SELF-CONSISTENT THEORY AND STRUCTURAL DYNAMICS OF EQUILIBRIUM APERIODIC SOLIDS

A Dissertation Presented to

the Faculty of the Department of Chemistry

University of Houston

In Partial Fulfillment

of the Requirements for the Degree

Doctor of Philosophy

By

Dmytro Bevzenko

August 2013

SELF-CONSISTENT THEORY AND STRUCTURAL DYNAMICS OF EQUILIBRIUM APERIODIC SOLIDS

Dmytro Bevzenko

APPROVED:

Dr. Vassiliy Lubchenko, Chairman

Dr. Eric R. Bittner

Dr. Donald J. Kouri

Dr. Chengzhi Cai

Dr. Peter Vekilov

Dean, College of Natural Sciences and Mathematics

ACKNOWLEDGMENTS

I would like to express my sincere gratitude to Vas Lubchenko, whose support often extended well beyond of what is normally required from the graduate advisor. I am also thankful to him for very careful, critical, and multiple reading of this manuscript which greatly contributed to its quality. This work would not be possible without help of my family: my parents, my wife, and my son. I am deeply grateful to Eric R. Bittner who, by being such a wonderful graduate advisor to my wife, made an inconspicuous, but very important, influence on everything I did. I also would like to thank to Anne Goj, Jon Golden, Pyotr Rabochiy, and other members of Bittner and Lubchenko's groups who made this place such a nice professional home. I am indebted to Elena and Phil Motuzko for helping me in the time of need. Last but not least, I thank Sergei Lukyanets without whom I would never became a scientist.

The numerical part of this work was completed using TLC2 HPC facility of the University of Houston and Ares cluster of the Texas Southern University. I am especially indebted to C. J. Tymczak for providing the access to the latter.

I also gratefully acknowledge support by the Donors of the ACS Petroleum Research Fund, the Arnold and Mabel Beckman Foundation, the Welch Foundation Grant E-1765, and the NSF Grant CHE 0956127.

SELF-CONSISTENT THEORY AND STRUCTURAL DYNAMICS OF EQUILIBRIUM APERIODIC SOLIDS

An Abstract of a Dissertation Presented to
the Faculty of the Department of Chemistry
University of Houston

In Partial Fulfillment
of the Requirements for the Degree
Doctor of Philosophy

By
Dmytro Bevzenko
August 2013

ABSTRACT

Essential microscopic aspects of activated transport in liquids, which precedes the glass transition, have evaded explanation for decades. These poorly understood aspects include: the molecular underpinning of the excess, configurational entropy; the transition state configurations for the activated transport; the chemical origin of the fragile vs. strong liquid behavior; and many others. This dissertation puts forth a radically novel way to address these open questions, in which liquids near their glass transition are viewed as structurally degenerate assemblies of strongly interacting, local sources of frozen-in stress. The thermodynamics and activated barriers for rearrangement of this stress field have been mapped onto a Heisenberg model with six-dimensional spins. A meanfield analysis of the spin model has shown glasses can be viewed as frozen-in patterns of shear stress and/or uniform compression/dilation, the two extremes corresponding to the strong and fragile behaviors. A self-consistent elasticity theory of aperiodic, metastable solids emerges in the present analysis; it supersedes the traditional elasticity theory, which fails to self-consistently account for the structural degeneracy stemming from the inherent mismatch between cohesive forces and steric repulsion. The observable elastic constants self-consistently emerge in the present theory similarly to how the dielectric susceptibility is determined by the properties of molecular dipoles. First simulations of the spin model have been carried out. In addition to direct observations of transition states for the activated transport, several key features of the glass transition are yielded by the spin model, including a strongly non-exponential, non-Arrhenius character of the relaxations and its correlation with the Poisson ratio of the substance.

CONTENTS

LIST OF FIGURES

INDEX OF FREQUENTLY USED SYMBOLS

$\mathbf{r}$, x_i	Position vector
$\mathbf{u}$, u_i	Deformation field
ε, ε_{ij}, ε_α	Strain tensor (compatible)
σ, σ_{ij}, σ_α	Stress tensor (compatible)
ρ, ρ_{ij}, ρ_α	Frozen-in stress field of amorphous structure (incompatible)
η, η_{ij}, η_α	Strain corresponding to ρ (incompatible)
ϵ^*, ϵ^*_{ij}, ϵ^*_α	Eigenstrain corresponding to ρ
$\mathbf{f}$, f_i	Body force field
C, C_{ijkl}, $C_{\alpha\beta}$	Elastic moduli tensor
λ, μ	Lamé coefficients
$\varkappa$	Bulk modulus
ν	Poisson ratio
g	Order parameter of the crystal-to-glass transition
a	Size of the effective particle, or bead, in a glass
s_c	Configurational entropy per bead
ϵ_{ijk}	Levi-Civita symbol
c	Number density
ρ_{M}	Mass density
c_t	Transverse sound velocity
c_l	Longitudinal sound velocity
V	Volume of a macroscopic body $\mathcal{B}$
v	Volume of a mesoscopic inclusion $\mathcal{I}$
β	Inverse temperature, $\beta = (k_B T)^{-1}$
θ	Dimensionless inverse temperature, $\theta = \beta g^2 a^3$

ACRONYMS

RFOT	random first order transition
MCT	mode-coupling theory
TLS	two-level systems
MF	mean field
BC	boundary conditions
MC	Monte Carlo
RCP	random close packed
PES	potential energy surface
rhs	right-hand side
lhs	left-hand side

1

MOTIVATION AND NON-TECHNICAL OVERVIEW OF THE DISSERTATION

Practical use of glasses by hominins, in the form of obsidian tools, dates back to between 1.7 and 0.2 Ma,[1] and precedes the appearance of modern humans, which happened approximately by 200 ka.[2, 3] Despite such a long history of their use, our understanding of how the microscopic structure of glasses arises and leads to their remarkable physical properties still contains many gaps.

The most conspicuous feature of liquids, upon supercooling towards a glass transition, is the dramatic increase in the viscosity, see Fig. 1.[5] Since the recent works of Wolynes and co-workers, see e.g. [4] for review, we have gained much understanding of the microscopic basis of this slowing down. In this microscopic picture, often called the random first order transition (RFOT) theory, the glass transition is preceded by the emergence of activated transport in the liquid.[6] This low-temperature type of transport is distinct from the better understood high-temperature, collisional transport. At high temperatures, the particle density distribution in liquids is uniform as it is in a dilute gas. In contrast, at low enough temperatures or high enough densities, the particle distribution function is more like that of a traditional, periodic crystal: it consists of well separated sharp peaks. In important distinction, however, the peaks in the glassy liquid form an *aperiodic* lattice. Such aperiodic lattices are bulk degenerate and, thus, exhibit intrinsic dynamics. A quantitative description of these dynamics is key to our understanding of the structural glass transition and controlling properties of glassy materials .

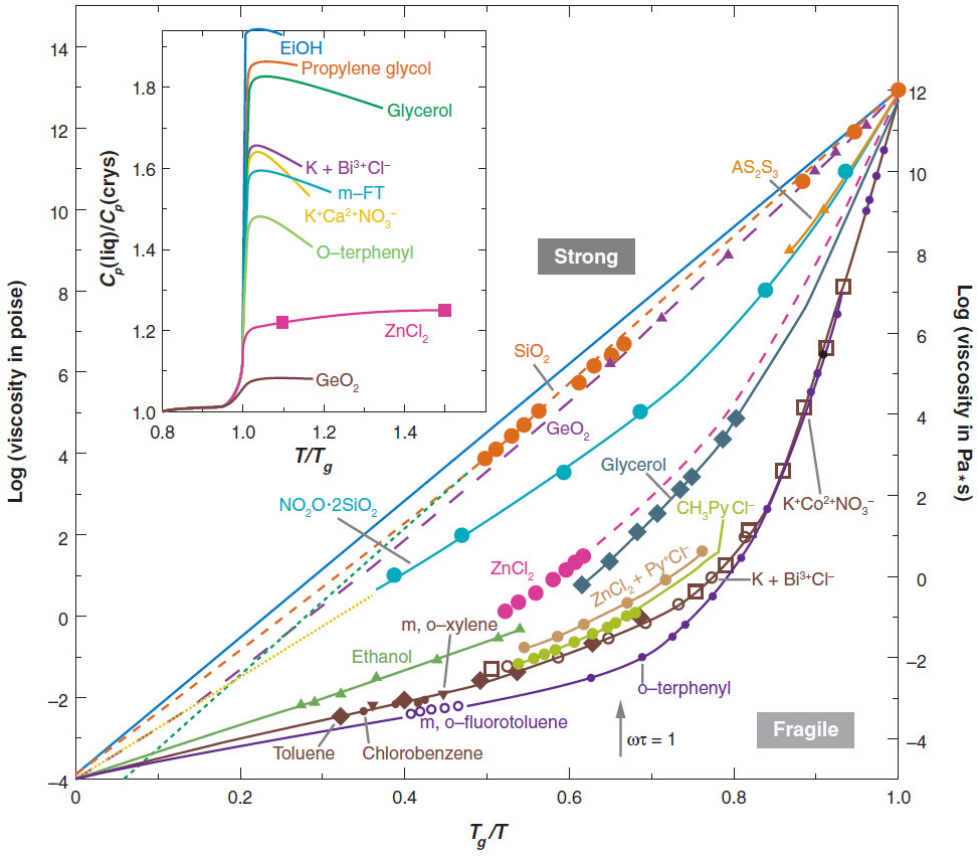

Figure 1.: The viscosities of several supercooled liquids plotted as functions of the inverse temperature. Substances with almost-Arrhenius-like dependences are said to be strong liquids, whereas the visibly convex curves are described as fragile substances. The full dynamic ranges from approximately 1 ps, on the lower viscosity side, to approximately 10^4 s when the viscosity reaches 10^{13} poise. Figure is reproduced from Reference [4] with permission.

Wolynes and co-workers have established that particle transport in the activated regime occurs via nucleation-like events: particle move when a distinct aperiodic arrangement is nucleated within the present structure.[7] In equilibrium, these nucleation events are driven by the multiplicity of the aperiodic structures. A quantitative measure of this multiplicity is the configurational entropy of the liquid, which is essentially the difference between the entropies of the liquid and the corresponding crystal. In the RFOT theory, the configurational entropy is a parameter determined experimentally; the procedure is not without ambiguity.[8] There is no theory at present that allows one to compute

this quantity for a specific substance. As a result, we are unable to estimate the viscosity and the glass-forming ability of a substance from first principles.

The aforementioned nucleation events are subject to a mismatch penalty between the initial and subsequent structures. There is a general semi-quantitative estimate for this surface-tension-like quantity.[9] Recently Rabochiy and Lubchenko have proposed a method of estimating this mismatch penalty for specific substances using their measured structure factors, elastic constants, and calorimetric data.[10] Despite these advances, the thus computed barriers for particle transport are often wrong by as much as a factor of two, implying relaxation rates which are off by many orders of magnitudes.

Even further in sight is an answer to the following deceptively simple question: where are the atoms in a glass? Owing to the astronomically broad dynamical range of relaxation in supercooled liquids, this question is not solvable by the present-day computer technology even for the simplest, non-realistic force fields. The dynamical range is broad because is must cover vibrational motions, which occur on the femtosecond scale, while glasses form on the scales of seconds to hours. Given the well developed machinery in the field of phase transitions and high-energy physics one but wonders why the glass transition problem is so difficult.

One difficulty is that even *writing* down a field theory for a liquid is problematic because there is no fixed reference frame. One of the main results of the present work is about circumventing this difficulty. Here we establish that the particle dynamics in the activated regime can be mapped on the dynamics of a Hamiltonian defined on a *fixed* lattice. The dynamic variables in this Hamiltonian are six-component spins; the six components correspond to the six independent entries of the deformation tensor in the linear elasticity theory. The 6-spins correspond to groups of several atoms that do not snugly fit in their immediate environments, resulting in frozen-in stress. The mismatch—and the resulting frustration—emerges because the cohesive forces and steric repulsion generally have different local symmetries. We thus arrive at the following picture for a crystal-to-glass transition: On the crystal side, the cohesive forces dominate, resulting in a higher density

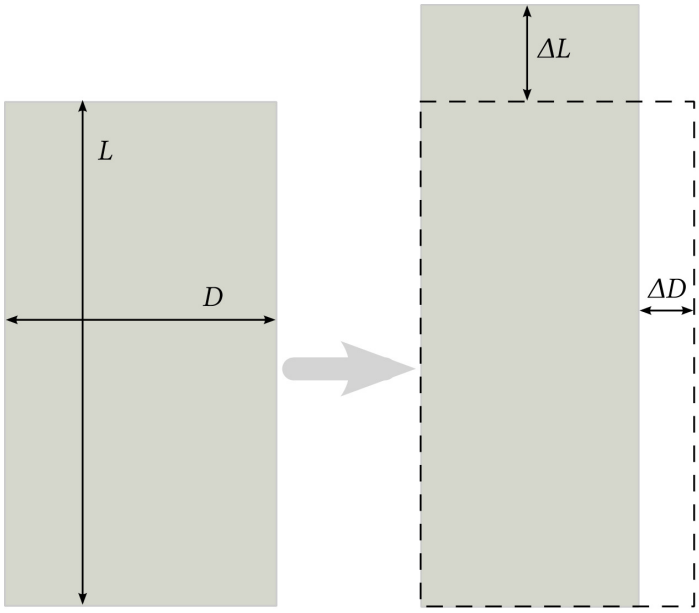

Figure 2.: The Poisson ratio, originally called the squeeze-stretch ratio,[11] is defined as a proportionality coefficient between lateral and longitudinal deformation of a rod under either purely longitudinal or lateral tension: $\nu = -\frac{\Delta D}{D}\Big/\frac{\Delta L}{L}$. The smaller the Poisson ratio, the stronger is the shear resistance of the material and, hence, the larger the ratio of the shear and bulk moduli.

and stronger bonding. On the glass side, the steric repulsion wins, giving rise a lower density and somewhat weaker bonding, but, at the same time, a possibility of many more mutual arrangements.

Aside from the formal progress achieved by the mapping, the motivation is to estimate, for the first time, the configurational entropy of the liquid and elucidate the spatial characteristics of the particle configurations occurring in the activated transport regime. In the present picture, motions in the liquid correspond to flipping of the 6-spins, while the configurational entropy is the log-number of the distinct mutual orientations of the spins.

The liquid-to-spin mapping comes at a cost, however, in that the interaction between the spins is very long-ranged, $1/r^3$, similar to the electric dipole-dipole interaction. Such long-ranged interactions are difficult to tackle either analytically or in computer simulations. We attempt this problem in steps of increasing difficulty. First, we solve the spin model in a mean field (MF) limit, in which the spin-spin interaction does not depend on the mutual separation between the spins.

Remarkably, some of the anisotropy of the original non-MF interactions is retained in this limit. This anisotropy reflects the Poisson ratio of the material, see fig. 2 for definition, which is known to correlate with the type of bonding and lattice connectivity of the material.[12] In this approximation we establish that supercooled liquids and glasses cover a range of situations, extremes of which correspond to the glass being a frozen-in *shear* stress and an *isotropic* deformation pattern. We discover that these two extremes are separated by a phase transition in the MF limit. By exploiting the known thermodynamics of this transition in finite dimensions, we establish that the stress pattern in strong glasses, such as silicates or oxides, corresponds mostly to frozen-in shear. In fragile systems, such as molecular liquids, the stress pattern corresponds largely to frozen-in compression/dilation.

To achieve the main goal of this work, i.e., establish the non-MF thermodynamic and dynamic behavior of the 6-spin model, we set up and perform Monte Carlo simulations. The long range of the spin-spin interaction prevents one from using traditional, periodic boundary conditions. Instead, we will exploit an analogy with dielectric polar liquids, which can be thought of as consisting of permanent dipoles. The bulk response of a polar liquid to an external electric field can be well approximated by a continuum with a dielectric constant. Likewise, here we consider a compact subset of the 6-spins explicitly, while modeling the surroundings using a continuum characterized by effective elastic moduli.

We immediately face a challenge similar to that of encountered by Debye, Onsager, Kirkwood, and others, some eight decades ago, who used the properties of molecular dipoles to determine the dielectric constant of a liquid self-consistently.[13] Similarly, here we develop, for the first time, a self-consistent theory of elasticity for a general uniform solid. We establish that the standard elasticity theory, although seemingly robust at long wavelengths, is, in fact, naive. It simply *postulates* mechanical stability, with no regard to local chemical bonding patterns, based on a general expectation that at long wavelengths, details of molecular interactions enter into the elastic response not directly but only through bulk elastic constants. In the present picture, in contrast,

the mechanical (meta)stability emerges self-consistently, starting from a liquid in the activated transport regime. The corresponding mechanical response is determined by the magnitude of the frozen-in stress, similarly to how the dielectric response is determined by the magnitude of the molecular dipoles. The calculation already at the level of a cavity approximation, similar to that of Debye and Onsager for dielectrics, turns out to be both more difficult and richer than the dielectric case. Owing to the tensor nature of the spin-spin coupling, the interaction between a spherical region of frozen-in stress and its environment exhibits a non-trivial fixed point: the frozen-in stress does not modify the Poisson ratio of the medium if the latter is equal to $\frac{1}{5}$. Remarkably, this is the same value of the Poisson ratio, at which the mean-field version of the 6-spin Hamiltonian, discussed above, exhibits a transition between the frozen-in shear and the uniform compression/dilation.

These developments enable to us to set up the Monte Carlo simulation in the following way: We consider a compact region in which the frozen-in stress self-interacts via bare, elastic interactions. (This is similar to molecular dipoles interacting by exchanging photons in vacuum.) The rest of the material is approximated by a mechanical continuum with renormalized elastic constants. (This corresponds with the bulk dielectric in the Onsager cavity construction.) We thus rid ourselves of the necessity to consider very remote spins, however at the expense of having to include in the simulation the spin-boundary interaction, as well as the spin-spin interaction mediated by the boundary. (These effects are analogous to the interaction of a charge with polarization charges at a dielectric discontinuity, which is vividly visualized in the method of images.) Already the interaction of a charge with a dielectric discontinuity is complicated in that there are an infinite number of images, except when one of the dielectrics is a metal. The elastic interactions are even more complicated. Despite these difficulties, we demonstrate that meaningful system sizes can be simulated. We obtain the first, to our knowledge, explicit demonstration of activated transport in a computer simulation. We recover what appears to be the deepest, to date, quench of a glassy system. We discover the dynamics of the 6-spin model are highly non-exponential and non-Arrhenius. The

extent of these anomalies correlates with the Poisson ratio, as expected from the our earlier, MF analysis, and consistent with experiment.

The dissertation is organized as follows: In Chapter 2, we work out the mapping between a liquid in the activated regime and a 6-spin model on a fixed lattice. There we also provide a mean-field solution of the spin model. In Chapter 3, the cavity construction is developed to establish self-consistently the metastability of the liquid and the corresponding elastic constants. In Chapter 4, we describe the details of the Monte Carlo simulation and present the results. Chapter 5 summarizes some of the present results and outlines future work.

2

GLASS AS A FROZEN-IN, DEGENERATE STRESS PATTERN: MAPPING BETWEEN ACTIVATED LIQUID MOTIONS AND A HAMILTONIAN DEFINED ON A FIXED LATTICE

Substantial portion of this Chapter is based on the published work.[14]

2.1 INTRODUCTION

If cooled sufficiently rapidly, a liquid may fail to crystallize, but will instead remain in a metastable, supercooled state. Upon further cooling, the relaxation times in a supercooled liquid grow very rapidly as the mass transport becomes activated, in contrast with the mainly collisional transport near the fusion temperature, see Fig. 1. Because the local structures are much longer-lived than the vibrational equilibration times, the activated-transport regime represents a state with a broken translational symmetry, even though the corresponding, aperiodic structure shows no obvious distinction from a snapshot of an ordinary, uniform liquid. (It is said the heterogeneity is "dynamical.") Since the symmetry is broken *gradually* with lowering the temperature—beginning with the highest frequency motions—a transition into this "aperiodic-crystal" state is not sharp, but, instead, is a soft cross-over centered at a temperature T_{cr}, [15, 16] corresponding universally to viscosity 10 Ps or so.[16, 17] The crossover into the activated regime is a finite-dimensional analog of a mean-field kinetic catastrophe of the mode-coupling theory (MCT), whereby the motional barriers would diverge at a temperature T_{A}, even though the configurational entropy is still extensive.[18, 19] the catastrophe comes about as the particle auto-correlation functions begin to exhibit progressively

long tails, because of frequent collisions. The thus slowed-down particles from transient cages around each other.[20] The thermodynamic basis of the transition is that by being confined to their individual cells in space, particles gain same entropy, while losing the translational entropy afforded by the uniform density distribution typical at low densities.

In additional contrast to the mean-field transition at T_{A}, the cross-over at T_{cr} exhibits two emerging length scales. The first one is the molecular length a that signifies the volumetric size of a chemically rigid unit, often called the *bead*, that is not significantly perturbed during activated transport. Conversely, the beads interact with each other weakly, comparably to the Lennard-Jones interaction.[16] A size of the bead may be thought of as a coarse-graining length, beyond which activated motions are largely independent of chemical detail, but fully characterized by a single, *bulk* quantity. This bulk quantity is the excess liquid entropy relative to the corresponding crystal, usually called the configurational entropy. The magnitude of the configurational entropy per bead, s_c, directly gives the number of alternative aperiodic configurations

$$\exp\left[\frac{s_c N}{k_B}\right]$$

available to a region of a supercooled liquid containing N beads. Structurally, the bead usually correspond to several atoms; it could be quite large for molecular liquids containing large rigid units such as benzene, see [16] for details.

The second length scale emerging during the crossover is the so-called Lindemann length d_L,[15, 21, 22] which is the molecular displacement at the mechanical stability edge. This length is nearly universal: $d_L \simeq \frac{1}{10}a$, and characterizes bead displacements during transitions between distinct aperiodic packings in the metastable, aperiodic crystal phase. One may view the crossover into the activated liquid regime as a "localization" transition, whereby the emerging metastability of local structures is signaled by a *discontinuous* transition from a uniform liquid to a state with a non-zero force constant of an effective Einstein oscillator; the one particle distribution function thus breaks

up into individual peaks, each corresponding to an Einstein oscillator.[15] The RFOT theory utilizes this view to analyze the activated transport in chemically distinct (non-polymeric) fluids in a *unified* fashion.[7, 9, 23] (See Ref.[4] for a review.) The RFOT theory predicts that in a fully developed activated regime, the structural relaxation time is determined solely by the configurational entropy per bead:[9, 16]

$$\tau = \tau_{vibr} \exp\left[\frac{32 k_B}{s_c}\right], \tag{2.1}$$

where $\tau_{vibr} \simeq 1$ psec is the microscopic time scale characterizing vibrational relaxation. By Eq. (2.1), system-specific deviations from the pure Arrhenius temperature dependence of τ result from variations in the value of the heat capacity jump at the glass transition temperature T_g per bead:

$$\Delta c_p = T \frac{\partial s_c}{\partial T}\bigg|_{T=T_g}.$$

The so-called fragility index

$$m = \frac{1}{T} \frac{d \log \tau}{d(1/T)}\bigg|_{T=T_g}$$

gives a quantitative measure of that deviation. Small and large deviations from the Arrhenius T-dependence (corresponding to small and large m respectively) are often called strong and fragile behaviors,[24, 25] see Fig. 1. The RFOT theory predicts $m \simeq 34.7 \Delta c_p$,[9, 16, 26] in good agreement with experiment.

Hall and Wolynes have put forth a simple qualitative model that relates the degree of molecular connectivity to the heat capacity jump Δc_p.[27] Establishing such connections between local chemistry and thermodynamics for actual substances is difficult, however, hampering the efforts to make first principles estimates of the configurational entropy and, ultimately, the glass-forming ability of those substances. Indeed, since the viscosity is directly related to the average relaxation time,[28]

$$\eta = \frac{2 k_B T}{\pi a d_L^2} \langle \tau \rangle \simeq 60 \, \frac{k_B T}{a^3} \langle \tau \rangle, \tag{2.2}$$

the crystal nucleus growth, which is subject to viscous drag,[29] is determined by the configurational entropy s_c per bead. The actual chemical identification of beads is relatively straightforward in molecular, but less so in covalently bonded compounds, where, for instance, the apparent bead often corresponds to a non-integer fraction of a stoichiometric unit.[16, 30] We note that these challenges are, of course, not unique to theories of the glass transition but equally pertain to quantitative descriptions of the ordinary liquid-to-crystal transition. Yet perhaps in reflection of these open questions, many believe fragile and strong behaviors actually have distinct mechanisms.

In an effort to develop a microscopic description of the configurational dynamics in specific substances, here we propose and work out several consequences of a novel quasi-continuum ansatz for local stress distribution that implements direct interactions in the activated regime semi-empirically, via the local elastic properties of the material. The ansatz incorporates the possibility of local, short-length motions that are similar in spirit to Einstein oscillators, but are strongly anharmonic and account explicitly for the tensorial nature of the relation between local deformation and stress in solids. In particular, explicitly treated is (high-frequency) *shear* resistance, which is characteristic of deeply supercooled liquids and, generally, activated liquid transport. This fully tensorial treatment of stress may be viewed, among other things, as a systematic improvement on self-consistent scalar-phonon theories of aperiodic crystals.[15, 31]

The many-body effects that lead to the emergence of shear resistance in liquids at high densities do not lend themselves easily to perturbative treatments that use the uniform liquid as the reference state. In contrast, we use a fully mechanically stable state as the reference state, and then uniformly allow for local, short-length anharmonic motions. Within this ansatz, a *metastable*, aperiodic frozen-in stress pattern emerges self-consistently, whereby the bead size is identified as the typical length scale of the stress heterogeneity. This result implies that even in a covalently bonded material, the concept of a bead is entirely unambiguous. The frozen-in stress pattern is multiply *degenerate*, whereby the transitions between alternative configurations can be mapped onto the dynamics of a classical Heisenberg model with six-component spins. The six components correspond to

the independent entries in the local frozen-in deformation tensor. The average length of the spin emerges as an order parameter for the aperiodic-to-periodic crystal transition. The transitions between different spin configurations are rare events implying the corresponding liquid states are long-lived and thus supporting the view of liquids in the activated-transport regime as aperiodic crystals. In other words, we explicitly confirm the non-trivial notion of the RFOT theory that aperiodic molecular assemblies can exhibit multiple states and, at the same time, support shear.

Already in a mean-field analysis of the spin model, we establish that the broken-symmetry state can exhibit a range of behaviors interpolating between frozen-in shear and uniform compression/dilation. These two limits correspond to a 5-component Heisenberg- and Ising-like ferromagnets respectively. The resulting heat capacity variations, together with the RFOT-derived intrinsic relation between thermodynamics and kinetics, as reflected in the m vs. Δc_p relation, implies that the spin model exhibits a broad range of fragile-to-strong behaviors during activated rearrangements. The heat-capacity jump per bead of the corresponding liquid will also depend on the ultraviolet cutoff of the theory, as specified by the bead size. We will observe that the fragility depends on the Poisson ratio of the material, but in a complicated, non-monotonic fashion. In any case, in view of the apparent broad range of strong-to-fragile behaviors exhibited in the present model, the present analysis strongly suggests the activated dynamics have the same mechanism in both strong and fragile liquids, consistent with the basic picture of the RFOT theory.

A potential formal benefit of the present approach is that it is possible to map the activated-transport liquid regime onto a spin model on a *fixed* lattice, thus opening the possibility of applying to liquids the many computational techniques developed in the context of spin models. Importantly, this mapping may provide a first principles basis for computing the configurational entropy for specific substances and the rate of crystallization from the supercooled state, since elastic constants at the length scale of a bead, which are the input into the theory, can be determined by ab initio methods.

2.2 ORDER PARAMETER FOR THE CRYSTAL-TO-GLASS TRANSITION: INFORMAL MOTIVATION AND QUANTITATIVE DISCUSSION

Let us begin with an *informal motivation* for a minimal ansatz for local stress distribution in a glass. Consider a substance that can both crystallize and vitrify and assume for concreteness that the glass has a greater specific volume than the corresponding crystal, as it is usually, but not always, the case.[1] A quenched melt or frozen glass of such a substance may be thus viewed as a result of the following action: Apply negative pressure to slowly expand the crystal until the lattice relaxes into one of the myriad available glass structures. (We assume that cracking does not occur.) Then release the negative pressure. The sample will remain in the metastable, glass state; the eventual transition to the lower free energy, crystal state will eventually occur by nucleation, but is subject to the surface tension between the two phases. In a standard fashion, the surface tension implies that the dependence of the free energy on the extent of dilation exhibits a concave down portion.[37] We can see qualitatively how it arises by estimating the free energy of the solid using a simple, *non-linear* Einstein-oscillator model.

Consider a collection of Einstein oscillators with the configurational partition function given by

$$Z^{\text{EO}} = \int_g^\infty \mathrm{d}\mathbf{r}\; e^{-\frac{1}{2}\beta k r^2}, \tag{2.3}$$

where we incorporate the non-linearity qualitatively by assuming a sharp lower cutoff in the configurational integral, at a displacement g. The non-linearity here comes down to the inability of the degree of freedom r to relax to values less than g. The latter corresponds to a frozen-in stress. The parameters k is a force constant in the harmonic limit. For $g = 0$ this model corresponds to the textbook, Einstein model for solids.[38, chap. 23]

1 Exceptions usually imply the glass was not generated by quenching an *equilibrium* liquid. Examples include: pressure induced amorphization,[32–34] densification of a glass,[35] and strain glasses.[36]

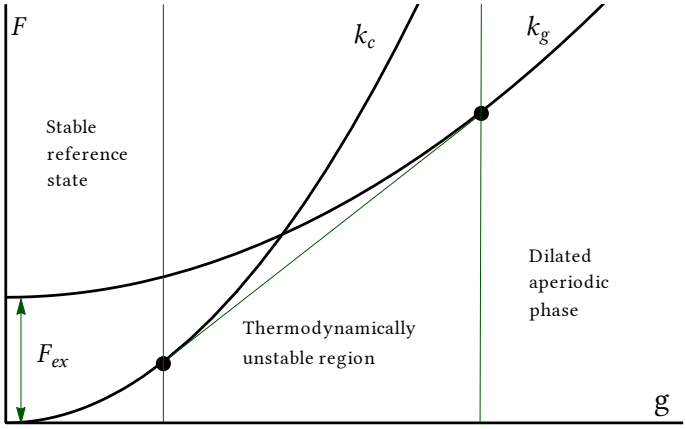

Figure 3.: Illustration of the notion of an aperiodic metastable state as a dilated crystal that was allowed to relax. F_{ex} is a free energy after the relaxation of the expansion which results in the "softening" of the crystal's force constant, $k_c \to k_g$.

Let us denote the force constants in the crystal and the expanded state as k_c and k_g respectively. Since the glass phase was assumed to be less dense than the crystal, we expect $k_g < k_c$. We sketch the free energies of the states as functions of g in Fig. 3, taking into account that the curve corresponding to the expanded state is shifted upward from the crystal state by the free energy cost of expansion. According to Fig. 3, under sufficient negative pressure (essentially equal to the negative slope of the common tangent of the two curves), the crystal will indeed begin converting into a collection of non-linear oscillators. The vast majority of the configurations of these oscillators are of course aperiodic, implying the metastable phase is aperiodic, too. This qualitative free energy graph tentatively confirms the view above of a quenched-melt/frozen-glass as a sufficiently expanded crystal that was allowed to relax. The interaction that stabilizes the lower density state is the steric repulsion. The graph also suggests an appropriate order parameter for the transition, namely the amplitude of short-wavelength, strongly anharmonic motions.

In writing a *formal* ansatz for a solid that allows short-wavelength anharmonic motions (to be defined below), we first point out that local mechanical instabilities are perfectly compatible even with macroscopic rigidity, examples including orientational glasses[39] and ferroelectrics

of order-disorder type.[40] The latter systems consist of rigid, periodic scaffolds where a *subset* of local motions could be marginally stable resulting in a vanishing frequency of transverse optical phonons.[40] In contrast, we wish to consider here a situation where *all* motions with the wavelength less than a certain cutoff distance are allowed to be multistable. The resulting material may or may not be macroscopically stable, as will be determined self-consistently. We will limit ourselves to a dynamical regime, in which relative distortions of individual bonds during lattice reconfigurations are only within 10% or so,[15, 21, 22] as appropriate both for activated transport and stable crystals. Such small distortions imply the harmonic approximation for local stress is semiquantitative.

Consider the elastic energy E of a solid, in the linear elasticity approximation, as a function of the local displacement $\mathbf{u}$ relative to a steady-state reference state:[41]

$$E = \frac{1}{2}\int \mathrm{dV}\epsilon_{ij}C_{ijkl}\epsilon_{kl}, \tag{2.4}$$

where C_{ijkl} is the elastic moduli tensor and

$$\epsilon_{ij} = \frac{1}{2}\left(u_{i,j} + u_{j,i}\right) \tag{2.5}$$

is the strain. Hereafter Latin indexes run from 1 to 3 and Einstein's summation convention for two repeating indexes is always implied, e.g.: $u_i u_i = \sum_{i=1}^{3} u_i u_i$. We also use index notations to label derivatives. For example, for $\mathbf{u}(\mathbf{r})$ we write

$$u_{i,j} \qquad \text{instead of} \qquad \frac{\partial u_i}{\partial x_j}.$$

We decompose the strain tensor into long- and short-wavelength components:

$$\epsilon_{ij} = \varepsilon_{ij} + \eta_{ij}, \tag{2.6}$$

where ε_{ij} now includes only the Fourier components with wave vectors *inside* a certain cutoff surface in k-space, while η_{ij} contains only Fourier components *outside* of the cutoff surface. Let us evaluate the free energy of the system subject to a constraint on the elastic self-energy density of the short-wavelength component,

$$\eta_{ij} C_{ijkl} \eta_{kl} = g^2(\mathbf{r}), \tag{2.7}$$

which forces the short-wavelength motions to be essentially a collection of anharmonic Einstein oscillators. If the cutoff surface in the Fourier space is generically at $k \simeq k_{micro}$, the anharmonic oscillators fill space, approximately one per volume $(\pi/k_{micro})^3$, but not necessarily in a periodic fashion. The detailed lattice in which the oscillators are arranged depends on the precise shape of the cutoff surface.

Since the presence of strongly anharmonic degrees of freedom generally requires expanding the lattice from the reference state, we must include in the full free energy of our solid a penalty for increasing g, which we denote as $F_{ex}(g)$. The precise form of this function is not essential for the majority of our conclusions; clearly it is a monotonically increasing, *concave up* function of g, to ensure the compressibility is positive. As a result, the full free energy is:

$$F_a(g) = F(g) + F_{ex}(g), \tag{2.8}$$

where the free energy $F(g)$ of the ansatz is computed by summing over all configurations of the local stress, subject to the constraint (2.7), at a constant temperature T:

$$e^{-\beta F(g)} = \sum_{\eta(\mathbf{r})} \sum_{\mathbf{u}(\mathbf{r})} e^{-\beta E}. \tag{2.9}$$

Note that in calculating $F(g)$, the long-wavelength displacement field $\mathbf{u}(\mathbf{r})$ and short-wavelength tensor field $\eta(\mathbf{r})$ are understood to be dynamical variables. The use of $\mathbf{u}$ is a standard way of calculating the free energy of, e.g., phonons in a solid.[38] However, no continuous deformation

field corresponds to $\eta(\mathbf{r})$ in general. Summation over $\eta(\mathbf{r})$ in (2.9) corresponds to averaging over short-wavelength structural states of the material. Similar approaches have been employed, e.g., to study martensitic transformations in functional materials.[42]

Even though we have written $\eta(\mathbf{r})$ as a continuum field, it is understood that it is defined on a fixed lattice given by the positions of the Einstein oscillators. For all known crystals classes, the elastic tensor is symmetric with respect to interchanging the first two indices: $C_{ijkl} = C_{jikl}$, and likewise for the last pair: $C_{ijkl} = C_{ijlk}$. Thus the tensor η can be taken as symmetrical without loss of generality and as a result has 6 independent components (we assume here that η is symmetric similarly to ε) it corresponds to 6 degrees of freedom, and thus every lattice site must correspond to at least two atoms. A change of $\eta(\mathbf{r})$ reflects a reconfiguration of particles constituting the lattice in the vicinity of $\mathbf{r}$. The field $\mathbf{u}(\mathbf{r})$ describes elastic deformation of the lattice with wavelengths exceeding $2\pi/k_{micro}$, which we generically will call acoustic phonons. Note that the number of the acoustic modes is three per lattice site reflecting three translational degrees of freedom which describe change in the position of the center of mass of a group of atoms, while disregarding the mutual displacements within the group. Switching between discrete summation over lattice sites and continuous integration over space can be done according to the rule:

$$a^3 \sum \rightarrow \int_{\mathcal{B}} \mathrm{dV}, \tag{2.10}$$

where $a = \pi/k_{micro}$ is the length scale corresponding to the cutoff wave vector k_{micro}. The index $\mathcal{B}$ signifies integration over the volume of the body $\mathcal{B}$.

For the sake of argument, hereafter we assume the order parameter is uniform:

$$g^2(\mathbf{r}) = g^2 = \mathrm{Const.} \tag{2.11}$$

Formal extension to a nonuniform $g(\mathbf{r})$ is possible to do. However, since $|g(\mathbf{r})|$ is finite in the first place, local variations will introduce higher order effects. Also, we limit the analysis to the simplest case of an isotropic reference state:

$$C_{ijkl} = \lambda\delta_{ij}\delta_{kl} + \mu\left(\delta_{ik}\delta_{jl} + \delta_{il}\delta_{jk}\right), \tag{2.12}$$

where λ and μ are the Lamé coefficients (μ is also called the shear modulus).[43, §5.2] Such choice allows one to considerably simplify tensor algebra making use of the notation scheme outlined in the next section.

2.3 A DIGRESSION ON TENSOR ALGEBRA

Throughout this manuscript we will often need to write different inner products, e.g, $\varepsilon_{ij}C_{ijkl}\varepsilon_{kl}$. We always use Einstein's summation rule. By construction, Latin indexes run from 1 to 3. Very often, however, it is convenient to drop indexes in inner products altogether,[44] as it is usually done when writing inner products of vectors. For instance, **ab** is widely used for labeling the inner product of vectors **a** and **b**, $\sum_{i=1}^{3} a_i b_i$. Similarly we will write

$$\sigma = \mathrm{AB}\varepsilon \qquad \text{instead of} \qquad \sigma_{ij} = A_{ijkl}B_{klpq}\varepsilon_{pq},$$

and

$$\sigma\varepsilon \qquad \text{instead of} \qquad \sigma_{ij}\varepsilon_{ij}.$$

To avoid confusion we use upright font to label tensors (both fourth- and second-order) if their indexes are dropped. Note, that some of the Greek letters are conventionally reserved for scalars. For instance, μ and $\varkappa$ label the shear and bulk moduli, ν is the Poisson ratio, and

$$\beta = (k_B T)^{-1}.$$

Here we deal mostly with isotropic tensors. The corresponding algebra can be much simplified using the system of notations developed by L. J. Walpole.[44] We use the symbolic notation $\mathrm{L}[a\,, b]$ to label a generic isotropic tensor of the fourth order. Such a tensor can be written as a spectral decomposition[44]

$$\mathrm{L}[a\,, b] = a\mathrm{J} + b\mathrm{K}, \tag{2.13}$$

where the fourth-order isotropic tensors J and K,

$$\begin{aligned} J_{ijkl} &= \frac{1}{3}\delta_{ij}\delta_{kl}, \\ K_{ijkl} &= \frac{1}{2}\left(\delta_{ik}\delta_{jl} + \delta_{il}\delta_{jk} - \frac{2}{3}\delta_{ij}\delta_{kl}\right), \end{aligned}$$

are idempotent, i.e., they satisfy relations

$$\mathrm{JJ} = \mathrm{J} \qquad \text{and} \qquad \mathrm{KK} = \mathrm{K}, \tag{2.14}$$

and are mutually "orthogonal",

$$\mathrm{JK} = \mathrm{KJ} = 0.$$

Acting on a symmetric second-order tensor, say υ, tensors J and K extract its isotropic (diagonal) and deviatoric (zero-trace) parts respectively

$$\begin{aligned} J_{ijkl}\upsilon_{kl} &= \frac{1}{3}\upsilon_{kk}\delta_{ij}, \\ K_{ijkl}\upsilon_{kl} &= \upsilon_{ij} - \frac{1}{3}\upsilon_{kk}\delta_{ij} = {}'\upsilon_{ij}. \end{aligned} \tag{2.15}$$

The elastic moduli tensor C of an isotropic medium with Lamé coefficients λ and μ,

$$C_{ijkl} = \lambda\delta_{ij}\delta_{kl} + \mu\left(\delta_{ik}\delta_{jl} + \delta_{il}\delta_{jk}\right), \tag{2.16}$$

can be written using Eq. (2.13) as

$$\mathrm{C} = \mathrm{L}\left[3\varkappa\ , 2\mu\right] = 2\mu\ \mathrm{L}\left[\frac{1+\nu}{1-2\nu}\ , 1\right], \tag{2.17}$$

where ν,

$$\nu = \frac{1}{2\left(1+\mu/\lambda\right)}, \tag{2.18}$$

is the Poisson ratio of the medium and $\varkappa$,

$$\varkappa = \lambda + \frac{2}{3}\mu = \frac{2\mu}{3}\frac{1+\nu}{1-2\nu}, \tag{2.19}$$

is the bulk modulus, which is the same as the inverse compressibility

$$\varkappa^{-1} = -\frac{1}{V}\left(\frac{\partial V}{\partial p}\right)_T, \tag{2.20}$$

where V is the volume of the body $\mathcal{B}$, p is the external pressure, and T is the temperature. For $\nu = 0$, C is proportional to the fourth-order unit tensor I,

$$\mathrm{I} = \mathrm{L}[1\ , 1] = \mathrm{J} + \mathrm{K} = \frac{1}{2}\left(\delta_{ik}\delta_{jl} + \delta_{il}\delta_{jk}\right). \tag{2.21}$$

Decomposition (2.13) simplifies the algebra for isotropic tensors considerably. For example, for two isotropic tensors $\mathrm{L}_1 = \mathrm{L}[a_1\ , b_1]$ and $\mathrm{L}_2 = \mathrm{L}[a_2\ , b_2]$, the sum and the product are given simply by

$$\mathrm{L}_1 + \mathrm{L}_2 = \mathrm{L}[a_1 + a_2\ , b_1 + b_2]$$

and

$$\mathrm{L}_1\mathrm{L}_2 = \mathrm{L}[a_1 a_2\ , b_1 b_2]$$

respectively. Also, the tensor equation $\mathrm{L}_1 = \mathrm{L}_2$ is equivalent to the system of two scalar equations, $a_1 = a_2$ and $b_1 = b_2$. The n-th power of the tensor can be found as

$$\mathrm{L}[a\ , b]^n = \mathrm{L}[a^n\ , b^n]\,, \tag{2.22}$$

where, note, n can be non-integer. Also note that isotropic tensors commute with each other, a property which also holds for cubic symmetry, but no other point group symmetries.[44]

This system of notations allows us to express Eq. (2.4) and the constraint (2.7) in a more compact form. Absorbing the tensor C into the definition of ε and η,

$$\varepsilon = \mathrm{C}^{-1/2}\phi, \qquad \text{and} \qquad \eta = \mathrm{C}^{-1/2}\psi, \tag{2.23}$$

we can write

$$E = \frac{1}{2}\int_{\mathcal{B}} \mathrm{dV}\,(\varepsilon + \eta)\,\mathrm{C}\,(\varepsilon + \eta) = \frac{1}{2}\int_{\mathcal{B}} \mathrm{dV}\,(\phi + \psi)^2\,, \tag{2.24}$$

and

$$\eta\mathrm{C}\eta = \psi_{ij}\psi_{ij} = \psi^2 = g^2 \tag{2.25}$$

It is known that the linear elasticity formalism can be written in a six component second-order tensor representation.[45] In this picture, second-order tensors, such as σ_{ij} and ε_{ij}, are recast as six component vectors, σ_α and ε_α, respectively, where it is always assumed that Greek indexes run

from 1 to 6. Since both notations are completely equivalent, we will often drop indexes by writing, e.g. ε instead of ε_α or ε_{ij}. To avoid any confusion we will *always* label the norm of a 6-vector by $|\cdot|$.

In the 6-vector representation, the constraint (2.25) acquires a clear geometrical meaning: it becomes equivalent to fixing the length of the 6-vector corresponding to ψ_{ij}:

$$\psi_{ij}\psi_{ij} = \psi_\alpha\psi_\alpha = |\psi|^2 = g^2. \tag{2.26}$$

Thus, the structural states of η, permitted by the constraint (2.7) or (2.25), can be mapped onto all possible orientations of the 6-vector ψ while the Boltzmann average over η in the definition of $F(g)$, Eq. (2.9), corresponds to an averaging over all orientations of ψ. This will be considered in more detail in the next section.

In the 6-vector picture, fourth-order tensors are recast as second-order tensors, e.g. $C_{ijkl} \to C_{\alpha\gamma}$, which allows us to make use of the square matrix eigenvalue decompositions. We can write

$$\Big(\mathrm{L}[a\,,b]\Big)_{\alpha\beta} = U_{\alpha\gamma}\Big(\mathrm{D}[a\,,b]\Big)_{\gamma\delta}U^{\top}_{\delta\beta}, \tag{2.27}$$

where

$$\mathrm{U} = \begin{pmatrix} 1/\sqrt{3} & -1/\sqrt{6} & -1/\sqrt{2} & 0 & 0 & 0 \\ 1/\sqrt{3} & -1/\sqrt{6} & 1/\sqrt{2} & 0 & 0 & 0 \\ 1/\sqrt{3} & \sqrt{2}/\sqrt{3} & 0 & 0 & 0 & 0 \\ 0 & 0 & 0 & 1 & 0 & 0 \\ 0 & 0 & 0 & 0 & 1 & 0 \\ 0 & 0 & 0 & 0 & 0 & 1 \end{pmatrix} \tag{2.28}$$

is the tensor constructed from eigenvectors of $\mathrm{L}[a\,,b]$, and the symbol $\mathrm{D}[a\,,b]$ labels a diagonal tensor of the form

$$\mathrm{D}[a\,,b] = \begin{pmatrix} a & 0 & 0 & 0 & 0 & 0 \\ 0 & b & 0 & 0 & 0 & 0 \\ 0 & 0 & b & 0 & 0 & 0 \\ 0 & 0 & 0 & b & 0 & 0 \\ 0 & 0 & 0 & 0 & b & 0 \\ 0 & 0 & 0 & 0 & 0 & b \end{pmatrix}. \tag{2.29}$$

Note that U does not depend on a and b, $\mathrm{U}\mathrm{U}^{\top} = \mathrm{I}$, and the determinant $\det \mathrm{U} = -1$. Also $\mathrm{U}^{\top}$ stands for the transpose of the orthogonal matrix U. Hereafter we always imply 6-vector representation when applying the transpose to a fourth-order tensor.

2.4 GLASS AS A FROZEN-IN STRESS PATTERN

We inquire about the possibility of (metastable) states with a non-zero g by testing $F_a(g) = F(g) + F_{ex}(g)$, Eq. (2.8), for the presence of a concave down portion. The latter peculiarity is only possible if $F(g)$ has an inflection point. It will suffice for our purposes here to extract the small and large g asymptotes of $F(g)$, which one may accomplish by first averaging the Boltzmann weight $e^{-\beta E}$ in Eq. (2.9) over all possible η subject to the constraint (2.7). As was demonstrated in the previous section, such averaging is equivalent to the averaging over the orientations of the 6-vector $\psi = \mathrm{C}^{1/2}\eta$, cf. Eq. (2.23). By the aforementioned prescription for interchange between discrete summation over the oscillator sites and integration in space, Eq. (2.10), we break up the integral in the expression for E into a lattice sum

$$E = \frac{1}{2}\int_{\mathcal{B}} \mathrm{d}V \left[\phi(\mathbf{r}) + \psi(\mathbf{r})\right]^2 \approx \frac{a^3}{2}\sum_i \left[\phi(\mathbf{r}_i) + \psi(\mathbf{r}_i)\right]^2. \tag{2.30}$$

and swap the order of summations over $\mathbf{u}$ and over η to get

$$\sum_{\eta(\mathbf{r})} e^{-\beta E} \approx \prod_i e^{-\frac{\beta a^3}{2}\left[\phi^2(\mathbf{r}_i)+g^2\right]} \int \mathrm{d}\Omega_\psi^{(i)} e^{-\beta a^3 \phi_\alpha(\mathbf{r}_i)\psi_\alpha(\mathbf{r}_i)}, \tag{2.31}$$

where the integration is carried out for every lattice point at $\mathbf{r}_i$ over a solid angle in six-dimensional coordinate system. Labeling the corresponding angles by φ_j, we can write the solid angle element as[46, §A.10]

$$\mathrm{d}\Omega_\psi = \sin^4\varphi_1 \sin^3\varphi_2 \sin^2\varphi_3 \sin\varphi_4 \mathrm{d}\varphi_1 \mathrm{d}\varphi_2 \mathrm{d}\varphi_3 \mathrm{d}\varphi_4 \mathrm{d}\varphi_5,$$

$\varphi_i \in [0,\pi]$, for $\alpha < 5$, and $\varphi_5 \in [0, 2\pi]$. The integration can be accomplished analytically,[2] cf. [49, §9.6.18],

$$\int \mathrm{d}\Omega_\psi^{(i)} e^{-\beta a^3 \phi_\alpha(\mathbf{r}_i)\psi_\alpha(\mathbf{r}_i)} = \frac{16\pi^3}{3} \frac{I_2\left[\beta g a^3 |\phi(\mathbf{r}_i)|\right]}{\left[\beta g a^3 |\phi(\mathbf{r}_i)|\right]^2}, \tag{2.32}$$

where the norm of ϕ is defined via

$$|\phi| = \sqrt{\phi^2} = \sqrt{\phi_\alpha \phi_\alpha} = \sqrt{\varepsilon_{ij} C_{ijkl} \varepsilon_{kl}},$$

and $I_n(x)$ is the modified Bessel function of order n. Using Eq. (2.10) again, we finally obtain for the free energy density of the short-wavelength deformation component $f_\eta\,[\phi]$,

$$\sum_{\eta(\mathbf{r})} e^{-\beta E} \approx e^{-\beta \int_{\mathcal{B}} \mathrm{d}V f_\eta[\phi]}$$

where

$$f_\eta\,[\phi] = \frac{1}{2}\left(\phi^2(\mathbf{r}) + g^2\right) - \frac{1}{\beta a^3} \ln \frac{I_2\left[\beta g a^3 |\phi(\mathbf{r})|\right]}{\left[\beta g a^3 |\phi(\mathbf{r})|\right]^2}, \tag{2.33}$$

up to an additive constant. This free energy depends only on the absolute values of the 6-component vector ϕ and g, which characterize the long- and short-wavelength deformation respectively.

2 We note in passing that similar calculation is done for n-vector model of magnetic systems, see e.g., [47, §3.5] or [48].

To extract the behavior of $F(g)$ at small g, we note that at small values of either field, expression (2.33) yields

$$f_\eta\,[\phi] \xrightarrow[g|\phi(\mathbf{r})|\to 0]{} \frac{1}{2}\phi^2(\mathbf{r})\left(1-\frac{g^2\beta a^3}{6}\right)+\frac{1}{2}g^2, \tag{2.34}$$

implying the sole effect of the presence of the short-wavelength anharmonic displacement of magnitude g is a renormalization of all acoustic frequencies downwards by a factor of $(1-\frac{1}{6}\beta g^2 a^3)^{1/2} \simeq 1-\frac{1}{12}\beta g^2 a^3$ (if g is sufficiently small). Since the partition function of a classical harmonic oscillator with frequency ω is $(k_B T/\hbar\omega)$, this reduction in the acoustic frequency results in a free energy shift of $-\frac{1}{12}g^2a^3$ per phonon. As mentioned earlier, the number of the acoustic modes is three times the number of the lattice sites where η is defined, yielding that at small g (per phonon),

$$\frac{F(g)}{N} \sim \frac{g^2}{2} - 3\frac{k_B T}{a^3}\frac{g^2\beta a^3}{12} = \frac{g^2}{4}.$$

Thus at small g, the second derivative is positive.

According to the asymptotic expansion of the Bessel function, $I_n(x) \propto x^{-1/2}e^x$,[49, §9.7] and so the two leading terms in the large g limit of Eq.(2.33) are given by

$$f_\eta \xrightarrow[g\to\infty]{} \frac{1}{2}\left[|\phi(\mathbf{r})|-g\right]^2+\frac{5}{2}\frac{k_B T}{a^3}\ln g. \tag{2.35}$$

The g-dependent portion of the free energy is now uniform in space and thus no longer has short-wavelength components. As a result, we can always shift the $\mathbf{u}$ variable to eliminate the g-dependence from the integrand in the partition function corresponding to the free energy (2.35) so as to make the expression a pure quadratic in the new variable ϕ': $\mathbf{u} = \mathbf{u}_0 + \mathbf{u}' \to \phi = \phi_0 + \phi'$ where $|\phi_0| = g$. This latter reference state physically corresponds to a uniform distribution of stress (not displacement!) at a free energy density $\frac{1}{2}g^2$. The resulting integration over ϕ' becomes

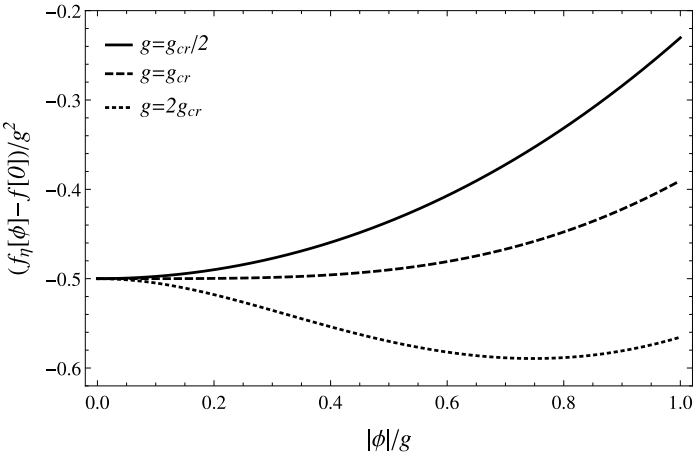

Figure 4.: Free energy profiles for local elastic strain at three representative values of the anharmonic displacement g, from Eq. (2.33). Above the critical value g_{cr} from Eq. (2.36), the lattice freezes in an aperiodic pattern at wavelength $2\pi/k_{micro}$.

asymptotically Gaussian in the large g limit, despite the non-analytical dependence on $\mathbf{u}$ in Eq. (2.35). As a result,

$$\frac{F(g)}{N} \xrightarrow[g\to\infty]{} \frac{5}{2}\frac{k_B T}{a^3}\ln g,$$

i.e. the second derivative of $F(g)$ becomes *negative* at large g, implying $F(g)$ has an inflection point at an intermediate value of g.

We thus conclude from the analysis of the asymptotic behavior of the free energy $F(g)$ that with a suitable form of $F_{ex}(g)$, such as $F_{ex}(g) \propto g^2$, it is possible for the full free energy $F_a(g)$ to have a concave down portion, also consistent with the mean-field solution in Section 2.6, see Fig.8. We reiterate that the presence of the concave down portion means the system exhibits a metastable state at a *non-zero* value of g. We do not explicitly treat the steric repulsion which is needed to stabilize the $g > 0$ phase. The methodology is, nevertheless, internally consistent, see also Chapter 3. The quantity g, therefore, can be used as an order parameter for a transition between the lowest free energy, fully stable state and the metastable state at non-zero g.

The free energy $f_\eta\,[\phi]$ of our ansatz helps to understand the origin of the peculiar behavior of $F(g)$. At large enough magnitude of anharmonic displacement g, the equilibrium value of the

acoustic displacements becomes non-zero. According to Eq. (2.34) this transition occurs at a critical value:

$$g_{cr}^2 = \frac{6k_BT}{a^3}. \tag{2.36}$$

We show the ϕ-dependence of the free energy from Eq. (2.33) in Fig. 4, for several representative values of g. In the metastable phase at $g > 0$, the thermodynamic potential from Eq. (2.33) is dominated by aperiodic configurations of the anharmonic field ψ, implying the modulation of the harmonic field is aperiodic, too. This potential becomes particularly vivid in the $g^2/k_BT \to \infty$ limit, i.e. $\frac{1}{2}\left(g - |\phi|\right)^2 = \frac{1}{2}\left(g - \sqrt{\varepsilon C \varepsilon}\right)^2$. Consistent with this identification, the form $\left(g - \sqrt{\varepsilon C \varepsilon}\right)^2$ is similar to broken-symmetry functionals that arise in systems with self-generated disorder.[50, 51] Importantly, the free energy (2.33) is an equilibrium quantity, implying the metastable aperiodic state corresponds to a melt *above* the glass transition. Furthermore, the aperiodic phase corresponds to a frozen-in stress pattern at half-wave length $a = \pi/k_{micro}$. Thus we must associate the length a with the bead size of the RFOT theory. We reiterate that the bead size a corresponds to size of a chemically rigid unit. Conversely, motions on length scales below a do not appreciably affect the activated reconfigurations.

2.5 MINIMAL ANSATZ FOR LOCAL STRESS DISTRIBUTION

The aperiodic phase discussed above exhibits many distinct states separated by activation barriers. To see this structural degeneracy explicitly, we find the free energy cost of the short-wavelength deformation η, by averaging over the long-wavelength deformations $\mathbf{u}$ in Eq. (2.9),

$$F(g) = -\frac{1}{\beta}\sum_{\dot{\mathbf{u}}(\mathbf{r})}\sum_{\mathbf{u}(\mathbf{r})} e^{-\beta\left(E+K_{ph}\right)}, \tag{2.37}$$

where the elastic energy of the system is given by (2.4)

$$E = \frac{1}{2}\int_{\mathcal{B}} \mathrm{dV}\left[\varepsilon C\varepsilon + 2\eta C\varepsilon + \eta C\eta\right], \tag{2.38}$$

and K_{ph} is the kinetic energy of the phonon deformation,

$$K_{ph} = \frac{1}{2}\int_{\mathcal{B}} \mathrm{dV}\rho_{\mathrm{M}}\dot{\mathbf{u}}^2. \tag{2.39}$$

There is no kinetic energy contribution due to the field η, since the phonon part already accounts for the kinetic energy of all atoms. The integration is carried over the volume of the sample, a body $\mathcal{B}$, and ρ_{M} labels the corresponding mass density. The notation $F(g)$ emphasizes that the phonons are integrated out and so $F(g)$ is a thermodynamic potential for the degree of freedom ρ, which is the frozen-in stress. In what follows it will be more convenient to work in terms of the *stress* ρ resulting from the short-wavelength deformation:

$$\rho = C\eta. \tag{2.40}$$

This allows us not to write out explicitly the elastic moduli tensor in the interaction term in (2.38):

$$F(\rho) = \frac{1}{2}\int_{\mathcal{B}} \mathrm{dV}\rho\eta - \frac{1}{\beta}\sum_{\dot{\mathbf{u}}(\mathbf{r})}\sum_{\mathbf{u}(\mathbf{r})} e^{-\beta\left(K_{ph}+\int_{\mathcal{B}}\mathrm{dV}\left[\frac{1}{2}\varepsilon C\varepsilon+\rho\varepsilon\right]\right)}. \tag{2.41}$$

The integration can be accomplished in the standard manner, using the Fourier transform of $\mathbf{u}$,

$$\mathbf{u} = \frac{1}{\sqrt{\rho_{\mathrm{M}}V}}\sum_{\mathbf{k}\in\mathcal{D}(a)} \mathbf{w}\left(\mathbf{k},t\right)e^{i\mathbf{k}\mathbf{r}}, \tag{2.42}$$

where we have limited the domain of possible wave vectors $\mathcal{D}(a)$ to one inside a cutoff surface corresponding to $a = \pi/k_{micro}$, see Section 2.2 for discussion. The complex vector field $\mathbf{w}$ satisfy the property,

$$\mathbf{w}\left(\mathbf{k}, t\right) = \mathbf{w}^{*}\left(-\mathbf{k}, t\right), \tag{2.43}$$

ensuring that $\mathbf{u}$ is real. To enforce (2.43), we write

$$\mathbf{w} = \mathbf{x} + i\mathbf{y} \tag{2.44}$$

and reduce summation over $\mathbf{k}$ to a half-space only, labeling the corresponding sum and product symbols by a prime, in a standard fashion.[52, §5.7.2] This gives

$$K_{ph} + \int_{\mathcal{B}} \mathrm{dV}\left[\frac{1}{2}\varepsilon \mathrm{C}\varepsilon + \rho\varepsilon\right] = \sum_{\mathbf{k}}{}' \left(\dot{\mathbf{x}}^{2} + \dot{\mathbf{y}}^{2} + \frac{1}{\rho_{\mathrm{M}}}\left[x_i \zeta_{ij} x_j + y_i \zeta_{ij} y_j\right] - \mathbf{xs} - \mathbf{yc}\right), \tag{2.45}$$

where, cf. [43, Eq. (6.56)],

$$\zeta_{ij} = k_m C_{imlj} k_l, \tag{2.46}$$

$k = |\mathbf{k}|$, and

$$\begin{Bmatrix} c_i\left(\mathbf{k}\right) \\ \\ s_i\left(\mathbf{k}\right) \end{Bmatrix} = \frac{2}{\sqrt{\rho_{\mathrm{M}} V}} \int_{\mathcal{B}} \mathrm{dV} \begin{Bmatrix} \cos\mathbf{kr} \\ \\ \sin\mathbf{kr} \end{Bmatrix} \rho_{ij} k_j. \tag{2.47}$$

In writing Eq. (2.47), we explicitly used the fact that only the symmetric part of the field η enters the energy E, Eq. (2.38), since the tensor C satisfies[41]

$$C_{ijkl} = C_{jikl}.$$

Hence we can assume with no loss of generality $\eta_{ij} = \eta_{ji}$. Consequently, $\rho = \mathrm{C}\eta$ is also symmetric $\rho_{ij} = \rho_{ji}$, and so one may write

$$\varepsilon_{ij}\rho_{ij} = \frac{\partial u_i}{\partial x_j}\rho_{ij}.$$

Now, specifically for an isotropic

$$C_{ijkl} = \lambda\delta_{ij}\delta_{kl} + \mu(\delta_{ik}\delta_{jl} + \delta_{il}\delta_{jk}),$$

cf. Eq. (2.16), we get

$$\zeta_{ij} = \mu k^2\delta_{ij} + (\lambda + \mu)\, k_i k_j, \tag{2.48}$$

and

$$\left(\zeta^{-1}\right)_{ij} = \frac{1}{2\mu k^2}\left(2\delta_{ij} - \frac{1}{1-\nu}\frac{k_i k_j}{k^2}\right), \tag{2.49}$$

where we have used the following relation between the Lamé coefficients and Poisson ratio,

$$\frac{\lambda + \mu}{\lambda + 2\mu} = \frac{1}{2}\frac{1}{1-\nu}. \tag{2.50}$$

The determinant ζ,

$$\det\zeta = \mu^2\,(\lambda + 2\mu)\,k^6 = \rho_{\text{M}}^3 c_l^2 c_t^4 k^6, \tag{2.51}$$

where $\rho_{\text{M}} c_t^2 = \mu$ and $\rho_{\text{M}} c_l^2 = \lambda + 2\mu$ define the transverse, c_t, and the longitudinal, c_l, sound velocities, is related to the high temperature limit of the free energy of the acoustic phonons,

$$F^0 = -\frac{k_B T}{2}\sum_{\mathbf{k}} \ln\frac{\rho_{\text{M}}^3\,(k_B T)^6}{\hbar^6 \det\zeta}. \tag{2.52}$$

Replacing the sum over $\mathbf{u}$ with an integral over $\mathbf{x}$ and $\mathbf{y}$,[3]

$$\sum_{\dot{\mathbf{u}}}\sum_{\mathbf{u}} \to \left(\frac{1}{\pi\hbar}\right)^6 \prod_{\mathbf{k}}{}' \int_{-\infty}^{+\infty} \mathrm{d}\dot{\mathbf{x}}\,\mathrm{d}\dot{\mathbf{y}}\,\mathrm{d}\mathbf{x}\,\mathrm{d}\mathbf{x} \tag{2.53}$$

3 The normalization factor of $(\pi\hbar)^{-6}$ in Eq. (2.53) was chosen so that $F = F^0$ for $|\eta| = 0$.

and performing Gaussian integration, see, e.g., [53, §7.23.2], we get[14]

$$F(\rho) = F^0 - \frac{\rho_{\text{M}}}{8} \sum_{\mathbf{k}} \left(s_i \zeta_{ij}^{-1} s_j + c_i \zeta_{ij}^{-1} c_j \right),$$

which, after substitution of (2.47) and use of trigonometrical identities, produces,

$$F(g) = \frac{1}{2} \int_{\mathcal{B}} \mathrm{dV} \rho \eta + \frac{1}{2} \int_{\mathcal{B}} \mathrm{dV} \int_{\mathcal{B}} \mathrm{dV}' \rho_{ij}(\mathbf{r}) G_{ijlm} \left(\mathbf{r} - \mathbf{r}' \right) \rho_{lm} \left(\mathbf{r}' \right) + F^0. \tag{2.54}$$

The coupling tensor G is given by

$$G_{ijlm} = -\frac{1}{V} \sum_{\mathbf{k}} \zeta_{im}^{-1} k_j k_l \cos \mathbf{k} \left(\mathbf{r} - \mathbf{r}' \right).$$

As discussed above, the tensor ρ is symmetric:

$$\rho_{ij} = \rho_{ji} = \frac{1}{2} \left(\rho_{ij} + \rho_{ji} \right).$$

As a result, one can profitably employ a symmetrized form of G_{ijlm}:

$$G_{ijlm} = -\frac{1}{4V} \sum_{\mathbf{k}} \left(\zeta_{im}^{-1} k_j k_l + \zeta_{jm}^{-1} k_i k_l + \zeta_{il}^{-1} k_j k_m + \zeta_{jl}^{-1} k_i k_m \right) \cos \mathbf{k} \left(\mathbf{r} - \mathbf{r}' \right). \tag{2.55}$$

Substituting ζ^{-1} from Eq. (2.49) yields:

$$G_{ijml} \left(\mathbf{r} - \mathbf{r}' \right) = -\frac{1}{16 \mu \pi^3} \int_{\mathcal{D}(a)} \mathrm{d}\mathbf{k} \Big[\frac{1}{2k^2} \left(\delta_{im} k_j k_l + \delta_{jm} k_i k_l + \delta_{il} k_j k_m + \delta_{jl} k_i k_m \right) - \frac{1}{1-\nu} \frac{k_i k_j k_m k_l}{k^4} \Big] \cos \mathbf{k} \left(\mathbf{r} - \mathbf{r}' \right), \tag{2.56}$$

where we have replaced the sum over $\mathbf{k}$ by an integral,

$$\frac{1}{V}\sum_{\mathbf{k}\in\mathcal{D}(a)} \to \frac{1}{8\pi^3}\int_{\mathcal{D}(a)} \mathrm{d}\mathbf{k}. \tag{2.57}$$

$\mathcal{D}(a)$ denotes the *inside* of a compact region in $\mathbf{k}$-space; it is the aperiodic analog of the first Brillouin zone for vibrations in periodic crystals.

Apart from the limits of integration in the integral over $\mathbf{k}$, the coupling tensor G is equivalent to the Green tensor describing the strain field produced by a localized source of *stress*, see Appendix A for derivation and discussion. Indeed, G can be rewritten as

$$\begin{aligned} G_{ijml}(\mathbf{r}-\mathbf{r}') = \frac{1}{64\pi^3\mu_0\,(1-\nu_0)}&\left(\delta_{ip}\frac{\partial}{\partial x_j}+\delta_{jp}\frac{\partial}{\partial x_i}\right)\left(\delta_{ql}\frac{\partial}{\partial x_m}+\delta_{qm}\frac{\partial}{\partial x_l}\right)\\ &\times\left(2\,(1-\nu_0)\,\delta_{pq}\frac{\partial^2}{\partial x_s x_s}-\frac{\partial^2}{\partial x_p x_q}\right)\int_{\mathcal{D}(a)}\mathrm{d}\mathbf{k}\frac{e^{i\mathbf{k}(\mathbf{r}-\mathbf{r}')}}{k^4}, \end{aligned} \tag{2.58}$$

which has the same form as Eq. (A.11).

Interaction energy similar to $F(\rho)$ has been applied in the past to study amorphous materials in two types of models: it has been used to describe interaction between the empirical two-level systems (TLS) and to model interaction between substitutes in orientational glasses, see, e.g., [54–56] and [57–59] respectively. Despite these uses, $F(\rho)$ has not been studied in its full complexity. As it stands here, $F(\rho)$ describes the interaction part of the free energy of the short-wavelength deformation field ρ, which has six degrees of freedom at every point of space. Thus the model (2.54) is a Heisenberg model with 6-component spins (of the constant length if the constraint (2.25) is used) and anisotropic long-range couplings.

In the context of orientational glasses, which possess a fully periodic matrix, lattice anisotropy allows one to simplify the model by considering only a trace-less defect strain field:

$$\rho_{ij} \propto n_i n_j - \frac{1}{3}\delta_{ij},$$

where **n** is a *three*-component unit vector characterizing the orientation of a polar substitute. Thus the six degrees of freedom, available to ρ in every point where it is defined, are reduced to just three. Even for the simplified model, Grannan at el.[57] point out that magnets of the type in Eq. (2.54) are frustrated even on periodic lattices. Similar simplification as well as the frustrated interactions characteristic of solid ortho-hydrogen have been known for a long time.[60] The Quadrupole moments of ortho-hydrogen are somewhat more general than the defect type considered in [57] in that they correspond to four degrees of freedom. For the TLS, the simplifications are even more drastic since these systems can be represented by Ising spins, which have only two orientations and the coupling G is projected onto one direction in space (different for each TLS).[55] Here, in contrast, no simplifications are afforded except for fixing the length of 6-vector ψ, Eqs. (2.7) and (2.25),

$$\eta C \eta = \rho C \rho = |\psi|^2 = g^2,$$

which amounts to the assumption of the uniformity of the glass.

Another important feature of the coupling G is the presence of a compact cutoff surface, which limits integration over **k** to $\mathbf{k} \in \mathcal{D}(a)$. The precise geometry of $\mathcal{D}(a)$ is unknown and, by analogy with Brillouin zone in crystal, is expected to be system specific. We will not study this problem here. For reference we provide the result for the simplest case of a sharp cutoff at $k_{micro} = \pi/a$, where, cf. Eq. (2.60),

$$\int_{\mathcal{D}(a)} \mathrm{d}\mathbf{k} \frac{e^{i\mathbf{k}\mathbf{r}}}{k^4} = 2\pi \int_0^{\pi/a} \mathrm{d}k \int_0^{\pi} \mathrm{d}\theta \sin\theta \frac{e^{ikr\cos\theta}}{k^2} = -a\left[\pi^2 \frac{r}{a} + f_{sharp}\left(\frac{\pi r}{a}\right)\right], \tag{2.59}$$

and

$$f_{sharp}(x) = \frac{1}{x}\left(\sin x + x\cos x + x^2\left[\mathrm{Si}(x) - \frac{\pi}{2}\right]\right).$$

In practice, we will use the much simpler

$$\int \mathrm{d}\mathbf{k} \frac{e^{i\mathbf{k}\mathbf{r}}}{k^4} = -\pi^2 r, \tag{2.60}$$

as the spins are at least a distance a apart. The ensuing error is probably comparable to that stemming from not including higher multipole terms in the spin-spin interaction.

Below its Curie temperature, the classical Heisenberg magnet from Eq. (2.54) exhibits many distinct states separated by barriers. These states correspond to distinct configurations in the corresponding quenched liquid. The bead motions during transitions between these distinct states correspond to rotations of the six-component, classical "spins" $\psi(\mathbf{r}_i)$. The relative displacement of two beads, say i and j, during a transition is related to the transition-induced change in the vector $\Big(\psi(\mathbf{r}_i) - \psi(\mathbf{r}_j)\Big)$. The relation, however, is not obvious because of the tensorial nature of the frozen-in stress resulting in vectors being six-component. As in any magnet below its ordering transition, *typical* transitions between distinct metastable states of the spin system from Eq. (2.54) will involve the more spins the lower the temperature. Such bigger cooperative regions are necessary because the density of states for a region of fixed size decreases dramatically for lower energies. Specifically, according to the RFOT theory, the cooperativity size in the present case should increase as $s_c^{-2/3}$,[7] where s_c is the entropy per bead (spin). Consistent with the cooperativity, the individual 6-vectors rotate little relatively to each other so as to minimize local strain, implying the bead-bead bond will distort nearly harmonically most of the time. The overall transition is, nevertheless, strongly anharmonic, as reflected in a high free energy barrier for the reconfiguration. One appropriate progress coordinate is the number of beads that have already moved.[23]

We conclude this section by pointing out that the obtained mapping between activated liquid transport and the dynamics of the 6-spin Hamiltonian from Eq. (2.54) is not exact, of course, but nonetheless, does capture the essential features of the activated-transport regime in liquids. Systematic improvements, such as using a more flexible functional form for the non-linear oscillators,

including higher order multipole terms in the spin-spin interaction etc., are possible, however will likely result in largely quantitative corrections.

2.6 MEAN FIELD BEHAVIOR OF THE 6-SPIN MODEL

According to Eq. (2.56), the Fourier transform of G depends only on the *direction* of $\mathbf{k}$. This allows one to easily extract the long-wavelength limit of the coupling. Formally this is done by applying the limit $\lim_{k\to 0}$ and then replacing the summation over all $\mathbf{k}$ by averaging over all possible orientations of $\mathbf{k}$

$$\lim_{k\to 0}\sum_{\mathbf{k}} = \lim_{k\to 0}\frac{V}{8\pi^3}\int_{\mathcal{D}(a)} d\mathbf{k} \to \frac{V}{4\pi}\int d\Omega_{\mathbf{k}}. \tag{2.61}$$

This procedure amounts to a mean-field limit, because retaining $k \to 0$ values only is equivalent to making the spin-spin interaction $|\mathbf{r}|$-independent. Using $\lim_{k\to 0}\cos\mathbf{k}\,(\mathbf{r}-\mathbf{r}') = 1$ and averaging over directions of $\mathbf{k}$, Eq. (2.56) for the spin-spin coupling reduces to

$$G\,(\mathbf{r}-\mathbf{r}') \to \frac{G^{MF}}{V} = \frac{1}{3\mu V\,(1-\nu)}\,L\left[\frac{1}{2}\,(1-2\nu)\,,\frac{1}{5}\,(4-5\nu)\right], \tag{2.62}$$

where we have used notations defined in Section 2.3. Thus in this limit, the coupling does not depend on the distance, while the integration over $\mathbf{r}$ and $\mathbf{r}'$ reduces now to the volume average of ρ. We get, as a result

$$\frac{F^{MF}(\rho)}{V} = \frac{1}{2}\overline{\rho\eta} + \frac{1}{2}\overline{\rho}\;G^{MF}\;\overline{\rho}, \tag{2.63}$$

where we have dropped the phononic free energy F^0 which does not depend on the state of short-wavelength component and simply shifts the energy reference. The bar denotes the volume average, e.g.,

$$\overline{\rho} = \frac{1}{V}\int dV\rho(\mathbf{r}). \tag{2.64}$$

Now we recall that $\rho = C\eta$ is defined on a lattice and is subject to constraint (2.7), which fixes the density of the frozen-in energy:

$$\eta(\mathbf{r})C\eta(\mathbf{r}) = \eta^{(i)}C\eta^{(i)} = g^2 = \text{Const}, \tag{2.65}$$

where $\eta^{(i)}$ is the lattice approximation for $\eta(\mathbf{r})$, and we have used the following notation for brevity

$$\eta(\mathbf{r}_i) = \eta^{(i)}.$$

We will never use the Einstein summation convention of the superscripts.

It is convenient to represent the constraint in the 6-vector picture in a somewhat distinct from Eq. (2.23):

$$\eta^{(i)} = gC^{-1/2}U\tau^{(i)}, \tag{2.66}$$

where U is an othogonal 6×6 matrix constructed from the eigenvectors of $L[a\,, b]$, see Eq. (2.28), included for future convenience,

$$U = \begin{pmatrix} 1/\sqrt{3} & -1/\sqrt{6} & -1/\sqrt{2} & 0 & 0 & 0 \\ 1/\sqrt{3} & -1/\sqrt{6} & 1/\sqrt{2} & 0 & 0 & 0 \\ 1/\sqrt{3} & \sqrt{2}/\sqrt{3} & 0 & 0 & 0 & 0 \\ 0 & 0 & 0 & 1 & 0 & 0 \\ 0 & 0 & 0 & 0 & 1 & 0 \\ 0 & 0 & 0 & 0 & 0 & 1 \end{pmatrix} \qquad \text{((2.28) revisited)}$$

Substitution into (2.65) reduces the constraint to the condition

$$|\tau^{(i)}| = 1. \tag{2.67}$$

Thus, all the structural states allowed by the constraint can be mapped onto the orientations of the *unit* 6-vector $\tau^{(i)}$. Using the stress-strain relation $\rho = C\eta$, together with (2.66), we can reduce (2.63) to

$$\frac{F^{MF}}{V} = \frac{1}{2}g^2\left(1 + \frac{1}{N^2}\left[\sum_i \tau^{(i)}\right] U^\top C^{1/2} G^{MF} C^{1/2} U \left[\sum_j \tau^{(i)}\right]\right). \tag{2.68}$$

The tensor product can be calculated using the approach outlined in Section 2.3,

$$C^{1/2} G^{MF} C^{1/2} = C G^{MF} = -\frac{1}{3(1-\nu)} L\left[1+\nu\,, \frac{2}{5}(4-5\nu)\right]. \tag{2.69}$$

This tensor is well known in the theory of elasticity. It is a particular realization of the Eshelby tensor, which is related to the volume average of the fourth-order Green tensor,

$$S = -\int_{\mathcal{I}} dV' G^A(\mathbf{r}-\mathbf{r}')\, C^{-1}, \qquad \text{((B.4) revisited)}$$

see Appendix B for the derivation and discussion. For $\mathbf{r} \in \mathcal{I}$ and ellipsoidal $\mathcal{I}$, the Eshelby tensor S does not depend on $\mathbf{r}$. If $\mathcal{I}$ is a sphere, the tensor S has a particularly simple form:[44]

$$S = \frac{1}{3(1-\nu)} L\left[1+\nu\,, \frac{2}{5}(4-5\nu)\right], \tag{2.70}$$

which is identical to Eq. (2.69).

After establishing the physical meaning of G^{MF}, we can better appreciate why Eq. (2.61) leads to a MF approximation. Employing the latter equation is equivalent to replacing the interaction term $F(\rho)$ by the product of the volume averages of its constituents:

$$\int dV \int dV' \rho(\mathbf{r}) G(\mathbf{r}-\mathbf{r}')\, \rho(\mathbf{r}') \approx V^3 \overline{\rho}\, \overline{G}\, \overline{\rho},$$

which is equivalent to the assumption that ρ on different sites interact via a $\mathbf{r}$-independent, mean field. Note that in the above equation we have dropped the arguments of G writing simply $\overline{\mathrm{G}}$ for the volume average. This is possible, if the averaging volume is an ellipsoid,[44] leading to

$$\int_{\mathcal{I}} \mathrm{dV} \mathrm{G}^{\mathrm{A}}(\mathbf{r}-\mathbf{r}') = \int_{\mathcal{I}} \mathrm{dV}' \mathrm{G}^{\mathrm{A}}(\mathbf{r}-\mathbf{r}') = -\mathrm{S}\mathrm{C}^{-1}, \tag{2.71}$$

where, we remind, G is computed using Eq. (2.60), $\mathrm{G} \approx \mathrm{G}^{\mathrm{A}}$. Note that the tensors S and C commute only if $\mathcal{I}$ is a sphere.

Now, let us get back to Eq. (2.68) for F^{MF}. It can be written as

$$\frac{F^{\mathrm{MF}}}{V} = \frac{1}{2} g^2 + \frac{1}{N} H^{\mathrm{MF}}, \tag{2.72}$$

where we have labeled the part that governs the frozen-in stress τ by H^{MF}. Using Eqs. (2.69) and (2.27) one can write

$$H^{\mathrm{MF}} = -\frac{g^2}{2N} \sum_{i,j} \tau^{(i)} \mathrm{Y}\, \tau^{(j)}, \tag{2.73}$$

where Y is a *diagonal* matrix composed of the eigenvalues of S,

$$\mathrm{Y} = \mathrm{U}^{\top} \mathrm{S} \mathrm{U} = \frac{1}{3\,(1-\nu)} \mathrm{D}\left[1+\nu\,, \frac{2}{5}\,(4-5\nu)\right], \tag{2.74}$$

cf. Eq. (2.69).

Note that according to the definition in Eq. (2.66), the trace of η is give by

$$\mathrm{Tr}\ \eta = \frac{g}{\sqrt{\varkappa}} \tau_1, \tag{2.75}$$

where

$$\varkappa = \frac{2\mu}{3} \frac{1+\nu}{1-2\nu} \tag{2.76}$$

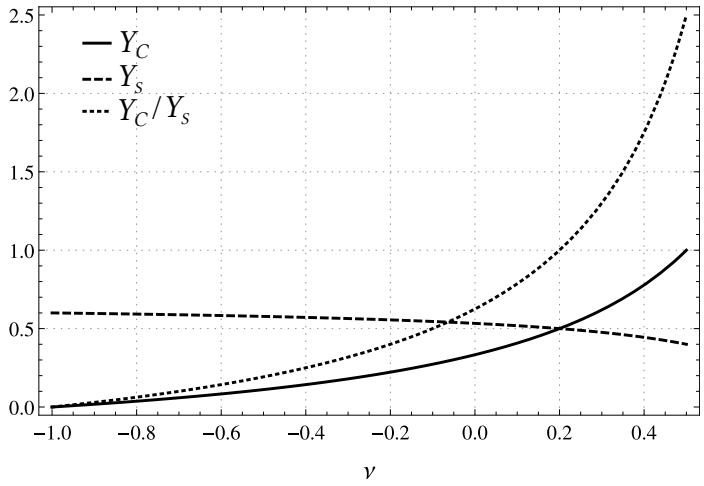

Figure 5.: Eigenvalues of the Eshelby matrix S for a sphere, which play the role of the coupling parameters in H^{MF}. The ratio Y_c/Y_s is the measure of anisotropy in the model. Remarkably, the isotropic case $Y_c = Y_s$, at $\nu = \frac{1}{5}$ (corresponding to the ratio of sound velocities $c_t^2/c_l^2 = \frac{3}{8}$), is within experimentally accessible range.

is the bulk modulus. Thus the first component of τ reflects local density variations of the frozen-in stress, while the rest of the components describe isochoric deformation and thus correspond to the shear portion of the frozen-in stress. In view of the physical meaning of the τ components, we label the eigenvalues of the matrix S as,

$$\begin{aligned} Y_c &= \frac{1+\nu}{3\,(1-\nu)}, && \text{compression/dilation,} \\ Y_s &= \frac{2\,(4-5\nu)}{15\,(1-\nu)}, && \text{pure shear,} \end{aligned} \tag{2.77}$$

and write the Hamiltonian in the following, simplified form

$$\frac{2N}{g^2} H^{\text{MF}} = -Y_c \left(\sum_i \tau^{(\text{i})}{}_1 \right)^2 - Y_s \sum_{\alpha=2}^{6} \left(\sum_i \tau_\alpha^{(i)} \right)^2 . \tag{2.78}$$

Since both Y_c and Y_s are positive, see Fig. 5, the model (2.78) corresponds to a ferromagnet. The

numerical value of the Y_c/Y_s ratio,

$$\frac{Y_c}{Y_s} = \frac{5}{2}\,\frac{1+\nu}{4-5\nu} = \frac{5}{2}\,\frac{\varkappa}{\varkappa+2\mu} = \frac{5}{2}\,\frac{3c_l^2-4c_t^2}{3c_l^2+2c_t^2}, \tag{2.79}$$

varies between 0.88 and 1.6 for nonmetallic glasses surveyed by Novikov and Sokolov.[61, 62] Bigger values of the Y_c/Y_s ratio correspond to a greater Poisson ratio and smaller $\mu/\varkappa$ ratio, i.e. to a lower shear modulus relative to the bulk modulus. We thus observe that the MF Heisenberg model (2.78) has anisotropic couplings, the anisotropy directly related to the Poisson ratio of the material. Remarkably, the purely isotropic case $Y_c = Y_s$, corresponding to

$$\nu = \tfrac{1}{5}, \qquad c_t^2/c_l^2 = \tfrac{3}{8},$$

falls within the experimental range, the implications to be discussed in the last section of this chapter.

The MF Hamiltonian (2.78) can be solved in a standard fashion, using a Hubbard-Stratonovich transformation. Since all the structural state available to the system are mapped onto the orientations of $\tau^{(i)}$, the partition function can be found, according to

$$Z^{\text{MF}} = \int \left\{\prod_i \mathrm{d}\Omega_\tau^{(i)}\right\} e^{-\beta F^{\text{MF}}} = e^{-\beta\frac{Vg^2}{2}} \int \left\{\prod_i \mathrm{d}\Omega_\tau^{(i)}\right\} e^{-\beta a^3 H^{\text{MF}}}, \tag{2.80}$$

where we have used $V = a^3N$. The Habbard-Stratonovich transformation in the particular case of Eq. (2.80) can be written as

$$e^{\frac{\beta g^2}{2N}\sum_{\alpha=1}^{6}\chi_\alpha\left(\sum_i \tau_\alpha^{(i)}\right)^2} = \left(\frac{N}{2\pi g^2\beta}\right)^3 \frac{1}{\sqrt{\det \mathrm{Y}}} \prod_{\alpha=1}^{6} \int_{-\infty}^{\infty} d\xi_\alpha e^{-\frac{N}{2g^2\beta\zeta_\alpha}\xi_\alpha^2 + \xi_\alpha\sum_i \tau_\alpha^{(i)}}. \tag{2.81}$$

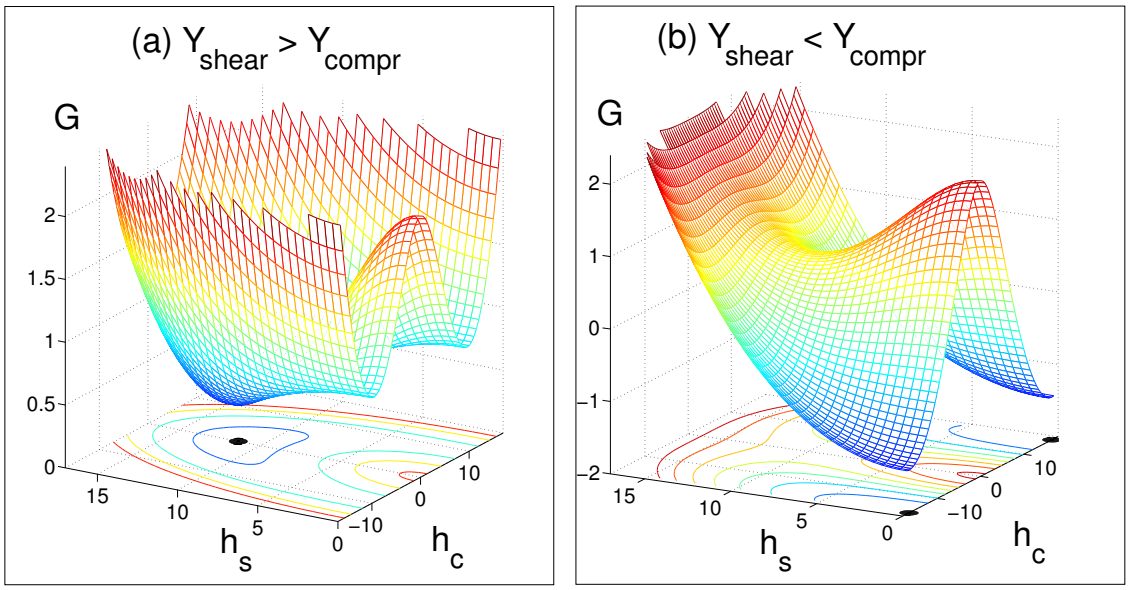

Figure 6.: Free energy from Eq. (2.83) corresponding to the elastic constants of (a) silica ($Y_c/Y_s \simeq 0.88$) and (b) salol ($Y_c/Y_s = 1.5$) Cases (a) and (b) exhibit frozen-in shear and uniform compression/dilation respectively. Solid circles at bottom plane denote the locations of minima.

where we define a 6-vector χ composed of the diagonal entries of the matrix Y:

$$\chi_\alpha = Y_{\alpha\alpha},$$

and no summation convention is implied in the last equation. After substituting Eq. (2.81) into Z^{MF}, the angular average can be easily performed.[48] Upon the angular averaging, the integration over ξ can be accomplished asymptotically exactly by the method of steepest descent. In the leading order in N, the corresponding free energy equals to

$$\frac{F^{\text{MF}}}{N} = \frac{a^3 g^2}{2} + G_{min}, \tag{2.82}$$

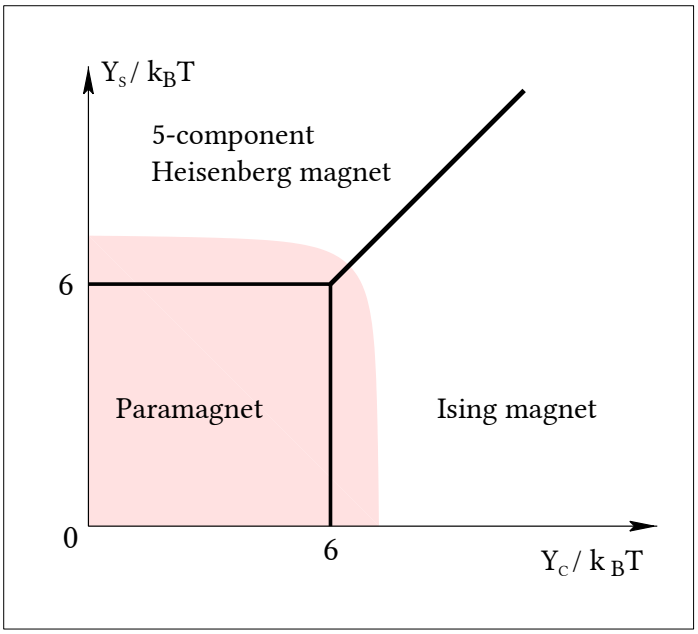

Figure 7.: The phase diagram corresponding to the mean-field Hamiltonian (2.78). The shaded region schematically denotes the regime where the mapping between liquid dynamics and the spin model does not apply. Labels "Ising magnet" and "Heisenberg magnet" indicate ordering of the compression and shear components in Eq. (2.78) in the respective regions of the diagram.

where G_{min} is the minimum value of the following function, c.f. [48, Eq. (2.3)],

$$\frac{G}{N} = \frac{h_c^2}{2\beta Y_c} + \frac{h_s^2}{2\beta Y_s} - \ln \frac{I_2(\sqrt{h_c^2 + h_s^2})}{h_c^2 + h_s^2}, \tag{2.83}$$

with respect to the variables $h_c = \xi_1$ and $h_s = (\sum_{\alpha=2}^{6} \xi_\alpha^2)^{1/2}$. The first quantity, h_c, gives the effective field on each spin in the direction of uniform compression/dilation; it can be of either sign. The second one, h_s is the *magnitude* of the total field in the direction of pure shear and can be only non-negative. The free energy from Eq. (2.83) is graphed in Fig. 6 for two distinct values of anisotropy, at a temperature below the Curie temperature.

The Curie temperature itself, according to Eq. (2.83), is determined by the bigger of the two coupling constants:

$$k_B T_{Curie}^{\text{MF}} = \frac{1}{6} \max\left[Y_c, Y_s\right]. \tag{2.84}$$

We remind the reader that the activated regime corresponds to the ordered state of the magnet. If $Y_c > Y_s$, the ordering is along the compression/dilation component of the local displacement, which corresponds to the first sum in Eq. (2.78), see Fig. 6. Note the depths of the two minima are equal, implying there is no net volume change during the ordering transition. From the spin perspective, this state is essentially an ordered Ising ferromagnet. Conversely, if $Y_c < Y_s$, it is the shear component that becomes ordered; this component corresponds to the second sum in Eq. (2.78). The frozen-in shear state is an ordered 5-component Heisenberg ferromagnet, from the spin viewpoint. We summarize these notions graphically in the phase diagram shown in Fig. 7.

We may further connect the MF parameters Y_s and Y_c to the material constants by enforcing the aforementioned notion that the large g asymptote of the function $F(g)$ be logarithmic in the large g limit, i.e. when the vector length or spin-spin coupling is large. According to Eqs. (2.33) and (2.83), the quadratic term in g from Eq. (2.33) will cancel out at large g, if

$$\max\left[Y_c, Y_s\right] = g^2 a^3. \tag{2.85}$$

As a result,

$$g^2 = \frac{6 k_B T_{Curie}^{\mathrm{MF}}}{a^3}. \tag{2.86}$$

After comparing this equation with Eq. (2.36), we conclude that the MF Curie temperature of our magnet is significantly higher than the temperature at which the aperiodic stress pattern sets in, since the actual value of g in the metastable phase is significantly greater than the critical value from Eq. (2.36), see Fig. 8. Hence, at least in the MF limit, the proposed mapping of activated transport onto an ordered spin model is internally consistent.

We further use Eq. (2.85) to compute the mean-field expression for $F(g)$, by numerically minimizing the free energy from Eq. (2.83). The result is shown with the dash-dotted line in Fig. 8. To compute the full free energy of the solid $F_a(g)$, from Eq. (2.8), we must make a specific assumption on the penalty $F_{ex}(g)$ for dilating the sample. For the sake of argument, we have used a quadratic

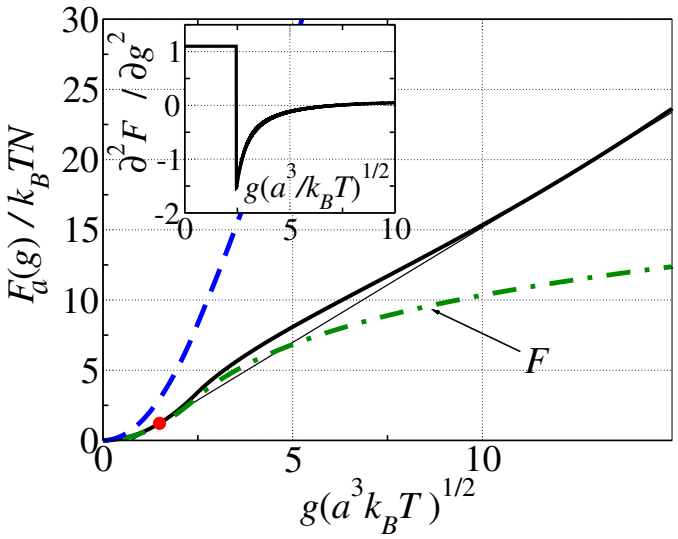

Figure 8.: The dashed-dotted line shows the mean-field expression for the $F(g)$ function. The thick solid line shows the full free energy from Eq. (2.8), with a specific choice of the function $F_{ex}(g)/N = c(g^2a^3)$, where the coefficient $c = 0.05$. The thin solid line is the common tangent of the two portions on the $F_a(g)$ that correspond to the mechanically stable reference state and the aperiodic metastable state. The dashed line shows the curve with the largest value of this coefficient ($c = \frac{5}{3}$), at which the $F_a(g)$ curve still exhibits a concave down portion. In the inset, we plot the second derivative of the mean-field $F(g)$. The discontinuity is at $\beta g^2 a^3 = 6$, c.f. Eq. (2.86).

function $F_{ex}(g) = cNg^2a^3$. A specific value $c = 0.05$ was chosen so that the resulting barrier between the two phases is about k_BT, since it is known that the one-particle barrier for surface melting is about k_BT.[22]

The mean-field solution supports the asymptotic analysis from Section 2.4 in that the fully mechanically stable solid is indeed the lowest free energy state; whereas the aperiodic state, though significantly higher in free energy, is metastable owing to the surface tension between the two phases.

2.7 SUMMARY, DISCUSSION, CONSEQUENCES FOR CORRELATION BETWEEN THE FRAGILITY COEFFICIENT AND THE POISSON RATIO

We have mapped the liquid activated-transport regime onto the dynamics of a spin model on a *fixed* lattice. The long-lived aperiodic arrangements, which are characteristic of the activated regime, correspond to aperiodic spin configurations below the Curie point of the spin system. The presence of non-zero shear resistance in the long-lived structures is reflected in the spins having six components, which correspond to the six independent entries of the local deformation tensor. Individual spins corresponds to a rigid, weakly interacting molecular units (or "beads") of the RFOT theory. The size of the bead is set unambiguously as the length scale of the inhomogeneity of frozen-in stress distribution in the activated regime. The length of the vectors is determined self-consistently as the value of the order parameter for the periodic-to-aperiodic crystal transition. The mutual angles between spins change modestly during the cooperative reconfigurations, implying individual bonds are deformed nearly harmonically most of the time. The anharmonicity of the reconfigurations is reflected in a high nucleation barrier in the free energy profile of the transition, the progress coordinate being the number of beads that have already switched their positions to their value in the new arrangement. The present approach exhibits clear parallels with earlier, self-consistent phonon theories of aperiodic crystals,[31, 63] which considered the uniform liquid state as the reference state and have demonstrated that the uniform liquid can cross-over to an aperiodic-crystal state, accompanied by a discontinuous change of an order parameter corresponding to the bead localization length. In contrast, here we construct the aperiodic crystal using a fully mechanically stable state as the starting point, thus allowing for a straightforward treatment of local, high-frequency shear resistance. We have also explicitly demonstrated that aperiodic crystals exhibit multiply degenerate states whose mutual interconversions can be mapped onto the dynamics of a long-range, 6-spin model with anisotropic interactions.

The present microscopic picture has implications for the temperature dependence of the activated barriers in supercooled melts that we can begin to discuss already at the MF level. In the allowed part of the phase diagram in Fig.7, consider a transition from the $Y_c < Y_s$ sector to the $Y_c > Y_s$ sector. As already mentioned, this transition would correspond to ordering of an Ising-like assembly of spins and vice verse for the 5-component Heisenberg spins. To avoid confusion, we emphasize that this Ising-like ordering takes place along one component of randomly oriented, *six*-component vectors. Now, according to accurate calculations,[64] the heat capacity jump upon ordering in the classical Heisenberg model tends to increase with lowering the dimensionality of the spins and reaches its largest value in the Ising model. This implies that the right-hand side (rhs) part of the phase diagram should generically exhibit a higher specific heat. In view of the RFOT-derived connection between the fragility index and the heat capacity jump, i.e. the mentioned $m \simeq 34.7\Delta c_p$ relation, we may expect that substances with a larger Y_c/Y_s ratio will generically be more fragile, but under several, rather restrictive circumstances, as we discuss next.

First, we reiterate the present approach is a minimalist way to explicitly account for the interactions that give rise to (high frequency) shear resistance in supercooled liquids. Already in this minimal model, the entropy and heat capacity per bead depend on the bead size a, which is, formally, the ultraviolet cutoff in the theory. In addition to the purely volumetric affect—one vector occupies a volume a^3—the bead size will affect the precise, self-consistently determined value of the order parameter g in the glass phase. Further, the isotropic assumption for local elastic response, from Eq. (2.16), is an approximation. Contributions other than purely elastic terms Eq. (2.9) will be generally present as well. One source of such contribution is the reconfiguration-induced electric dipole moment. Earlier estimates[65] suggest that even though the local polarization resulting from bead movements contributes only about a percent to local elastic constants, the resulting elemental electric dipoles interact comparably strongly to the elastic dipoles of the type we have considered. This effect should be especially significant in ionic glasses.[28] A careful treatment of polymeric materials, on the other hand, should include the effects of chain rigidity and other types of local

anisotropy that could not be accounted for by only two elastic constants and the bead size a, which are the parameters of our ansatz. Novikov and Sokolov have argued electronic contributions must be considered in metallic glasses.[66]

According to Fig. 7, we should expect that actual substances will exhibit a continuous range of local stress distributions and heat capacities. Indeed, to distinct points on the phase diagram in Fig. 7, there correspond very different values of the heat capacity. Furthermore, the heat capacity of an anisotropic Heisenberg model on a periodic lattice should exhibit a nonmonotonic behavior as a function of anisotropy, namely a spike at a transition that would occur at $Y_c = Y_s$ in the mean-field limit. The case of $Y_c = Y_s$ corresponds to the following value of the ratio of the longitudinal and transverse velocities: $c_l/c_t \simeq 1.63$. This is roughly consistent with a very broad range of fragilities observed for substances from a relatively narrow range of the c_l/c_t ratio centered at 1.75 or so.[66, 67] We point out that the correlation between the Poisson ratio and the fragility has been a subject of debate for some time.[61, 62, 66–69]

Our results suggest that a correlation between the fragility and the Poisson ratio might in fact be expected for nonmetallic substances that are far from the transition region $Y_c = Y_s$. Yet for substances near the "critical region" $Y_c = Y_s$, little correlation is expected. Note that the view of the activated regime in a *fragile* substance as a random Ising model below symmetry breaking is consistent with recent results of Stevenson at el.[70] who have mapped the localization transition in fiducial liquid structures of a Lennard-Jones mixture onto a replica-symmetry breaking transition in a random Ising model.

Regardless of the detailed value of the heat capacity, our results indicate that supercooled liquids exhibit local stress distribution ranging from frozen-in compression to frozen-in shear. Furthermore, the present findings that the activated liquid regime arises self-consistently from a mechanically stable reference state merge nicely with the self-consistent phonon view of the emergence of the aperiodic crystal state from the uniform *liquid*.[31, 63] This notion suggests that a unified, quantitative treatment of the liquid, aperiodic-crystal, and periodic-crystal regimes is in sight. We

conclude by reiterating that despite system-specific variations in direct interactions, accounted for, semi-empirically, in the variation of the elastic constants in Fig. 7, the underlying mechanism of activated transport in non-polymeric liquids is system independent, consistent with the conclusions of the RFOT theory.

3

SELF-CONSISTENT ELASTICITY THEORY OF METASTABLE SOLIDS

3.1 EFFECTIVE ELASTIC MODULI OF METASTABLE CONTINUUM

The elastic moduli of a glassy system are determined by the dynamics of the frozen-in stress distribution. The microscopic details of this dependence can be very complex.[71] The long-wavelength limit of the elastic response is, nevertheless, well defined. Similar to crystals, the linear elasticity approximation is valid for sufficiently small, smooth deformations. In contrast with crystals, however, a deformation field in an amorphous material subject to an external load contains an additional contribution, i.e., deformation due to the frozen-in stress "polarized" by the load. This is completely analogous to how the permanent dipoles comprising a dielectric determine the response of the latter to external electric field. This part of the response is a result of the multitude of structural states available to amorphous materials: states which favor the deformation produced by an external load will be visited more often; thereby the volume average of the frozen-in stress becomes different from zero on time scales shorter than the structural relaxation time. In this Chapter, we will quantitatively account for this effect providing the linear response type description of the elasticity of amorphous materials.

3.1.1 *Definition of the effective elastic moduli*

We begin by considering a body $\mathcal{B}$ characterized by an intrinsic elastic moduli tensor C_0, and also subject to a frozen-in stress field distribution $\rho(\mathbf{r})$, see Fig. 9. C_0 characterizes the material if

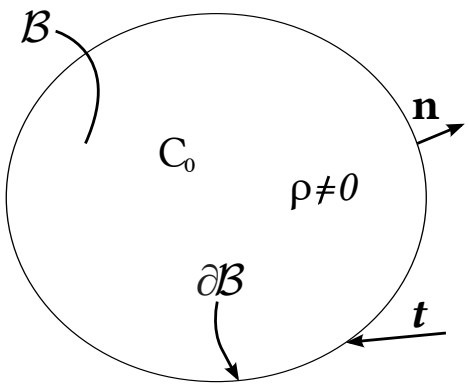

Figure 9.: A cartoon illustrating the problem considered in Section 3.1.1: a homogeneous body $\mathcal{B}$ with elastic constants given by the fourth-order tensor C_0 is subject to an external load in the form of a traction force $\mathbf{t}$ applied to the boundary $\partial\mathcal{B}$ of the body. Unit vector $\mathbf{n}$ is normal to $\partial\mathcal{B}$. The body also contains a distribution of frozen-in stress given by the tensor field $\rho(\mathbf{r})$.

the activated dynamics are completely frozen and the lattice is stable. If, on the other hand, the activated dynamics are present, the elastic moduli measured in a macroscopic experiment will be different from C_0 owing to the polarization of ρ discussed above. In the simplest experimental situation, $\mathcal{B}$ is deformed by a traction force applied to its surface. For small enough deformations, the corresponding strain will be related to the traction, or the stress produced by it, by Hooke's law, which allows one to find the effective, apparent elastic moduli tensor labeled hereafter by C. Note, that C_0 is inaccessible in experiment since one can only measures the combined response of the lattice and the frozen-in stress.

If an external traction force $\mathbf{t}(\mathbf{r})$ is applied to the boundary $\partial\mathcal{B}$ of $\mathcal{B}$, the resulting deformation field, $\mathbf{u}$, is a solution of the boundary value problem:

$$\begin{cases} \left(\sigma_{ij} + \rho_{ij}\right)_{,j} = 0, \\ \sigma_{ij} n_j \Big|_{\partial\mathcal{B}} = t_i, \end{cases} \tag{3.1}$$

supplemented by the constitutive relation (the Hooke law)

$$\sigma = C_0 \varepsilon. \tag{3.2}$$

Here σ (ε) is the elastic stress (strain) inside $\mathcal{B}$,

$$\varepsilon_{ij} = \frac{1}{2}\left(\frac{\partial u_i}{\partial x_j} + \frac{\partial u_j}{\partial x_i}\right) = \frac{1}{2}\left(u_{i,j} + u_{j,i}\right), \tag{3.3}$$

and $\mathbf{n}$ is the external unit normal to $\partial\mathcal{B}$. Equation (3.1) is essentially Newton's 3rd law, the top and the bottom entry corresponding to bulk and surface response respectively. The elastic stress σ is a sum of two components:

$$\sigma = \sigma^{\mathrm{T}} + \sigma^{\mathrm{S}}, \tag{3.4}$$

where the stress σ^{T} produced by the traction obeys

$$\begin{cases} \sigma^{\mathrm{T}}_{ij,j} = 0, \\ \sigma^{\mathrm{T}}_{ij} n_j \Big|_{\partial\mathcal{B}} = t_i, \end{cases} \tag{3.5}$$

while the stress σ^{S} produced by the source field ρ satisfies

$$\begin{cases} \left(\sigma^{\mathrm{S}}_{ij} + \rho_{ij}\right)_{,j} = 0, \\ \sigma^{\mathrm{S}}_{ij} n_j \Big|_{\partial\mathcal{B}} = 0, \end{cases} \tag{3.6}$$

The latter equations follow from Eqs. (3.1) and (3.5). The elastic strain ε can be similarly written as a sum of two components,

$$\varepsilon = \varepsilon^{\mathrm{T}} + \varepsilon^{\mathrm{S}}, \tag{3.7}$$

where the strain produced by the traction force $\mathbf{t}$ and the frozen-in stress ρ are defined as

$$\sigma^{\mathrm{T}} = \mathrm{C}_0 \varepsilon^{\mathrm{T}} \qquad \text{and} \qquad \sigma^{\mathrm{S}} = \mathrm{C}_0 \varepsilon^{\mathrm{S}} \tag{3.8}$$

respectively. We also assume that no frozen-in sources of stress lie at the boundary $\partial\mathcal{B}$ of the sample,

$$\rho\Big|_{\partial\mathcal{B}} = 0, \tag{3.9}$$

and limit consideration to symmetric sources, as before:

$$\rho_{ij} = \rho_{ji}. \tag{3.10}$$

The choice of the boundary condition is the same as the one conventionally applied when studying defects in solids.[72] It entails an important relation between volume average of σ^{S} and ρ,

$$\int_{\mathcal{B}} \sigma^{\mathrm{S}}\, \mathrm{dV} = -\int_{\mathcal{B}} \rho\, \mathrm{dV}, \tag{3.11}$$

which is straightforward to show by writing $\sigma^{\mathrm{S}}_{ij} = \sigma^{\mathrm{S}}_{ik} x_{k,j}$ and using the Gauss theorem together with Eq. (3.6).[73]

We define the effective elastic moduli C of $\mathcal{B}$ as a fourth-order tensor connecting the volume average of the *total* stress in $\mathcal{B}$ with the volume average of the total elastic strain:

$$\int_{\mathcal{B}} (\sigma + \rho)\, \mathrm{dV} = \mathrm{C} \int_{\mathcal{B}} \varepsilon\, \mathrm{dV}. \tag{3.12}$$

This definition is equivalent to the relation

$$\int_{\mathcal{B}} \sigma^{\mathrm{T}} \mathrm{dV} = \mathrm{C} \int_{\mathcal{B}} \varepsilon\, \mathrm{dV}, \tag{3.13}$$

which is easy to see using Eqs.(3.4) and (3.11). The volume average of ε in the rhs can be expressed in terms of ε^{T} and ρ. Using Eqs. (3.7), (3.11), (3.4), and (3.8) we get

$$\int_{\mathcal{B}} \varepsilon\, \mathrm{dV} = \int_{\mathcal{B}} \left(\varepsilon^{\mathrm{T}} - \mathrm{C}_0^{-1}\rho\right) \mathrm{dV}. \tag{3.14}$$

Now, consider an experiment in which ε^{T} is uniform. We can thus rewrite (3.13) as

$$\mathrm{C}_0\varepsilon^{\mathrm{T}} = \mathrm{C}\varepsilon^{\mathrm{T}} - \frac{1}{V}\mathrm{C}\mathrm{C}_0^{-1}\int_{\mathcal{B}} \rho \, \mathrm{dV}, \tag{3.15}$$

where V denotes the volume of $\mathcal{B}$ and we used Eqs. (3.8) and (3.14). Since the value of C can not depend on the configuration of the load and the shape of $\mathcal{B}$ used in the macroscopic experiment, below we consider only a homogeneous ε^{T}, treating Eq. (3.15) as a general definition of the effective elastic moduli. The field ρ undergoes activated dynamics. In equilibrium, Eq. (3.15) becomes

$$\mathrm{C}_0\varepsilon^{\mathrm{T}} = \mathrm{C}\varepsilon^{\mathrm{T}} - \mathrm{C}\mathrm{C}_0^{-1}\langle\tilde{\rho}\rangle, \tag{3.16}$$

where hereafter we use tildes to signify averaging over the volume of $\mathcal{B}$,

$$\tilde{\rho} = \frac{1}{V}\int_{\mathcal{B}} \rho \, \mathrm{dV}. \tag{3.17}$$

Note, that ε^{T} equilibrates on the time scale of the activated reconfigurations, which is much longer than the vibrational (phononic) equilibration.

We expect $\langle\rho\rangle = 0$ in an equilibrated amorphous solid in the absence of external load, $\varepsilon^{\mathrm{T}} = 0$, that the bonds between select atoms are permanent, which does not apply to equilibrium liquids. Since our approach is limited to linear response, it will suffice to consider the first two terms in the expansion

$$\langle\tilde{\rho}_{ij}\rangle \approx \langle\tilde{\rho}_{ij}\rangle\Big|_{\varepsilon^{\mathrm{T}}=0} + \frac{\partial\langle\tilde{\rho}_{ij}\rangle}{\partial\varepsilon^{\mathrm{T}}_{kl}}\bigg|_{\varepsilon^{\mathrm{T}}=0} \varepsilon^{\mathrm{T}}_{kl}, \tag{3.18}$$

which results, together with Eq. (3.15), in a linear response-type relation connecting the effective and the "bare" elastic moduli of $\mathcal{B}$:

$$(\mathrm{C}-\mathrm{C}_0)_{ijkl} = \left(\mathrm{C}\,\mathrm{C}_0^{-1}\right)_{ijmn} \frac{\partial\langle\tilde{\rho}_{mn}\rangle}{\partial\varepsilon^{\mathrm{T}}_{kl}}\bigg|_{\varepsilon^{\mathrm{T}}=0}. \tag{3.19}$$

This relation is valid for any symmetry of C_0. In the following, we concentrate on the simplest, albeit the most relevant for amorphous materials, case of an isotropic solid. We will label "bare" elastic moduli of $\mathcal{B}$ corresponding to C_0 as μ_0, ν_0, and $\varkappa_0$ for the shear modulus, Poisson ratio, and bulk modulus respectively. We expect C to be isotropic as well, since, by definition, amorphous materials are isotropic in the long-wavelength limit. Then, for Eq. (3.19) to be consistent, the derivative $\partial\langle\tilde{\rho}_{ij}\rangle/\partial\varepsilon^{\mathrm{T}}_{kl}$ must be an isotropic tensor, and, as we will show in Section 2.3, the tensor equation (3.19) is equivalent to two scalar equations. If the derivative is a known function of C_0, one can thus compute the tensor C and the corresponding effective moduli μ, $\varkappa$, and ν. Below we will show how the derivative $\partial\langle\tilde{\rho}\rangle/\partial\varepsilon^{\mathrm{T}}$ can be calculated in a near-MF approximation equivalent to Onsager's cavity construction. The approximation is higher order that the lowest order MF because it partially accounts for the "reaction field", i.e., the self-interaction of the spin mediated by its environment. Our task is complicated by the tensor nature of the problem. Fortunately, for isotropic tensors, the necessary algebra can be much simplified by using the system of notations developed by L. J. Walpole,[44] which was reviewed earlier in Section 2.3.

3.1.2 *The trivial fixed points of Eq.* (3.16)

We end this Section by noting that Eq. (3.15), which connects bare and renormalized elastic constants, has two trivial fixed points, in which the Poisson ratio does not renormalize. Indeed, consider the case of $\nu_0 = \frac{1}{2}$, which corresponds to a liquid since $\mu_0 = 0$ by Eq. (2.18). Then, $\varkappa_0 = \lambda_0$ leading to

$$\lim_{\nu_0 \to \frac{1}{2}} C_0 = L[3\varkappa_0\,, 0] = 3\varkappa_0 J.$$

As noted before, Eq. (2.15), the tensor J extracts the isotropic part when acting on any second-order tensor. Thus, multiplying (3.15) by C_0 and using the commutative property of isotropic tensors, one can write

$$\mathrm{C}_0\,(\mathrm{C}-\mathrm{C}_0)\,\boldsymbol{\varepsilon}^{\mathrm{T}} = \mathrm{C}\,\langle\tilde{\boldsymbol{\rho}}\rangle, \tag{3.20}$$

which becomes, for $\nu_0 = \frac{1}{2}$:

$$3\varkappa_0\,(\varkappa-\varkappa_0)\,\varepsilon^{\mathrm{T}}_{kk}\delta_{ij} = C_{ijkl}\,\langle\rho_{kl}\rangle. \tag{3.21}$$

Since the rhs is diagonal, the left-hand side (lhs) must be diagonal as well, leading to

$$\mathrm{C}\propto\mathrm{J} \qquad \text{for} \qquad \nu_0 = \frac{1}{2},$$

$\mu = \mu_0 = 0$ and $\nu = \nu_0 = \frac{1}{2}$. Equation (3.21) formally allows for $\varkappa \neq \varkappa_0$.

Similarly, consider a body with an infinite compressibility but non-zero shear resistance: $\varkappa_0 = 0$ while $\mu_0 \neq 0$ thus leading to $\nu_0 = -1$. One obtains, as a result,

$$\lim_{\nu_0\to-1}\mathrm{C}_0 = \mathrm{L}[0\,,2\mu_0] = 2\mu_0\mathrm{K}.$$

By Eq. (3.20),

$$4\mu_0\,(\mu-\mu_0)\,{}'\boldsymbol{\varepsilon}^{\mathrm{T}} = \mathrm{C}\,\langle\tilde{\boldsymbol{\rho}}\rangle. \tag{3.22}$$

Since the rhs is purely deviatoric, i.e. has zero trace, the equation can be satisfied if $\mathrm{C}\propto\mathrm{K}$ only, yielding $\nu = \nu_0 = -1$ and $\varkappa = \varkappa_0 = 0$. At the same time $\mu \neq \mu_0$ is perfectly allowed by Eq. (3.22).

3.2 CAVITY FIELD METHOD FOR THE ELASTIC RESPONSE OF SUPERCOOLED LIQUIDS

In this Section, we determine the effective elastic properties in an aperiodic solid in the presence of activated dynamics. Within the linear response approach, developed in the previous Section, we

must find the derivative of the average frozen-in stress as a function of the deformation due to the external load,

$$\left.\frac{\partial\langle\tilde{\rho}_{ij}\rangle}{\partial\varepsilon^{\mathrm{T}}_{kl}}\right|_{\varepsilon^{\mathrm{T}}=0}. \tag{3.23}$$

As we show below, this derivative can be expressed via the second cumulant of the stress distribution much the same way the compressibility reflects the magnitude of volume fluctuations at constant pressure. The calculation requires a specific model for the dynamics of ρ. In the preceding Chapter, we put forth a minimal ansatz for the stress distribution in equilibrated amorphous systems and showed that the activated dynamics in supercooled liquids can be mapped onto a classical Heisenberg model with six-component spins and long-range anisotropic coupling. The Hamiltonian defining the stress field ρ in the aperiodic phase can be written as follows,[14] cf. Eq. (2.54),

$$H_0 = \frac{1}{2}\int_{\mathcal{B}} \mathrm{dV}\rho \mathrm{C}_0^{-1}\rho + \frac{1}{2}\int_{\mathcal{B}}\mathrm{dV}\int_{\mathcal{B}}\mathrm{dV}'\rho_{ij}(\mathbf{r})\,G_{ijlm}(\mathbf{r}-\mathbf{r}')\,\rho_{lm}(\mathbf{r}'), \tag{3.24}$$

where the naught in H_0 refers to the absence of external load (i.e. zero field). The coupling tensor G is given by

$$\begin{aligned} G_{ijml}(\mathbf{r}-\mathbf{r}') = {} & \frac{1}{64\pi^3\mu_0\,(1-\nu_0)}\left(\delta_{ip}\frac{\partial}{\partial x_j}+\delta_{jp}\frac{\partial}{\partial x_i}\right)\left(\delta_{ql}\frac{\partial}{\partial x_m}+\delta_{qm}\frac{\partial}{\partial x_l}\right) \\ & \times\left(2\,(1-\nu_0)\,\delta_{pq}\frac{\partial^2}{\partial x_s x_s}-\frac{\partial^2}{\partial x_p x_q}\right)\int_{\mathcal{D}(a)}\mathrm{d}\mathbf{k}\frac{e^{i\mathbf{k}(\mathbf{r}-\mathbf{r}')}}{k^4}, \end{aligned} \tag{3.25}$$

where $\mathcal{D}(a)$ is a cutoff surface in the $\mathbf{k}$-space which depends on the bead size a, see Section 2.5 for discussion. Here we are interested in the long-wavelength response of amorphous materials, whereby the detailed shape of the cutoff surface is not essential. Replacing $\mathcal{D}(a)$ by the full $\mathbf{k}$-space we find $\int \mathrm{d}\mathbf{k}\exp[i\mathbf{k}\mathbf{r}]/k^4 = -\pi^2 r$.[43] The stress-stress coupling, which we label in this

approximation by G^{A}, can be expressed via the well known Green tensor γ^{A} for a point force inside an infinite, homogeneous, and isotropic medium (Kelvin's solution)[43] with elastic moduli C_0

$$G^{A}_{ijml}(\mathbf{r}-\mathbf{r}') = \frac{1}{4}\left(\delta_{ip}\frac{\partial}{\partial x_j}+\delta_{jp}\frac{\partial}{\partial x_i}\right)\left(\delta_{ql}\frac{\partial}{\partial x_m}+\delta_{qm}\frac{\partial}{\partial x_l}\right)\gamma^{A}_{pq}(\mathbf{r}-\mathbf{r}') \tag{3.26}$$

where

$$\gamma^{A}_{ij}(\mathbf{r}) = \frac{1}{16\pi\mu_0\,(1-\nu_0)}\frac{1}{r}\left[(3-4\nu_0)\,\delta_{ij}+\frac{x_i x_j}{r^2}\right]. \tag{3.27}$$

Note that, apart from the complicated tensorial form of the coupling, its distance dependence is $1/r^3$, similarly to the electric dipole-dipole interaction. As we show in Appendix A, tensor G^{A} is the Green tensor for a point *stress* source inside an infinite, homogeneous, and isotropic medium. The corresponding elastic strain ε^{S} caused by ρ can be calculated according to

$$\varepsilon^{S}(\mathbf{r}) = \int_{\mathcal{B}} dV' G^{A}(\mathbf{r}-\mathbf{r}')\rho(\mathbf{r}'), \tag{3.28}$$

while the Hamiltonian (3.24) becomes

$$H_0 \approx H_0^{A} = \frac{1}{2}\int_{\mathcal{B}} dV\rho\left(\varepsilon^{S}+C_0^{-1}\rho\right). \tag{3.29}$$

If $\mathcal{B}$ is subject to an external traction force and $\varepsilon^{T} \neq 0$, H_0 must be supplemented by a corresponding interaction term. This latter term equals $\int_{\mathcal{B}} dV\varepsilon^{T}\rho$, as will be shown in Section 3.2.2 below, see Eq. (3.62). The Hamiltonian for the frozen-in stress in the field of the external load is equal to

$$H^{A} = H_0^{A} + \int_{\mathcal{B}} dV\varepsilon^{T}\rho = H_0^{A} + V\varepsilon^{T}\tilde{\rho}. \tag{3.30}$$

The derivative (3.23) can be expressed, in a standard fashion, in terms of a second order response function,

$$\left.\frac{\partial\langle\tilde{\rho}_{ij}\rangle}{\partial\varepsilon^{\mathrm{T}}_{kl}}\right|_{\varepsilon^{\mathrm{T}}=0} = \left.\frac{\partial}{\partial\varepsilon^{\mathrm{T}}_{kl}}\frac{\int\mathcal{D}\rho\,\tilde{\rho}_{ij}\exp\left[-\beta H^{\mathrm{A}}\right]}{\int\mathcal{D}\rho\exp\left[-\beta H^{\mathrm{A}}\right]}\right|_{\varepsilon^{\mathrm{T}}=0} = -\beta\,V\Big[\langle\tilde{\rho}_{ij}\tilde{\rho}_{kl}\rangle_0 - \langle\tilde{\rho}_{ij}\rangle_0\langle\tilde{\rho}_{kl}\rangle_0\Big], \tag{3.31}$$

where we have assumed ε^{T} is homogeneous and labeled the thermodynamic average in external zero field, $\varepsilon^{\mathrm{T}}=0$, by $\langle\cdots\rangle_0$, e.g.,

$$\langle\tilde{\rho}\rangle_0 = \frac{\int\mathcal{D}\rho\,\tilde{\rho}\,\exp\Big[-\beta H_0^{\mathrm{A}}\Big]}{\int\mathcal{D}\rho\,\exp\Big[-\beta H_0^{\mathrm{A}}\Big]}. \tag{3.32}$$

The ground state of H_0 is given by $\rho(\mathbf{r})=0$, which corresponds to a uniform periodic crystalline structure. However, the model describes also a metastable aperiodic phase, $\rho\neq 0$, separated from the ground state by a free energy barrier.[14] The relaxation towards the ground state, $\rho\to 0$, is subject to nucleation and is suppressed by a surface tension between two phases.[37] This feature is translated into the continuum approximation considered here as the so-called *incompatibility* of the strain η corresponding to the metastable stress pattern in the aperiodic phase, $\rho = C_0\eta$,[43]

$$(\mathrm{inc}\,\eta)_{ij} = -\epsilon_{ikl}\epsilon_{jmn}\eta_{ln,km}\neq 0, \tag{3.33}$$

where ϵ_{ijk} is the Levi-Civita symbol.[1] Mathematically Eq. (3.33) means that there is *no* continuous deformation field, say $\mathbf{v}$, such that $\eta_{ij} = \left(v_{i,j}+v_{j,i}\right)/2$, and the relaxation $\eta\to 0$ can not be accomplished without breaking bonds or adding material. An equality in Eq. (3.33) is a necessary and sufficient condition for the existence of a continuous deformation field v if body $\mathcal{B}$ is simply-connected.[43, §2.7]

1 Occasionally, we use the same letter, ϵ, to label strain tensors, as, e.g., in Eq. (2.4). This will not lead to confusion since the Levi-Civita symbol is third-order tensor and we never write it without indexes.

In Chapter 2, we introduced a specific order parameter connecting the uniform crystalline ground state and the metastable glassy continuum. It directly reflects the frozen-in local energy of local anharmonic degrees of freedom

$$\rho(\mathbf{r})C_0^{-1}\rho(\mathbf{r}) = g^2(\mathbf{r}). \tag{3.34}$$

We have also showed that H_0, Eq. (3.24), is equivalent to a classical long-range Heisenberg model with anisotropic coupling and six-component spins. Then the assumption of a homogeneous distribution of the order parameter, $g(\mathbf{r}) = g = \text{Const}$, is equivalent to fixing the length of the spins. This approximation is discussed in greater detail is Section 3.2.3.

Evaluation of the cumulant in Eq. (3.31) is prohibitively difficult to accomplish analytically for the Heisenberg model discussed above. On the other hand, numerical methods, such as Monte Carlo simulation, face difficulties stemming from the very long interaction range. However, we are helped here by an analogy with the electric dipole-dipole interaction, for which a cavity method can be employed. In this method, a few degrees of freedom can be treated explicitly, while the surrounding degrees of freedom are approximated by a medium with a dielectric susceptibility. This analogy was noticed a long time ago and used mainly to study crystalline materials with a low concentration of defects.[74, 75] In crystals, however, defects dynamics are strongly influenced by lattice anisotropy which normally allows for just a few energetically equivalent structural states for a defect.[76] Similar features pertain to orientational glasses, which are formed in periodic crystalline materials with a high enough density of anisotropic substitutes that destroys the orientational but not translational long-range order.[39] Reorientational dynamics of the substitutes leads to a marked temperature dependence of the elastic moduli,[77] which is well accounted for theoretically, largely owing simplifications stemming from known symmetry of the crystalline lattice.[58] The latter simplifications are not possible for structural glasses, where there is no crystalline anisotropy to limit the phase space of the stress distribution; the allowed structural states correspond to the full rotational space of a Heisenberg 6-spin. This makes an effective field approximation for the

elasticity of supercooled liquids conceptually very similar to that for the dielectric properties of polar liquids where rotational dynamics of permanent electrical dipoles leads to a *renormalization* of the dielectric susceptibility. In fact, as we will show below, it is possible to use Onsager's cavity construction to find a relation between bare and renormalized effective moduli of a supercooled liquid, which, incidentally, is controlled by the order parameter of the crystal-to-glass transition. Below, for the reader's convenience, we outline the relevant part of Onsager's cavity construction for polar liquids, to which we will refer, as a matter of analogy, during the corresponding construction for the case of the stressed elastic continuum.

3.2.1 *Brief historical summary of the theory of polar liquids*

Here we briefly review early developments in the theory of polar liquid dielectrics, to set the stage for developing an analogous theory for effective elastic moduli in supercooled liquids.

In 1895, Pierre Curie experimentally showed that the magnetic susceptibility of certain materials (oxygen, palladium, air, iron sulfate) is inversely proportional to temperature.[78] This trend was theoretically accounted for by Paul Langevin who assumed that the corresponding molecules possess permanent magnetic dipole moments which can rotate freely.[79] The dielectric susceptibility of gases displayed similar behavior unexplained by the theory of dielectrics based on the view of electrons as elastically bound inside molecules. In 1912, Peter Debye developed a theory of "polarization by orientation" assuming, analogously to Langevin, that molecules in dielectrics possess permanent dipole moments.[80, 81] This assumption allows one to satisfactory account for the temperature the dependence of dielectric constant for *all* experimental data known at the time.

Debye's argument was as follows. Starting from the definition of the electric displacement $\mathbf{D}$,

$$\mathbf{D} = \mathbf{E} + 4\pi\mathbf{P},$$

and the dielectric constant ϵ, $\mathbf{D} = \epsilon\mathbf{E}$, which gives

$$\mathbf{P} = \frac{\epsilon - 1}{4\pi}\mathbf{E}, \tag{3.35}$$

he assumed that the polarization $\mathbf{P}$, i.e., the dipole moment per unit volume, is generated by two contributions: a temperature independent term describing polarization due to elastic displacements of electrons in the external electric field and a contribution due to permanent dipoles,

$$\mathbf{P} = c\mathbf{p} = c(\alpha\mathbf{F} + \langle\mathbf{d}\rangle). \tag{3.36}$$

Here $\mathbf{p}$ is the average dipole moment per molecule of a liquid, c is the dipoles' number density, α is the polarizability, and $\langle\mathbf{d}\rangle$ is an ensemble average of the permanent dipole moment $\mathbf{d}$. The field $\mathbf{F}$ is the "actual electric intensity acting upon one molecule of the substance",[81, §1] which must be calculated approximately.

The first estimate of the *internal* field $\mathbf{F}$ is due to H. A. Lorentz,[82, §117] who showed that it is different from the macroscopic average field $\mathbf{E}$. Indeed, to calculate the field acting on a particular molecule inside the dielectric, the *microscopic* field, $\mathbf{E}_{micro}$, of the molecule's immediate neighborhood must be found. Lorentz considered a spherical region,[2] containing a large number of molecules, but of the size "small in physical sense". The molecule, at whose position the internal field is to be calculated, is situated at the center of the region. The macroscopic average field $\mathbf{E}$ is defined in the continuum approximation, whereby the actual molecular composition of the dielectric is approximated by a continuum with dielectric constant ϵ. This is a long wavelength approximation. In order to find the field $\mathbf{F}$, the reverse procedure must be carried out: the effective continuum inside the region is to be removed and replaced by the actual molecular lattice of the dielectric.[83, §4.5] Thus, the field $\mathbf{F}$ is a combination of three components: the macroscopic average

2 It is interesting to note that the cavity construction, used by Lorentz, draws its inspiration from analogous reasoning "by which Kelvin long ago came to distinguish between the magnetic force and the magnetic induction."[82, p. 137]

field $\mathbf{E}$ minus the field $\mathbf{E}_{sphere}$, due to the effective medium removed from the cavity, and the field $\mathbf{E}_{micro}$ of the inserted microscopic lattice:

$$\mathbf{F} = \mathbf{E} - \mathbf{E}_{sphere} + \mathbf{E}_{micro}.$$

An elementary calculation shows that $\mathbf{E}_{sphere}$ is related to the macroscopic polarization in the dielectric[83, p. 153]

$$\mathbf{E}_{sphere} = -\frac{4\pi}{3}\mathbf{P},$$

so that

$$\mathbf{F} = \mathbf{E} + \frac{4\pi}{3}\mathbf{P} + \mathbf{E}_{micro}.$$

It is much more difficult to estimate the microscopic field $\mathbf{E}_{micro}$. Lorentz showed, however, that for a cubic lattice $\mathbf{E}_{micro} = 0$. He also noted that this is "a result that can be applied with a certain degree of approximation to isotropic bodies in general, such as glass, fluids and gases."[82, p. 138] Since Debye originally considered gases and diluted polar solutions only, he dropped $\mathbf{E}_{micro}$ arriving at the estimate[80]

$$\mathbf{F} = \mathbf{E} + \frac{4\pi}{3}\mathbf{P} = \frac{\epsilon + 2}{3}\mathbf{E}, \tag{3.37}$$

where we have used Eq. (3.35). He also assumed that the same field orients permanent dipole moments and calculated the average $\langle \mathbf{d} \rangle$ as

$$\langle \mathbf{d} \rangle = \frac{\int \mathrm{d}\Omega \mathbf{d} \exp(\beta \mathbf{d}\mathbf{F})}{\int \mathrm{d}\Omega \exp(\beta \mathbf{d}\mathbf{F})} \approx \frac{1}{3}\beta d^2 \mathbf{F}, \tag{3.38}$$

for $\beta dF \ll 1$. In Eq. (3.38), the integration is over all possible orientations of the vector $\mathbf{d}$ and $\mathrm{d}\Omega$ labels an infinitesimal element of the corresponding solid angle. Substituting the above result into (3.36) to get

$$c(\alpha + \frac{1}{3}\beta d^2)\mathbf{F} = \mathbf{P} = \frac{\epsilon - 1}{4\pi}\mathbf{E},$$

and using (3.37), we obtain a simple relation between the dielectric constant ϵ, polarizability α and the magnitude of the permanent dipole moment d:

$$\frac{\epsilon - 1}{\epsilon + 2} = \frac{4\pi}{3} c \left(\alpha + \frac{1}{3} \beta d^2 \right). \tag{3.39}$$

Eq. (3.39) can not be satisfied at sufficiently low temperatures, since the left hand side of (3.39) does not exceed unity while the rhs can be made arbitrarily large. This signifies the presence of a Curie point in polar liquids (at rather high temperatures [84]). It was not until 1932, however, that the experimental evidence mounted showing clear discrepancy between (3.39) and the actual data for polar solutions.[85]

The next theoretical advance came in 1936 from L. Onsager, who made an important correction to Debye's estimate of the internal field **F**.[86] Onsager noted that Debye's cavity construction did not take into account the presence of the permanent dipole moment itself which induces polarization changes near the cavity edge. The field, inside the cavity, due to these polarization changes is:

$$\mathbf{E}_{reaction} = \frac{2(\epsilon - 1)}{2\epsilon + 1} \frac{\langle \mathbf{d} \rangle}{a^3},$$

where a is a radius of the cavity. The radius is set by the number density of dipoles $c = 3/(4\pi a^3)$, and the polarization is just $\mathbf{P} = c\langle \mathbf{d} \rangle$. The field $\mathbf{E}_{reaction}$ is parallel to the dipole and does not affect its orientation[3] and, for the purpose of estimating $\langle \mathbf{d} \rangle$, Eq. (3.38), the product $\mathbf{dF}$ in (3.38) must be replaced by $\mathbf{dF}'$, where

$$\mathbf{F}' = \mathbf{E} + \frac{4\pi}{3}\mathbf{P} - \mathbf{E}_{reaction} = \mathbf{E} + \frac{4\pi}{3}\mathbf{P}\left(1 - \frac{2(\epsilon - 1)}{2\epsilon + 1}\right).$$

3 This point will be elucidated below. Also see [87, chap. 13] for a thorough discussion of this point.

Substituting the usual $4\pi\mathbf{P} = (\epsilon - 1)\mathbf{E}$ yields

$$\mathbf{F}' = \frac{3\epsilon}{2\epsilon + 1}\mathbf{E},$$

i.e., the familiar expression for the filed $\mathbf{E}$ modified by the presence of an empty cavity.[83, §4.4] Thus, as first noted by Kirkwood (and elegantly shown by Hannay in [88]), Debye's cavity corresponds to "shrinking the macroscopic Lorentz cavity onto the surface of the molecule in which the local field is to be calculated".[89] We consider Onsager's reasoning more closely in the form of the following problem:

> *Consider a dielectric liquid with susceptibility ϵ, in which a certain number of chemically inert molecules have been dissolved. Determine how these molecules modify the dielectric susceptibility of the liquid, assuming each molecule can rotate freely and possesses a constant dipole moment of magnitude d. The number density of the molecules is c. The dipoles are rigid, so that their polarizability $\alpha = 0$.*

Such a formulation is more appropriate than that with $\alpha \neq 0$ to make a connection with a stressed elastic continuum, since for solids the dia-elastic effect can be neglected if the para-elastic effect is present, see [90, §15] for details.

First, we present the charge density due to the dipole moments as[91, 92]

$$\rho_d = -\sum_i (\mathbf{d}_i \cdot \boldsymbol{\nabla})\, \delta(\mathbf{r} - \mathbf{r}_i) = -\boldsymbol{\nabla}\mathbf{P},$$

where $\mathbf{P} = \sum_i \mathbf{d}_i \delta(\mathbf{r} - \mathbf{r}_i)$ is the spatial distribution of the dipoles; the corresponding volume average is equal to the polarization, in the usual way.[93] In a standard fashion, this dipole density modifies the electric displacement,

$$\mathbf{D} = \epsilon\mathbf{E} + 4\pi\mathbf{P},$$

and the effective dielectric susceptibility can be defined via $\mathbf{D} = \epsilon'\mathbf{E}$. Performing the volume average, one obtains

$$\epsilon'\mathbf{E} = \epsilon\mathbf{E} + \frac{4\pi}{V}\sum_i \mathbf{d}_i, \tag{3.40}$$

where we assume $\mathbf{E}$ is homogeneous. Note that Eq. (3.40) is an analog of Eq. (3.15) for charged dielectrics. To solve Eq. (3.40) and connect the effective dielectric constant ϵ' with its "bare" value ϵ we need to find the relation between the molecular dipole moment density $\sum_i \mathbf{d}_i/V$ and the electric field $\mathbf{E}$. Performing thermodynamic average over the ensemble of the dipole states, similarly to Eq. (3.16), we replace

$$\frac{1}{V}\sum_i \mathbf{d}_i \to \langle\mathbf{P}\rangle. \tag{3.41}$$

It is not necessary to use here the expansion in powers of $\mathbf{E}$, as we did in Eq. (3.18), since the average dipole moment can be readily found for $\mathbf{E} \neq 0$. The same is not possible for the case of para-elasticity considered below where we will have to proceed through Eq. (3.19).

To calculate $\langle\mathbf{P}\rangle$, we use Onsager's cavity construction.[86] Assuming that correlations between dipoles are negligible, we replace the ensemble average of the dipole density approximately by the time average of a single dipole moment $\mathbf{d}$, located at the origin of the coordinate system,

$$\langle\mathbf{P}\rangle \approx c\langle\mathbf{d}\rangle. \tag{3.42}$$

Next we circumscribe the dipole by a sphere of radius a, so that no other dipole is located inside it. The material inside the sphere has the "bare" dielectric susceptibility ϵ, while outside, the distribution of dipoles is replaced by an effective medium with a "renormalized" dielectric susceptibility ϵ'. The radius of the cavity is set by the concentration, $c = 3/(4\pi a^3)$. The total field acting on the dipole is[83]

$$\mathbf{F} = \frac{2\,(\epsilon' - \epsilon)}{a^3\epsilon\,(2\epsilon' + \epsilon)}\mathbf{d} + \frac{3\epsilon'}{2\epsilon' + \epsilon}\mathbf{E}, \tag{3.43}$$

and the dipole's potential energy

$$W = -\mathbf{dF} = -\frac{2(\epsilon' - \epsilon)}{a^3\epsilon(2\epsilon' + \epsilon)}d^2 - \frac{3\epsilon'}{2\epsilon' + \epsilon}\mathbf{dE}.$$

Since the term proportional to d^2 in W is invariant with respect to the dipole's rotation, it does not contribute to $\langle\mathbf{d}\rangle$ which equals, in the high temperature limit, to

$$\langle\mathbf{d}\rangle = \frac{\int \mathrm{d}\Omega\mathbf{d}e^{-\beta W}}{\int \mathrm{d}\Omega e^{-\beta W}} \approx \frac{d^2\beta\epsilon'}{2\epsilon' + \epsilon}\mathbf{E}, \tag{3.44}$$

where the integration is over all possible orientations of $\mathbf{d}$ and $\mathrm{d}\Omega$ denotes an infinitesimal element of the corresponding solid angle. Upon substitution into Eqs. (3.41) and (3.40) we get

$$\frac{\epsilon'}{\epsilon} = 1 + \frac{b\epsilon'}{\epsilon(2\epsilon' + \epsilon)},$$

where

$$b = 4\pi c\beta d^2.$$

As a result,

$$\frac{\epsilon'}{\epsilon} = \frac{1}{4}\left(1 + \frac{b}{\epsilon} + \sqrt{\left(1 + \frac{b}{\epsilon}\right)^2 + 8}\right). \tag{3.45}$$

The latter equation coincides with Eq. (26) from Onsager's paper [86], if we take polarizability $\alpha = 0$ and set ϵ to unity. The solution is plotted at Fig. 10, where it is compared to the result of a similar calculation based on the approximation for the local field $\mathbf{F}$ due to P. Debye.[80] Not realizing the importance of the cavity's structure, Debye used Lorentz's cavity field, Eq. (3.37) to estimate the field acting on the dipole moment in a liquid. This effectively shrinks the cavity to the surface of the molecule[89] and fails to subtract the image field part of $\mathbf{F}$ (the first term in the rhs of Eq. (3.43)) which does not contribute to orienting the dipole. Formally this is equivalent to

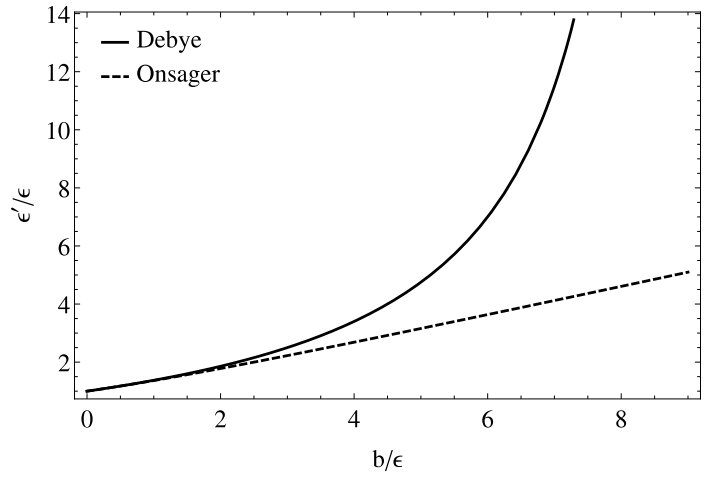

Figure 10.: Modification of dielectric susceptibility by the permanent dipole moments calculated based on Onsager's and Debye's approximations, Eqs. (3.45) and (3.48) respectively.

replacing $\mathbf{d}$ by $\langle\mathbf{d}\rangle$ in the expression for $\mathbf{F}$, which gives rise to a ferroelectric transition as dipoles are allowed to be aligned. Thus, according to Debye's method, we use (3.40) and (3.41) to get

$$\frac{\langle\mathbf{d}\rangle}{a^3} = \frac{4\pi}{3}\langle\mathbf{P}\rangle = \frac{\epsilon' - \epsilon}{3}\mathbf{E}. \tag{3.46}$$

Substituting this result in (3.43), we obtain for the potential energy of the dipole W,

$$W = -\frac{\epsilon' + 2\epsilon}{3\epsilon}\mathbf{dE}, \tag{3.47}$$

which is exactly the Loretz field, $\mathbf{E} + 4\pi\mathbf{P}/3$ times the dipole moment. Averaging similarly to (3.44), we obtain

$$\frac{\epsilon'}{\epsilon} = \frac{2b/\epsilon + 9}{9 - b/\epsilon}, \tag{3.48}$$

instead of (3.45). It is evident from (3.48) that Debye's approximation entails a Curie point with a diverging susceptibility at $b = 9$. This ferroelectric type of response is a result of the replacement $\mathbf{d} \to \langle\mathbf{d}\rangle$ which permits alignment of the dipoles in liquid. Onsager's expression (3.45), on the

contrary, does not exhibit a divergence, which, as was noted by Onsager,[94] is characteristic of solids, not liquids.

Another model of the cavity which can be readily solved analytically is the model in which the dipole moment is "smeared" uniformly over the whole cavity. In fact, it produces a result identical to that for the localized dipole since only the first term in rhs of Eq. (3.43) is changed but only the second one contributes to the final expression in Eq. (3.45). In contrast, as we will demonstrate below, this is not true for a stressed elastic continuum, where a homogeneously stressed inclusion and an inclusion with the stress concentrated at the center interact differently with external load. This is a direct result of the tensor structure of the elastic "dipole", implying one should be careful when using scalar elasticity for glasses.

A transition to modern theories of static dielectric susceptibility in polar liquids was accomplished by J. Kirkwood,[89] who provided a generalization of the Onsager's approach avoiding reference to a cavity at all. The result of Kirkwood's analysis is equivalent to Eq. (3.45) with b replaced by $4\pi c(3\alpha + \beta d\bar{d})$, where $\bar{d}$ is "the total moment of any finite macroscopic spherical specimen polarized by a fixed molecule, when immersed in a medium of its own dielectric constant". This quantity describes short-ranged angular correlations and is related to the pair correlation function of a liquid, see [95, chap.11] for the review. Accounting for such detail provides merely a quantitative correction to the theory (see, e.g., fig. 22 in [96]), but considerably complicates corresponding calculations, which must now rely on explicit models of the liquid's structure. Onsager's approach, however, provides a very powerful heuristic model for the development of effective continuum theories which is simple enough to be analyzed exactly. Thus it will be used below in a rather distinct realm of the elastic properties of supercooled liquids.

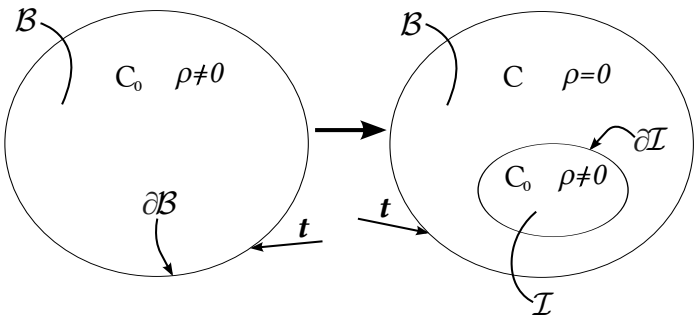

Figure 11.: A cartoon illustrating the present cavity construction for the elasticity of supercooled liquids. The original amorphous body $\mathcal{B}$ with a non-zero frozen-in stress distribution ρ and bare elastic moduli tensor C_0 is shown in the left part of the cartoon. By applying external traction force $\mathbf{t}$ to the surface $\partial\mathcal{B}$ and monitoring the resulting geometry of $\mathcal{B}$, the effective (apparent) elastic moduli C can be measured. As shown in Section 3.1.1, $C \neq C_0$ owing to the presence of ρ. To find the relation between C_0 and C, we replace the original body $\mathcal{B}$ by one with the moduli given by C everywhere except for the region $\mathcal{I}$ in the interior of the body far enough from $\partial\mathcal{B}$ so that the corresponding image field can be neglected. As explained in the text, the average of ρ, $\bar{\rho}$, over the volume of $\mathcal{I}$ can be calculated under certain assumptions as a function of C, C_0, $\mathbf{t}$, and the temperature. Neglecting correlations between ρ inside $\mathcal{I}$ and the rest of $\mathcal{B}$ we may replace $\tilde{\rho}$ by $\bar{\rho}$ in Eq. (3.19) to obtain a self-consistent equation for C as a function of C_0 and the temperature.

3.2.2 *Cavity construction for supercooled liquids*

In full analogy with the case of polar liquids we will use a cavity construction to estimate the mean field value of $\partial\langle\rho\rangle/\partial\varepsilon^{\mathrm{T}}$ and thus solve Eq. (3.19) for renormalized elastic constants. We consider an ellipsoidal region $\mathcal{I}$ inside the body $\mathcal{B}$ and assume that the stress distribution ρ outside $\mathcal{I}$ can be taken into account effectively, by switching the elastic moduli of the medium from C_0 to C while simultaneously replacing ρ by zero, see Fig. 11. Note that since both C_0 and C are assumed to be isotropic, all possible orientations of $\mathcal{I}$ in $\mathcal{B}$ are equivalent. The linear size of $\mathcal{B}$, $L_{\mathcal{B}}$, is assumed to be much larger than that of $\mathcal{I}$ and, consequently, we neglect the image forces coming from $\partial\mathcal{B}$ since the corresponding contribution is $\propto L_{\mathcal{B}}^{-3}$.

The thermodynamic average $\langle\tilde{\rho}\rangle$ is approximated by that computed by Boltzmann averaging over all structural states inside $\mathcal{I}$. First we need to find the potential energy E of the metastable

stress distribution inside the inclusion. The full elastic energy of $\mathcal{B}$ containing $\mathcal{I}$ that possesses non-zero frozen-in stress distribution ρ equals to

$$E_{el} = \frac{1}{2}\int_{\mathcal{B}} dV\,(\sigma+\rho)\left(\varepsilon + C_0^{-1}\rho\right), \tag{3.49}$$

where the integrand is the product of the total (compatible and incompatible) stress, $\sigma+\rho$, and the total strain, $\varepsilon + C_0^{-1}\rho$. The elastic stress σ and strain ε are solutions of Eq. (3.1), but since $\mathcal{B}$ is now inhomogeneous, Eq. (3.4) no longer holds. Instead, one should write:

$$\sigma = \sigma^{T} + \sigma^{P} + \sigma^{S}, \tag{3.50}$$

where $\sigma^{T} = C\varepsilon^{T}$ everywhere in $\mathcal{B}$ is a solution of the homogeneous problem (3.5) and

$$\sigma^{P} = \begin{cases} C\varepsilon^{P}, \text{ outside } \mathcal{I}, \\ C_0\varepsilon^{P}, \text{ inside } \mathcal{I}, \end{cases} \tag{3.51}$$

is the correction due to the inclusion. For an ellipsoidal $\mathcal{I}$ and homogeneous ε^{T} considered here, ε^{P} *inside* $\mathcal{I}$ is also homogeneous and is given by[44, 73, 97]

$$\varepsilon^{P} = SQ\,(C - C_0)\,\varepsilon^{T}, \tag{3.52}$$

where

$$Q = \left(C - [C - C_0]\,S\right)^{-1}, \tag{3.53}$$

and S is the so-called Eshelby tensor for the ellipsoidal inclusion $\mathcal{I}$.[44] As we show in the Appendix B, this tensor is straightforwardly related to the volume average of the Green tensor G^{A}. Note that

the order of tensors is important in (3.52) since in general S is not isotropic. If, however, $\mathcal{I}$ is a sphere, S is in fact isotropic:

$$\mathrm{S} = \frac{1}{3\,(1-\nu)}\,\mathrm{L}\left[1+\nu\,,\frac{2}{5}\,(4-5\nu)\right], \tag{3.54}$$

and depends only on the Poisson ratio ν of the matrix, i.e. the part of $\mathcal{B}$ outside $\mathcal{I}$. Below we will consider exclusively the case of a spherical $\mathcal{I}$. We note in passing that the Eshelby tensor S, Eq. (3.54), also emerges as the mean field limit of the coupling in the Hamiltonian H_0, Eq. (3.24).[14]

We will not need the expression for σ^{P} outside of $\mathcal{I}$ which is very complex.[73] The boundary conditions,

$$\sigma^{\mathrm{P}}_{ij} n_j \Big|_{\partial\mathcal{B}} = 0, \tag{3.55}$$

are important, however.

As before, σ^{S} is given by the solution of (3.6) but now, also taking into account the inhomogeneity of $\mathcal{B}$, due to the elastic discontinuity caused by the inclusion,

$$\sigma^{\mathrm{S}} = \begin{cases} \mathrm{C}\varepsilon^{\mathrm{S}}, \text{ outside } \mathcal{I}, \\ \mathrm{C}_0\varepsilon^{\mathrm{S}}, \text{ inside } \mathcal{I}. \end{cases} \tag{3.56}$$

The potential energy E of ρ is the difference between the elastic energy E_{el} and the work performed by an external load $\mathbf{t}$,

$$W = \int_{\partial\mathcal{B}} \mathbf{t}\,(\mathbf{u}^{\mathrm{T}} + \mathbf{u})\,\mathrm{dS}, \tag{3.57}$$

where $\mathbf{u}$ and $\mathbf{u}^{\mathrm{T}}$ are displacement vectors corresponding to ε and ε^{T} respectively. We also take the potential energy of a homogeneous $\mathcal{B}$, i.e. without $\mathcal{I}$, with $\rho = 0$,

$$E_h = \frac{1}{2}\int_{\mathcal{B}} \sigma^{\mathrm{T}}\varepsilon^{\mathrm{T}}\mathrm{dV} - \int_{\partial\mathcal{B}} \mathbf{t}\mathbf{u}^{\mathrm{T}}, \tag{3.58}$$

as our energy reference. Then,

$$E = E_{el} - W - E_h. \tag{3.59}$$

Multiple applications of the Gauss theorem together with Eqs. (3.5)-(3.9), (3.52), and (3.55) allows one to recast E in terms of the integral over $\mathcal{I}$ only (the interested reader is referred to Chapter 4 of Mura's monograph[73] for this derivation),

$$E = \frac{1}{2}\int_{\mathcal{I}} dV\Big(\rho\varepsilon^{S} + \rho\, C_0^{-1}\rho - \varepsilon^{T}C\,(C - C_0)\,Q\varepsilon^{T} + \varepsilon^{T}\,(I + C\,Q)\,\rho - \varepsilon^{T}\,(C - C_0)\,\varepsilon^{S}\Big). \tag{3.60}$$

The first two terms in the integral yield the same form as the earlier obtained Hamiltonian H_0^{A}, Eq. (3.29),

$$E_0 = \frac{1}{2}\int_{\mathcal{I}} dV\rho\left(\varepsilon^{S} + C_0^{-1}\rho\right). \tag{3.61}$$

In important distinction from Eq. Eq. (3.29), the integration domain is now the region $\mathcal{I}$ only. The third term is the potential energy of the system for $\rho = 0$. Since E is the difference between the full elastic energy E_{el} and the work of the external load W, see Eq. (3.59), this term describes the contribution due to the inhomogeneity introduced by inclusion $\mathcal{I}$ and vanishes for $C_0 = C$. The last two terms in the integrand in Eq. (3.60) describe the interaction between ρ and the external field ε^{T}. If $C = C_0$, i.e. $\mathcal{B}$ is homogeneous, as considered in Section 3.1.1,

$$E\Big|_{C=C_0} = E_0 + \int_{\mathcal{I}} dV\varepsilon^{T}\rho, \tag{3.62}$$

since $I + CQ = 2I$ for $C = C_0$. This equation has the same form as Eq. (3.30), showing that H^{A} is indeed the correct Hamiltonian for the stress distribution subject to an external field. Again the integration in (3.62) is over the region $\mathcal{I}$, not $\mathcal{B}$. Now, let's find the derivative $\partial\langle\rho\rangle/\partial\varepsilon^{T}$, which

describes the response of the material *inside* the inclusion $\mathcal{I}$ to external traction $\mathbf{t}$. Recalling that ε^{T} is homogeneous we get, using Eq. (3.60),

$$\left.\frac{\partial\langle\overline{\rho}_{ij}\rangle}{\partial\varepsilon^{\mathrm{T}}_{kl}}\right|_{\varepsilon^{\mathrm{T}}=0} = \left.\frac{\partial}{\partial\varepsilon^{\mathrm{T}}_{kl}}\frac{\int\mathcal{D}\rho\,\overline{\rho}_{ij}\exp\left[-\beta E\right]}{\int\mathcal{D}\rho\exp\left[-\beta E\right]}\right|_{\varepsilon^{\mathrm{T}}=0} = -\beta\Big[\langle\overline{\rho}_{ij}\zeta_{kl}\rangle_0 - \langle\overline{\rho}_{ij}\rangle_0\langle\zeta_{kl}\rangle_0\Big], \tag{3.63}$$

where

$$\zeta = \frac{1}{2}v\left[(\mathrm{I}+\mathrm{CQ})\,\overline{\rho} - (\mathrm{C}-\mathrm{C}_0)\,\overline{\varepsilon^{\mathrm{s}}}\right], \tag{3.64}$$

the bar signifies averaging over the volume v of $\mathcal{I}$, e.g.,

$$\overline{\varepsilon^{\mathrm{s}}} = \frac{1}{v}\int_{\mathcal{I}}\varepsilon^{\mathrm{s}}\,\mathrm{dV}, \tag{3.65}$$

and $\langle\cdots\rangle_0$, again, denotes thermodynamic averaging in zero field, $\varepsilon^{\mathrm{T}}=0$. Since now ρ is non-zero inside $\mathcal{I}$ only, in contrast with Eq. (3.32), the averaging reduces to the one over $\mathcal{I}$.

$$\langle\rho\rangle_0 = \frac{\int\mathcal{D}\rho\,\rho\exp[-\beta E_0]}{\int\mathcal{D}\rho\exp[-\beta E_0]}. \tag{3.66}$$

The last step in the cavity approximation is to replace the derivative $\partial\langle\tilde{\rho}\rangle/\partial\varepsilon^{\mathrm{T}}$ describing the response of the homogeneous body $\mathcal{B}$, Eqs. (3.31), by Eq. (3.63) for the purpose of calculating the effective elastic moduli from Eq. (3.19). This is completely analogous to how the true density $\mathbf{P}$ of the dipoles was approximated by the one calculated over Onsager's cavity in Eq. (3.42). Similarly to polar liquids, such approximation is permissible if the correlation length of the frozen-in stress ρ is smaller than the linear size of the inclusion $\mathcal{I}$. The quality of the approximation improves with the cavity size (at a fixed spin concentration) because many-particle effects are increasingly better accounted for.

Since the inclusion represents only a small portion of the body, calculations involved in Eq. (3.63) may be simplified by explicit assumptions about the structure of ρ inside $\mathcal{I}$. Importantly, however, Eq. (3.60) holds for any field ρ. Thus, it is possible to systematically improve the approximation by

increasing the size of $\mathcal{I}$ and thus explicitly account for many-particle effects. Such an approach can and be will implemented in a simulation, see Section 3.3.

Below we consider two specific, simple cases where all the necessary calculations can be performed analytically.

3.2.3 *The case of uniform frozen-in stress*

First we consider the case of a uniform $\rho = \text{Const}$, which allows us to simplify Eq. (3.60) considerably. Eshelby has shown that for a uniform ρ and spherical $\mathcal{I}$ [98]

$$\varepsilon^{S} = -QS\rho. \tag{3.67}$$

Thus, Eq. (3.60) simplifies to read

$$\frac{E}{v} = \frac{1}{2}\rho\, G\, \rho + \varepsilon^{T}\, C\, Q\, \rho - \frac{1}{2}\varepsilon^{T} C\, (C - C_0)\, Q\, \varepsilon^{T}, \tag{3.68}$$

where v is the volume of $\mathcal{I}$ and

$$G = C\, (I - S)\, Q\, C_0^{-1}. \tag{3.69}$$

Equation (3.68) is an expanded version of Eq. (25.24) from Mura's monograph written for an isotropic solid.[73]

Now, the dynamics of ρ can be mapped onto the rotations of an assembly of six-component classical spins. The full set of structural states realized in a supercooled liquid corresponds to the mutual configurations of these 6-spins. Here we show how this mapping arises from the cavity construction developed in the previous section.

Let us return to the original model of homogeneous $\mathcal{B}$ described by Eq. (3.30), and consider the spherical region $\mathcal{I}$ inscribed into a cube of volume a^3. Assume that the material outside $\mathcal{I}$ exhibits

only a rigid lattice response, that is $\rho = 0$, while inside $\mathcal{I}$, there is present frozen-in stress $\rho \neq 0$. By Eq. (3.68), together with taking $\varepsilon^{T} = 0$ and $C = C_0$, we get for the potential energy of ρ in $\mathcal{I}$

$$\frac{E^{F}}{v} = \frac{1}{2}\rho\, C_0^{-1}\,(I - S_0)\,\rho, \tag{3.70}$$

where S_0 is the Eshelby tensor for a medium with elastic moduli C_0, and, we remind, ρ is assumed to be uniform inside $\mathcal{I}$. Energy E^{F} is essentially the formation energy of the stressed aperiodic structure inside $\mathcal{I}$. It is a sum of the self-interaction energy, $\int_{\mathcal{I}} dV \rho C_0^{-1} \rho$, and the energy of the elastic relaxation in the sample, $\int_{\mathcal{I}} dV \varepsilon^{S} \rho$, cf. Eq. (3.67). Note, that E^{F} is not the formation energy of amorphous structure inside the periodic crystal phase discussed in Section 3.2 since the elastic moduli in that phase are different from C_0.

Assuming the amorphous phase is equilibrated and thus homogeneous, we may relate E^{F} and the order parameter of the crystal-to-glass transition defined above according to[14]

$$E^{F} = \frac{1}{2} g^2 a^3 = \text{Const.} \tag{3.71}$$

However, we also can fix the magnitude of ρ by assuming that only the self-interaction part of E^{F}, $\int_{\mathcal{I}} dV \rho C_0^{-1} \rho$, is homogeneous throughout the sample.[14] This assumption corresponds to the usual way of defining the eigenstrain $\eta = C_0^{-1}\rho$ via a cutting and pasting procedure proposed by Eshelby. Indeed, η can be defined as a "stress-free strain" attained in equilibrium by the inclusion in the absence of the outside matrix.[98, 99] The corresponding potential energy equal to zero. Indeed, by Eq. (3.53), $Q = -(C_0 S)^{-1}$ for $C = 0$, and so, by Eq. (3.67), we get for the strain inside the inclusion which has been removed from the matrix,

$$\varepsilon^{S} = -C_0 \rho = -\eta. \tag{3.72}$$

Note that the latter equation does not contradict Eq. (3.33) since ρ was assumed to be homogeneous throughout $\mathcal{I}$, i.e. only the discontinuity of ρ at the boundary $\partial\mathcal{I}$ is a source of incompatibility. Substituting Eq. (3.72) into expression (3.68) for E we get zero, since the elastic contribution completely balances the energy of self-interaction. Then the assumption that

$$\frac{E^{\mathrm{S}}}{v} = \frac{1}{2}\rho \mathrm{C}_0^{-1}\rho = \frac{1}{2}g^2a^3 = \mathrm{Const}, \tag{3.73}$$

is equivalent to saying that the energy of relaxation of $\mathcal{I}$ removed from $\mathcal{B}$ does not depend on the original position of $\mathcal{I}$ in the body.

In the rest of this section we will use the constraint (3.71). Transition to the constraint (3.73) can be accomplished at any step of the calculation by simply removing the factor $\mathrm{I} - \mathrm{S}_0$. The final solution of Eq. (3.19) will be provided in Fig. 12 for both constraints.

As already discussed in Section 2.3, the linear elasticity formalism can be written in a six-component second-order tensor representation.[45] In this picture, second-order tensors, such as σ_{ij} or ε_{ij}, are recast as six component vectors, σ_α or ε_α, respectively. Hereafter Greek indexes are always assumed to run from 1 to 6. Then fourth-order tensors become second-order tensors, e.g. $\mathrm{C}_{ijkl} \rightarrow \mathrm{C}_{\alpha\gamma}$. This system of notations allows us to express Eq. (3.70) and the constraint (3.71) in a more compact form. We can define a new 6-vector (second-order tensor) τ absorbing the fourth-order tensors from the expression for E^{F}, Eq. (3.70),

$$\rho = g\frac{a^3}{v}\mathrm{R}\ \mathrm{U}\ \tau, \tag{3.74}$$

where

$$\mathrm{R} = \sqrt{\frac{v}{a^3}\mathrm{C}_0\left(\mathrm{I} - \mathrm{S}_0\right)^{-1}}, \tag{3.75}$$

and the square root of a tensor is defined via (2.22). Substituting (3.74) into the expression for E^{F} we get,

$$E^{\mathrm{F}} = \frac{1}{2} g^2 a^3 \tau_{ij} \tau_{ij}. \tag{3.76}$$

Thus, in the 6-vector representation, the constraint (3.71) acquires a clear geometrical meaning: it becomes equivalent to fixing the length of the 6-vector corresponding to τ,

$$\tau_{ij}\tau_{ij} = \tau_\alpha \tau_\alpha = |\tau|^2 = 1.$$

Thus, all structural states of $\mathcal{I}$ or ρ, allowed by (3.71), are now mapped onto all possible orientations of a unit 6-vector τ and the thermodynamic average $\langle\overline{\rho}\rangle$ can be defined via the thermodynamic average of $\langle\tau\rangle$, cf. Eq. (3.44),

$$\langle\tau\rangle = \frac{\int \mathrm{d}\Omega_6 \tau e^{-\beta E}}{\int \mathrm{d}\Omega_6 e^{-\beta E}}, \tag{3.77}$$

where integration is carried out over the solid angle in the six dimensional spherical coordinate system,

$$\mathrm{d}\Omega_6 = \sin^4 x_1 \sin^3 x_2 \sin^2 x_3 \sin x_4 dx_1 dx_2 dx_3 dx_4 dx_5,$$

$x_\alpha \in [0, \pi]$, for $\alpha < 5$, and $x_5 \in [0, 2\pi]$.

The potential energy E of different structural states is given by Eq. (3.68). Using Eq. (3.74) we can write it as

$$E = \frac{1}{2} g^2 a^3 \tau \,\mathrm{D}\, \tau + g a^3 \varepsilon^{\mathrm{T}} \mathrm{C}\, \mathrm{Q}\, \mathrm{R}\, \mathrm{U}\tau - \frac{v}{2} \varepsilon^{\mathrm{T}} \mathrm{C}\, [\mathrm{C} - \mathrm{C}_0]\, \mathrm{Q}\, \varepsilon^{\mathrm{T}}, \tag{3.78}$$

where $\mathrm{D} = a^3\, \mathrm{U}^{\mathrm{T}} \mathrm{RGRU}/v = \mathrm{D}[\gamma_1\ , \gamma_2]$ is a diagonal matrix, see (2.29), with

$$\begin{aligned} \gamma_1 &= \frac{3\,(1-\nu_0)}{2 + \nu_0\,(\chi - 4) + \chi}, \\ \gamma_2 &= \frac{15\,(1-\nu_0)\,(7-5\nu)}{(7-5\nu_0)\,(7 + 8\chi - 5\nu\,[1+2\chi])}, \end{aligned} \tag{3.79}$$

and

$$\chi = \mu_0/\mu. \tag{3.80}$$

In the second-order tensor representation, Eq. (3.19) becomes

$$C_{\alpha\gamma} - (C_0)_{\alpha\gamma} = \frac{ga^3}{v} C_{\alpha\beta} \left(C_0^{-1}\right)_{\beta\delta} R_{\delta\zeta} U_{\zeta\xi} \left.\frac{\partial\langle\tau_\xi\rangle}{\partial\varepsilon_\gamma^{\mathrm{T}}}\right|_{\varepsilon_\gamma^{\mathrm{T}}=0}, \tag{3.81}$$

where we have used the relation between τ and ρ, Eq. (3.74). To find a closed equation for the effective elastic moduli C we need to calculate the derivative of $\langle\tau\rangle$ in zero field. To this end, we use Eqs. (3.77) and (3.78) to show that

$$\left.\frac{\partial\langle\tau_\alpha\rangle}{\partial\varepsilon_\gamma^{\mathrm{T}}}\right|_{\varepsilon^{\mathrm{T}}=0} = -\beta g a^3 \left[\langle\tau_\alpha\tau_\zeta\rangle - \langle\tau_\alpha\rangle\langle\tau_\zeta\rangle\right]_{\varepsilon^{\mathrm{T}}=0} \left(\mathrm{U}^{\top}\mathrm{R}\,\mathrm{Q}\,\mathrm{C}\right)_{\zeta\gamma}. \tag{3.82}$$

We remind the reader that $\overline{\rho} = \rho$, since ρ assumed to be uniform in this Section. The angular integration in Eq. (3.77) can be performed analytically since for $\varepsilon^{\mathrm{T}} = 0$,

$$\left.\frac{2E}{g^2a^3}\right|_{\varepsilon^{\mathrm{T}}=0} = \tau\mathrm{D}\tau = \frac{1}{2}\left[\gamma_1 + \gamma_2 + (\gamma_1 - \gamma_2)\cos 2x_1\right], \tag{3.83}$$

i.e. the elastic moduli are decoupled from the angular variables and the thermodynamic averages are functions of the single parameter

$$p = \frac{1}{4}\beta g^2 a^3 (\gamma_1 - \gamma_2). \tag{3.84}$$

A straightforward calculation yields

$$\left.\langle\tau\rangle\right|_{\varepsilon^{\mathrm{T}}=0} = \frac{\int \mathrm{d}\Omega_6 \tau e^{-p\cos 2x_1}}{\int \mathrm{d}\Omega_6 e^{-p\cos 2x_1}} = 0, \tag{3.85}$$

and

$$\langle \tau_\alpha \tau_\zeta \rangle \Big|_{\varepsilon^{\mathrm{T}}=0} = \mathrm{D}\left[1 - 5s(p)\ , s(p)\right]_{\alpha\zeta}, \tag{3.86}$$

where

$$s\,(p) = \frac{\int_0^\pi dx_1 \sin^6 x_1 e^{-p\cos 2x_1}}{\int_0^\pi dx_1 \sin^4 x_1 e^{-p\cos 2x_1}} = \frac{p\,(4p-1)\,I_0(p) + (2 + p\,[4p-3])\,I_1(p)}{10p\,\left[2pI_0(p) + [2p-1]\,I_1(p)\right]}, \tag{3.87}$$

and $I_n(p)$ labels the modified Bessel function of n-th order.

Substitution of these results into Eq. (3.81) gives:

$$\mathrm{C} - \mathrm{C}_0 = -\theta\,\mathrm{C}^2\,(\mathrm{I} - \mathrm{S}_0)^{-1}\,\mathrm{QL}\left[1 - 5s(p)\ , s(p)\right], \tag{3.88}$$

where

$$\theta = \beta g^2 a^3. \tag{3.89}$$

After rearranging, we finally get a numerically solvable version of the self-consistent equation connecting the effective elastic moduli C with C_0,

$$(\mathrm{I} - \mathrm{S}_0)\,(\mathrm{X} - \mathrm{I})\,(\mathrm{I} + [\mathrm{X} - \mathrm{I}]\,\mathrm{S}) = \theta \mathrm{L}\left[1 - 5s(p)\ , s(p)\right], \tag{3.90}$$

where

$$\mathrm{X} = \mathrm{C}_0 \mathrm{C}^{-1}. \tag{3.91}$$

The Eq. (3.90), although being tensorial, is equivalent to a system of two scalar equations. It connects the ratio of shear moduli $\chi = \mu_0/\mu$ with ν_0, ν, and the unitless temperature θ from Eq. (3.89). Thus, given a bare value of the Poisson ratio ν_0, its effective value ν as well as χ can be found for any θ. The solution is presented at Fig. 12.

Note that the dependence of χ on θ is nearly universal for any values of ν_0. Also, it is evident from Fig. 12 that Eq. (3.90) has three fixed points such that $\nu = \nu_0$ for any value of θ. The fixed points at $\nu_0 = -1$ and $\nu_0 = \frac{1}{2}$ are trivial as discussed previously in Section 3.1.

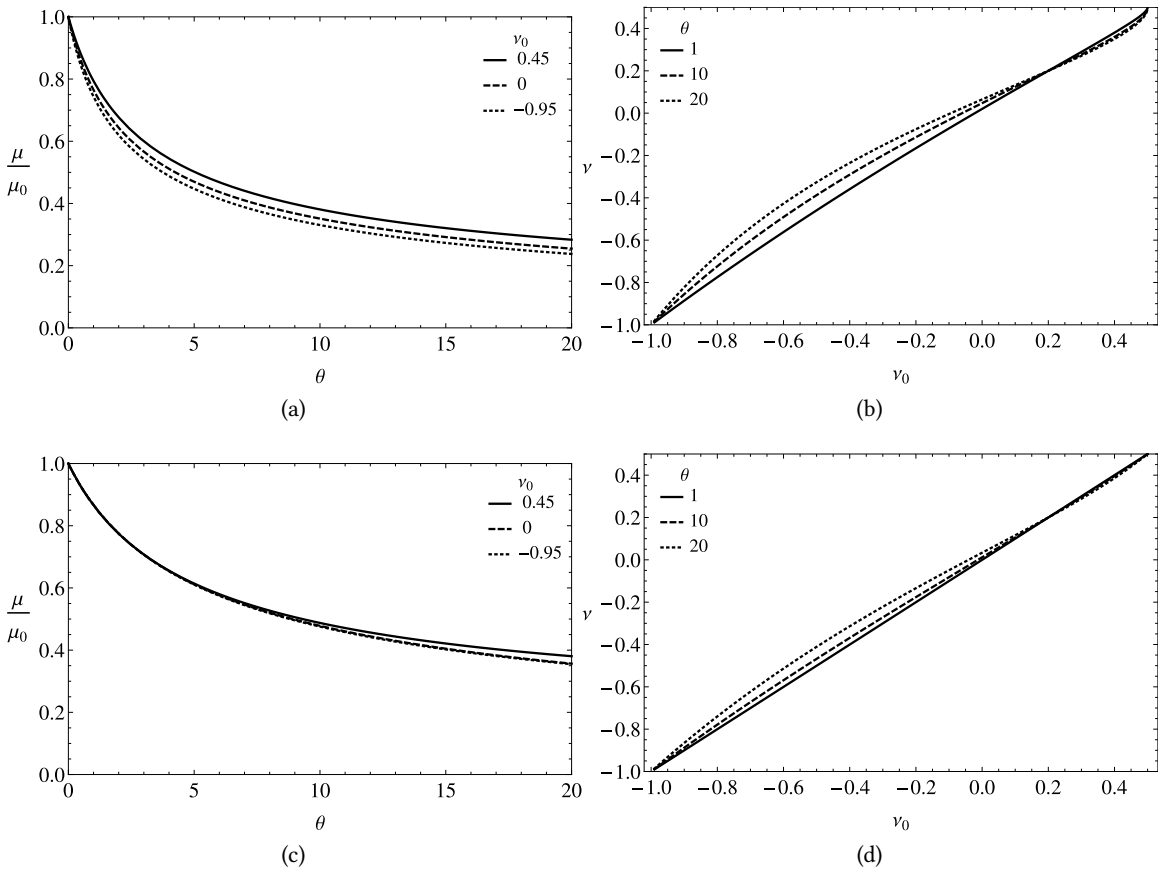

Figure 12.: Elastic moduli renormalization calculated using method of spherical inclusion and homogeneous ρ approximation. Figures (a) and (b) are solutions of Eq. (3.90). (a) Dependence of the ratio μ/μ_0 on $\theta = \beta g^2 a^3$ for different bare values of the Poisson ratio ν_0. (b) Dependence of the effective Poisson ratio ν on its bare value ν_0 for different θ. Corresponding solutions, when the constraint (3.73) is adopted so that $\mathrm{R} = (v\mathrm{C}_0/a^3)^{1/2}$ instead of Eq. (3.75), are given by (c) and (d) respectively. Note the presence of three fixed points where $\nu = \nu_0$ for any θ for both cases.

There appears to be a third fixed point. To test for its presence, we write Eq. (3.90) in a more compact form as

$$\mathrm{L}_x = \theta \mathrm{L}_s, \tag{3.92}$$

where

$$\mathrm{L}_x = (\mathrm{I} - \mathrm{S}_0)\,(\mathrm{X} - \mathrm{I})\,(\mathrm{I} + [\mathrm{X} - \mathrm{I}]\,\mathrm{S})\,,$$

and

$$\mathrm{L}_s = \mathrm{L}\left[1 - 5s(p)\ , s(p)\right], \tag{3.93}$$

and study the stability around $\nu = \nu_0$. Consider small deviations

$$\nu = \nu_0 + \epsilon,$$

$\epsilon \ll 1$. Taylor expanding both sides of Eq. (3.92) in terms of ϵ and rearranging terms we get the following tensor equation linear in ϵ,

$$\left(\mathrm{L}_x - \theta \mathrm{L}_s\right)_{\nu=\nu_0} = \epsilon \left(\theta \frac{\partial \mathrm{L}_s}{\partial \epsilon} - \frac{\partial \mathrm{L}_x}{\partial \epsilon}\right)_{\nu=\nu_0}. \tag{3.94}$$

A fixed point corresponds to a value of ν_0 such that the solution of Eq. (3.94) is $\epsilon = 0$ for any θ and χ. This is possible only if

$$\mathrm{L}_x\Big|_{\nu=\nu_0} = \theta \mathrm{L}_s\Big|_{\nu=\nu_0}. \tag{3.95}$$

Despite the complex form of Eq. (3.95) the solution can be readily found. Multiplying it, in view of Eqs. (3.84) and (3.89), by $(\gamma_1 - \gamma_2)$, we get for $\epsilon = 0$

$$(\gamma_1 - \gamma_2)\ \mathrm{L}_x\Big|_{\nu=\nu_0} = 4p\mathrm{L}\left[1 - 5s(p)\ , s(p)\right]\Big|_{\nu=\nu_0}. \tag{3.96}$$

The lhs of Eq. (3.96) does not contain θ; the rhs depends on it, but solely via the parameter $p \propto \theta\,(\gamma_1 - \gamma_2)$. Thus the solution for any value of θ is possible only if $\gamma_1 = \gamma_2$ and the dependence on θ disappears from both sides of the equation. This gives the condition that must be satisfied at the fixed point,

$$\gamma_1 - \gamma_2\Big|_{\nu=\nu_0} = \frac{9\,(1-\nu_0)\,(1-5\nu_0)\,(1-\chi)}{(2+\nu_0\,[\chi-4]+\chi)\,(5\nu_0\,[1+2\chi]-7-8\chi)} = 0. \tag{3.97}$$

The above equation is satisfied if

$$\nu_0^{\mathrm{FP}} = \frac{1}{5}.$$

This non-trivial fixed point is closely related to the properties of the tensor D, describing self-interaction of frozen-in stress and the Eshelby tensor S_0, cf. Eq. (3.78) and (3.54). For $\gamma_1 = \gamma_2$ tensor D is proportional to the unit tensor, $D \propto I$. By definition, $D \propto U^{\top} R^2 G U$, which means that Eq. (3.97) entails

$$R^2 G\Big|_{\nu=\nu_0} \propto I. \tag{3.98}$$

Consider the tensor G first. From its definition, Eq. (3.69), we have

$$G\Big|_{\nu=\nu_0} \propto C_0^{-1} (I - S_0) (I - [1 - \chi] S_0)^{-1}. \tag{3.99}$$

Using $R^2 \propto C_0 (I - S_0)^{-1}$ one can write

$$R^2 G\Big|_{\nu=\nu_0} \propto (I - [1 - \chi] S_0)^{-1}.$$

Thus, the condition $D \propto I$ is satisfied, if $S_0 \propto I$, which, using (3.54), gives again $\nu_0^{\mathrm{FP}} = 1/5$. Note that the position of the fixed point will not change if we take, instead of (3.75), $R \propto C_0$, as has been done previously.[14]

3.3 SPHERICAL INCLUSION WITH STRUCTURE: A GENERAL PROCEDURE TO DETERMINE THE EFFECTIVE ELASTIC CONSTANTS

In the previous section we considered the case of uniform $\rho = \mathrm{Const}$. Here we will study the other extreme: a point source of stress located at the center of a spherical $\mathcal{I}$. First, however, it is instructive to outline a general procedure for determining the effective elastic constants for an

arbitrary assembly of point sources inside a cavity. We start by considering a set of point sources arranged in an arbitrary (but uniform) lattice.[14] We replace the continuous tensor field $\rho(\mathbf{r})$ by a collection of *stress* sources $\sigma^{(i)}$ localized at points $\mathbf{r}_i$ inside $\mathcal{I}$,

$$\rho(\mathbf{r}) = \sum_i \sigma^{(i)} \delta(\mathbf{r} - \mathbf{r}_i). \tag{3.100}$$

Each source occupies a volume a^3, where a is the volumetric size of the bead in the glass.[14] The potential energy E of such a stress distribution can be calculated using Eq. (3.60) which is valid for arbitrary ρ. In the lattice approximation, however, it contains a singular term, $\rho \mathrm{C}_0^{-1} \rho$, which corresponds to the on-site frozen-in energy. This is the field $g(\mathbf{r})$, that serves as the order parameter of the crystal-to-glass transition, Eq. (3.34). Thus, the potential energy is

$$E = \frac{1}{2} \sum_i \varepsilon^{\mathrm{s}}(\mathbf{r}_i) \sigma^{(i)} + \frac{1}{2} \varepsilon^{\mathrm{T}} \left(\mathrm{I} + \mathrm{C}\, \mathrm{Q}\right) \sum_i \sigma^{(i)} - \frac{v}{2} \varepsilon^{\mathrm{T}} \left(\mathrm{C} - \mathrm{C}_0\right) \overline{\varepsilon^{\mathrm{s}}} + \frac{v}{2} g^2 + E^{\mathrm{T}}, \tag{3.101}$$

where we have assumed the order parameter $g(\mathbf{r})$ is uniform, $g(\mathbf{r}) = g = \mathrm{Const}$, and labeled the potential energy at $\rho = 0$ by E^{T}:

$$E^{\mathrm{T}} = -\frac{1}{2} \int_{\mathcal{I}} \mathrm{d}V \varepsilon^{\mathrm{T}} \mathrm{C} \left(\mathrm{C} - \mathrm{C}_0\right) \mathrm{Q} \varepsilon^{\mathrm{T}}. \tag{3.102}$$

As above, $\overline{\varepsilon^{\mathrm{s}}}$ denotes the average of ε^{s} over the region $\mathcal{I}$,

$$\overline{\varepsilon^{\mathrm{s}}} = \frac{1}{v} \int_{\mathcal{I}} \varepsilon^{\mathrm{s}} \, \mathrm{d}V. \tag{3.103}$$

To calculate the strain produced by point sources $\sigma^{(i)}$ we use the approach outlined in Appendix A, which leads to the expression,

$$\varepsilon^{\mathrm{s}}(\mathbf{r}) = \sum_i \mathrm{G}^{\mathrm{L}}(\mathbf{r}, \mathbf{r}_i) \sigma^{(i)}, \tag{3.104}$$

cf. Eq. (A.9). The Green tensor G^L is a sum of two contributions,

$$G^L(\mathbf{r},\mathbf{r}_i) = \begin{cases} G^A(\mathbf{r},\mathbf{r}_i) + G^I(\mathbf{r},\mathbf{r}_i), & \mathbf{r} \neq \mathbf{r}_i; \\ G^I(\mathbf{r},\mathbf{r}_i), & \mathbf{r} = \mathbf{r}_i, \end{cases} \tag{3.105}$$

where G^A is the Green tensor for a point stress inside an isotropic homogeneous medium with elastic moduli C_0 given by Eq. (3.26) and G^I is the image field contribution created by the boundary $\partial\mathcal{I}$. The image field Green tensor can be calculated using Eq. (A.10) from the corresponding second-order, image field Green tensor for a point *force*, γ^I, if the latter is known analytically. Calculation of γ^I is generally a very complicated problem which often can be solved only numerically. Obtaining γ^I for the case of a spherical isotropic inclusion inside an isotropic medium with distinct elastic moduli had been a longstanding problem in the theory of elasticity until finally solved by L. J. Walpole in 2002.[100] The resulting expression is a complicated combination of several harmonic series. Because of that, application of Eq. (A.10) to γ^I is very tedious. We provide the general result of the calculation in Appendix C, which is studied numerically in the following Chapter of the thesis. At the end of this Chapter we treat analytically the case of a single point source located at the center of the spherical inclusion.

The expression (3.103) can be simplified since, as shown in Appendix B, the volume average of G^A is related to the Eshelby tensor,

$$\overline{\varepsilon^S} = -QS\,\overline{\rho}. \tag{3.106}$$

Using Eq. (3.106) we get,

$$E = \frac{1}{2}\sum_i \varepsilon^S(\mathbf{r}_i)\sigma^{(i)} + \varepsilon^T CQ \sum_i \sigma^{(i)} + \frac{v}{2}g^2 + E^T, \tag{3.107}$$

since $I + QC + (C - C_0)QS = 2CQ$. Now from Eqs. (3.63) and (3.64) we obtain for the derivative of the average frozen-in stress,

$$\frac{\partial \langle \overline{\rho}_\alpha \rangle}{\partial \varepsilon^{\mathrm{T}}_\gamma} = \frac{1}{v} \sum_i \frac{\partial \langle \sigma^{(i)}_\alpha \rangle}{\partial \varepsilon^{\mathrm{T}}_\gamma} = Z_{\alpha\gamma}, \tag{3.108}$$

where

$$Z_{\alpha\gamma} = -\frac{\beta}{v} \sum_{ij} \left[\left\langle \sigma^{(i)}_\alpha \left(CQ\sigma^{(j)} \right)_\gamma \right\rangle_0 - \langle \sigma^{(i)}_\alpha \rangle_0 \left(CQ \langle \sigma^{(j)} \rangle_0 \right)_\gamma \right]. \tag{3.109}$$

We can not use this expression to determine C since the cumulant can only be calculated numerically for given C, C_0, and the temperature. Thus, using Eq. (3.19) with $\tilde{\rho}$ replaced by

$$\overline{\rho} = \frac{1}{v} \sum \sigma^{(i)}, \tag{3.110}$$

we obtain the tensor

$$F = C - C_0 - CC_0^{-1}Z \tag{3.111}$$

whose components are generally non-zero. Importantly, however, the value of F can be estimated in an equilibrium simulation with $\varepsilon^{\mathrm{T}} = 0$. Thus, by performing several such simulations with different C, we can iteratively reduce F to zero. The effective elastic moduli determined in such a way will mimic the long-wavelength response of the inclusion, i.e. the simulation sample. Since the size of the sample can be systematically increased, $\overline{\rho}$ can approach $\tilde{\rho}$ arbitrarily closely. The simulations constructed in such a way will allow to sample glassy dynamics inside the inclusion more accurately than other approaches available at present, since it will not rely on the restrictive and physically unmotivated choice of either periodic of fixed boundary conditions. Thus Eq. (3.111) and the approach outlined above may be considered the central result of this Section.

3.4 A POINT STRESS AT THE CENTER OF SPHERICAL INCLUSION

If the inclusion contains a single source $\sigma^{(0)}$, located at its center (the origin of the coordinate system $\mathbf{r} = 0$),

$$\varepsilon^{s}(0) = G_0^{I}\sigma^{(0)}, \tag{3.112}$$

where $G_0^{I} = G^{I}(0,0)$ can be found from Walpole's result[100] on the second-order Green tensor using Eq. (A.10). Assuming the radius of $\mathcal{I}$ equal to $a/2$ we get from the general solution obtained in Appendix C,

$$G_0^{I} = \frac{2}{\pi\mu a^3}L[\xi_1\,,\xi_2]\,, \tag{3.113}$$

where

$$\begin{aligned}\xi_1 &= \frac{(1-2\nu_0)^2(1-\chi)}{\chi(1-\nu)(2+\nu_0\,[\chi-4]+\chi)},\\ \xi_2 &= 3\frac{4-5\nu}{5\nu\,(2\chi+1)-8\chi-7} - \frac{5\nu_0^2\,(\chi-8)+7\,(\chi-5)+3\nu_0\,(\chi+20)}{\chi\,(1-\nu_0)\,(5\nu_0\,[\chi-8]+7\,[\chi+4])}.\end{aligned} \tag{3.114}$$

In order to find $\partial\langle\overline{\rho}\rangle/\partial\varepsilon^{T}$ and subsequently write down the self-consistent equation for the tensor C we will use the constraint (3.71) to the magnitude of $\sigma^{(0)}$ and map the set of structural states available to $\mathcal{I}$ onto the rotations of unit 6-vectors τ, similar to how it was done in Section 3.2.3. First taking the volume average of ρ, Eq. (3.100), assuming a single source, we get

$$\overline{\rho} = \frac{\sigma^{(0)}}{v}. \tag{3.115}$$

Then, replacing the uniform ρ in Eq. (3.71) by $\overline{\rho}$ we express the constraint via $\sigma^{(0)}$

$$\frac{1}{2v}\sigma^{(0)}C_0^{-1}\,(I-S_0)\,\sigma^{(0)} = \frac{1}{2}g^2a^3 = \text{Const}, \tag{3.116}$$

Now we can relate $\sigma^{(0)}$ to the unit 6-vector by using the conversion rule similar to Eq. (3.74),

$$\sigma^{(0)} = ga^3 \mathrm{RU}\tau, \tag{3.117}$$

where R is given by Eq. (3.75), thereby Eq. (3.116) is equivalent to $|\tau| = 1$.

The rest of the calculation is completely analogous to that performed in Section 3.2.3. The resulting self-consistent equation for the effective elastic moduli has the same form as Eq. (3.90),

$$(\mathrm{I} - \mathrm{S}_0)\,(\mathrm{X} - \mathrm{I})\,(\mathrm{I} + [\mathrm{X} - \mathrm{I}]\,\mathrm{S}) = \theta \mathrm{L}\big[1 - 5s(q)\ , s(q)\big]\,, \tag{3.118}$$

where the parameter q is given by

$$q = \pi\theta\chi\left[\xi_1 \frac{1 - \nu_0^2}{(1 - 2\nu_0)^2} - 10\xi_2 \frac{1 - \nu_0}{7 - 5\nu_0}\right]. \tag{3.119}$$

The solution is presented in Fig. 13. We also provide, for the reader's reference, the result of the calculation using the constraint (3.73). The relation (3.117) is still valid in this case with, however, the tensor R is redefined as

$$\mathrm{R} \to \sqrt{\frac{v}{a^3}\mathrm{C}_0}. \tag{3.120}$$

Since the radius of $\mathcal{I}$ was set to $a/2$, $v/a^3 = \pi^3/8$. The equation for C has now the from

$$(\mathrm{X} - \mathrm{I})\,(\mathrm{I} + [\mathrm{X} - \mathrm{I}]\,\mathrm{S}) = \theta \mathrm{L}[1 - 5s(t)\ , s(t)]\,, \tag{3.121}$$

where

$$t = \frac{\pi}{3}\theta\chi\left[2\xi_1 \frac{1 + \nu_0}{1 - 2\nu_0} - 2\xi_2\right]. \tag{3.122}$$

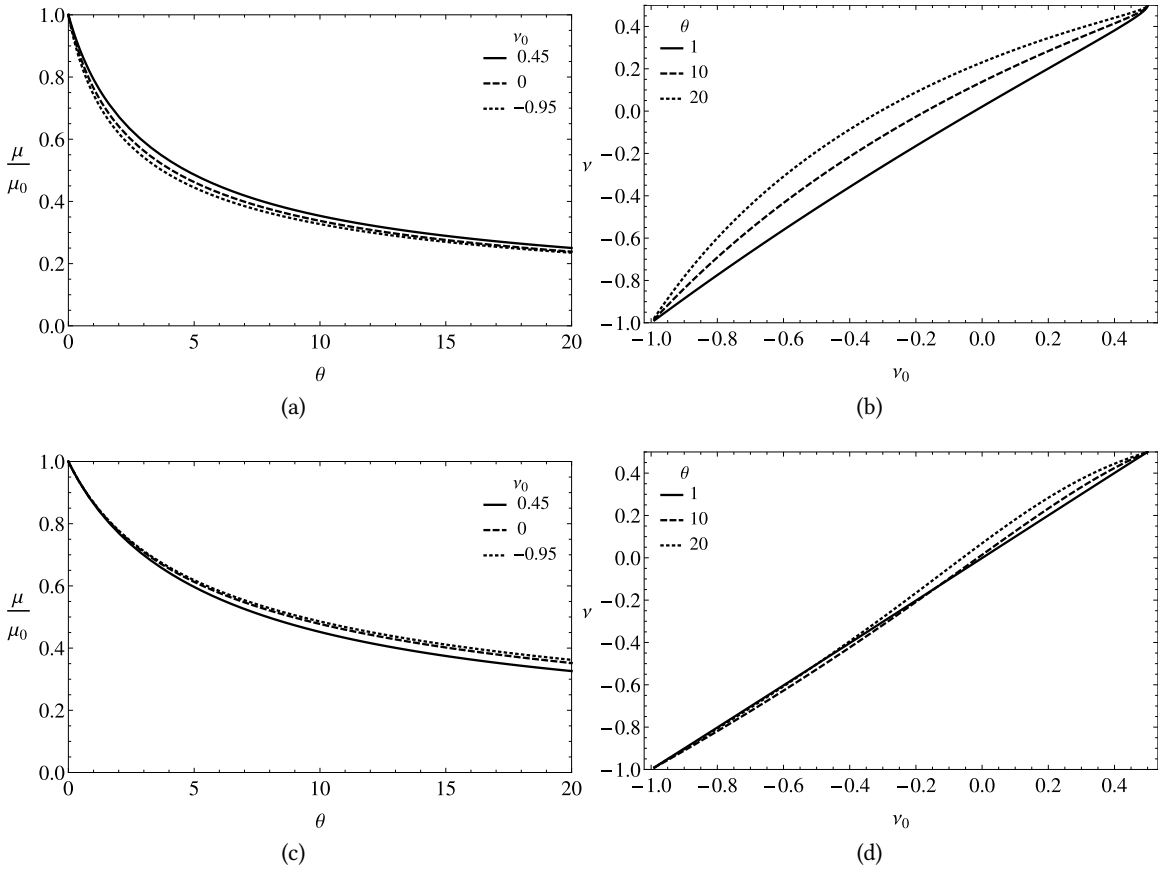

Figure 13.: Elastic moduli renormalization calculated using the model of a point stress source in the center of spherical inclusion. Figures (a) and (b) are solutions of Eq. (3.118). (a) Dependence of the ratio μ/μ_0 on $\theta = \beta g^2 a^3$ for different bare values of the Poisson ratio ν_0. (b) Dependence of the effective Poisson ratio ν on its bare value ν_0 for different θ. Corresponding solutions, when the constraint (3.73) is adopted, are given by (c) and (d) respectively (the solutions of Eq. (3.121)).

4

NUMERICAL SIMULATION OF THE 6-SPIN MODEL

4.1 GENERAL APPROACH

4.1.1 *Formulation of the model*

In the first part of this manuscript, we put forth a mapping between activated dynamics in supercooled liquids and a Heisenberg model for the frozen-in stress distribution ρ, Eq. (2.54). Here, we describe a Monte Carlo (MC) simulation developed to study thermodynamic properties of ρ and consequently, via the mapping, the properties of supercooled liquids. The simulational approach is a logical development of the cavity approximation for the elasticity of supercooled liquids studied in Chapter 3. In the present setup, the simulation volume $\mathcal{I}$ is part of a large body $\mathcal{B}$, see fig. 14. Outside the simulation volume, the elastic properties of $\mathcal{B}$ are taken into account in a mean field fashion as described in Chapter 3. Hereby, the spin dynamics in the environment are accounted for effectively by replacing bare elastic moduli of the matrix (the part of $\mathcal{B}$ outside $\mathcal{I}$) with their effective values. The cost of such a replacement is an elastic discontinuity at the boundary $\partial\mathcal{I}$ of the region $\mathcal{I}$. If the correlation length of ρ is smaller than the linear size of $\mathcal{I}$, such a mean field approximation is adequate for determining the effective elastic moduli of the matrix.[1] Conversely, this setup will allow for better sampling of the activate dynamics inside the simulation volume than other types of boundary conditions (BC), such as periodic or fixed BC, which would introduce an infinite number of spurious image charges.

1 See Section 3.1.1 for definition and discussion.

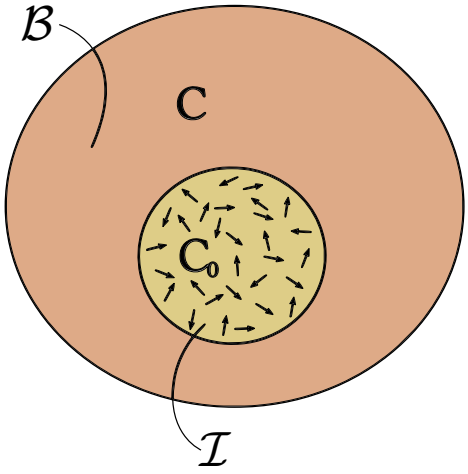

Figure 14.: The simulation setup. The simulation volume $\mathcal{I}$ is a sphere embedded into the matrix $\mathcal{B} \setminus \mathcal{I}$ with elastic moduli tensor C. The elastic moduli inside, C_0, and outside, C, $\mathcal{I}$ are different because the frozen-in stress ρ is treated explicitly inside $\mathcal{I}$, but only effectively outside. This is analogous to how one can treat the dielectric response of a liquid by either explicitly considering individual molecular dipoles or by using a dielectric constant $\epsilon \neq 1$. Arrows labels concentrated sources of stress $\sigma^{(i)}$ located on the random lattice given by $\mathbf{r}_i$.

For the purpose of simulation we adopt both the lattice approximation for the continuous tensor field $\rho(\mathbf{r})$,

$$\rho(\mathbf{r}) = \sum_i \sigma^{(i)} \delta(\mathbf{r} - \mathbf{r}_i). \tag{3.100 revisited}$$

and the long-wavelength approximation for the coupling tensor G,[2]

$$G(\mathbf{r}, \mathbf{r}') \approx G^{L}(\mathbf{r}, \mathbf{r}'), \tag{4.1}$$

where G^{L} is given by Eq. (3.105)

$$G^{L}(\mathbf{r}, \mathbf{r}') = \begin{cases} G^{A}(\mathbf{r}, \mathbf{r}') + G^{I}(\mathbf{r}, \mathbf{r}'), & \mathbf{r} \neq \mathbf{r}'; \\ G^{I}(\mathbf{r}, \mathbf{r}'), & \mathbf{r} = \mathbf{r}'. \end{cases} \tag{3.105 revisited}$$

2 For a sharp cutoff in $\mathbf{k}$-space, see Section 2.5, the long-wavelength limit is a quantitatively good approximation for the coupling starting from the third coordination shell.

To remind the reader, $G^{A}(\mathbf{r},\mathbf{r}')$ corresponds to the direct interaction between local units of frozen-in stress, while $G^{A}(\mathbf{r},\mathbf{r}')$ is the interaction mediated by the "image" charges stemming from the elastic discontinuity.

As in Chapter 3, we use C_0 and C to denote the bare elastic moduli of the inclusion and the effective moduli of the matrix respectively. The resulting Hamiltonian is obtained from Eq. (3.101) for the potential energy E of ρ inside the *spherical* inclusion in zero external field, $\varepsilon^{T} = 0$,

$$H = \frac{1}{2}\left(v g^2 + \sum_i \varepsilon^{S}(\mathbf{r}_i)\sigma^{(i)}\right) = \frac{1}{2}\left(v g^2 + \sum_{ij} \sigma^{(i)} G^{L}(\mathbf{r}_i,\mathbf{r}_j)\sigma^{(j)}\right), \tag{4.2}$$

where v is the volume of $\mathcal{I}$ and g is the order parameter of the crystal-to-glass transition, see Chapter 2. The latter corresponds to the frozen-in stress, as described in Section 3.3:

$$\eta(\mathbf{r})C_0\eta(\mathbf{r}) = \rho(\mathbf{r})C_0^{-1}\rho(\mathbf{r}) = \rho(\mathbf{r}_i)C_0^{-1}\rho(\mathbf{r}_i) = g^2 = \text{Const}, \tag{4.3}$$

We use the same equation to set a constraint on the magnitude of the localized sources of stress $\sigma^{(i)}$. Noting that $\sigma^{(i)}$ have the dimensions energy, we adopt the following correspondence between the continuous field ρ and the point sources $\sigma^{(i)}$:

$$\rho(\mathbf{r}_i) \to \frac{\sigma^{(i)}}{a^3}, \tag{4.4}$$

where a^3 is the volume per single point source corresponding to the volumetric size of a bead, see Chapter 2 for discussion. This expression results from the following equation relating the average of ρ over a lattice cell with the magnitude of the concentrated source of stress located in its center,

$$\frac{1}{a^3}\int\limits_{i\text{th lattice cell}} \rho \, dV = \frac{\sigma^{(i)}}{a^3}. \tag{4.5}$$

Thus, by Eq. (4.3),

$$\frac{\sigma^{(i)}}{a^3} C_0^{-1} \frac{\sigma^{(i)}}{a^3} = g^2,$$

which allows one to recast H in terms of *unit* 6-vectors $\tau^{(i)}$ defined via[3]

$$\sigma^{(i)} = g a^3 C_0^{1/2} \tau^{(i)}. \tag{4.6}$$

The resulting expression for H is

$$\frac{H}{a^3 g^2} = \frac{1}{2} \left(\tilde{v} + \sum_{ij} \tau^{(i)} Y^{(ij)} \tau^{(j)} \right), \tag{4.7}$$

where $\tilde{v} = v/a^3$ and

$$Y^{(ij)} = a^3 C_0^{1/2} G^{L}(\mathbf{r}_i, \mathbf{r}_j) C_0^{1/2}. \tag{4.8}$$

Note that in the equation above, tensors do not commute with each other since the tensor G^{L} is not isotropic. Also, we *do not use* the summation convention for superscripts.

The model given by Eq. (4.7) is a Heisenberg model with six-component classical spins defined on a lattice in three spacial dimensions. Using the notation [ ] to denote the dimensions of a given quantity, we have:

$$\begin{aligned}
[g] &= (\text{energy density})^{1/2}, \\
[\rho] &= \text{energy density}, \\
\left[\sigma^{(i)}\right] &= \text{energy}, \\
\left[\tau^{(i)}\right] &= 1, \\
[C_0] &= \text{energy density}, \\
[G^{L}] &= (\text{energy})^{-1},
\end{aligned}$$

3 See Chapter 3 for the other examples of such transformation and discussion of its physical significance.

$$[\mathrm{Y}] \quad = \quad 1.$$

Thus, the rhs of Eq. (4.7) is dimensionless; this is the final form of the Hamiltonian studied in the MC simulation, as described below.

The main difference between the model (4.7) and the existing models of glassy systems studied by MC simulations is that the interaction matrix $\mathrm{Y}^{(ij)}$ is not a random matrix and so *no* quenched disorder is assumed at the onset. According to Eq. (3.105), the interaction is a sum of two parts, G^{A} and G^{I}, both of which can be calculated from the corresponding second-order Greens tensors γ^{A} and γ^{I} using Eq. (A.10). For G^{A} we obtain,

$$\begin{aligned} &16\pi\mu_0(1-\nu_0)|\mathbf{r}_o-\mathbf{r}_s|^3 G^{\mathrm{A}}_{ijlm}(\mathbf{r}_o,\mathbf{r}_s) = \delta_{ij}\delta_{kl} - (1-2\nu_0)\left(\delta_{jk}\delta_{il}+\delta_{ik}\delta_{jl}\right) \\ &- 3\left(\delta_{ij}n_k n_l + \delta_{kl}n_i n_j\right) - 3\nu_0\left(\delta_{ik}n_j n_l + \delta_{jk}n_i n_l + \delta_{il}n_j n_k + \delta_{jl}n_i n_k\right) + 15 n_i n_j n_k n_l, \end{aligned} \tag{4.9}$$

where

$$n_i = \frac{x_i^o - x_i^s}{\mathbf{r}_o - \mathbf{r}_s},$$

and $\mathbf{r}_s$ and $\mathbf{r}_o$ are position vectors for the source and observation points, while x_i^s and x_i^o label corresponding vector components. This is a well known equation studied in the context of orientational glasses,[57], TLS,[54–56], as well as structural glasses in general.[14] The expression for the image field Green tensor G^{I}, given in app. C, Eq. (C.5), is much more complex, and has not been studied previously. Note that both G^{A} and G^{I} are explicitly proportional to μ_0^{-1}. Since $\mathrm{C}_0 \propto \mu_0$, $\mathrm{C}_0^{1/2}\mathrm{G}^{\mathrm{A}}\mathrm{C}_0^{1/2}$ depends on the bare value of the Poisson ratio ν_0 only. Also it is obvious, by elementary dimensional analysis, that G^{I} is a function of $\chi = \mu_0/\mu$. Thus, in general $\mathrm{Y}^{(ij)}$ is a function of five variables

$$\mathrm{Y}^{(ij)} = \mathrm{Y}^{(ij)}(\chi, \nu_0, \nu, a, R), \tag{4.10}$$

where R is the radius of $\mathcal{I}$.

Since we use spherical samples, the most convenient choice for the lattice is random close packed (RCP). In practice, we have generated samples with a given number of lattice points by cutting spherical chunks from several large ($N = 10^5$) RCP lattices generated[4] using the Bennett algorithm.[101] The nearest neighbor distance in the Bennett algorithm was set to unity; accordingly, we use $a = 1$. The full algorithm for sample generation and computations of the interaction is described in Appendix D.

4.1.2 *The algorithm for the Monte Carlo simulation*

A frequent problem encountered in simulations of a cooperative phenomena is a critical slowing down or trapping in metastable states that often occur in the most interesting parameter range. This problem is especially severe for glassy models such as the one studied here. There are many algorithms which are designed to improve sampling close to a transition point. The combination of algorithms often used in the context of short-range Heisenberg spin glasses in three dimensions [102–104] consists of the heat bath [105] and over-relaxation [106] spin update algorithms, augmented by employing temperature exchange,[107] also called simulated tempering. Such an approach allows one to study critical properties of the systems: still, achieving equilibration is very difficult.[103] It is fair to say that Heisenberg glasses in three dimensions represent one of the most difficult system for numerical studies. The long-range character of interaction in our model is expected to make equilibration of a simulation sample even more problematic.

Another important feature of the present model is that the diagonal term of the interaction matrix is non-zero; it contains the image field part of the interaction:

$$\mathrm{Y}^{(ii)} = a^3 \mathrm{C}_0^{1/2} \mathrm{G}^{\mathrm{I}}(\mathbf{r}_i, \mathbf{r}_i) \mathrm{C}_0^{1/2} \neq 0.$$

4 The MATLAB implementation of the Bennett algorithm was done by Pyotr Rabochiy.

This term describes the self-interaction of the spin $\tau^{(i)}$ and makes it impossible to use both heat bath and over-relaxation methods, in their standard formulations. To show this, consider a change of the energy upon rotation of a single spin

$$\tau^{(k)} \to \tilde{\tau}^{(k)} = \tau^{(k)} + \Delta\tau.$$

Energy of the new configuration H_{fin} is given by

$$\begin{aligned}\frac{2H_{fin}}{g^2a^3} - \tilde{v} &= \sum_{pq}\left(\tau^{(p)} + \Delta\tau\delta_{pk}\right)\Upsilon^{(pq)}\left(\tau^{(q)} + \Delta\tau\delta_{qk}\right)\\ &= \sum_{pq}\left[\tau^{(p)}\Upsilon^{(pq)}\tau^{(q)}\right] + \sum_{p}\left[\tau^{(p)}\Upsilon^{(pk)}\Delta\tau + \Delta\tau\Upsilon^{(kp)}\tau^{(p)}\right] + \Delta\tau\Upsilon^{(kk)}\Delta\tau,\end{aligned}$$

which after a rearrangement gives for the energy change upon the update of the k-th spin, $\Delta H^{(k)} = H_{fin} - H_{in}$,

$$\frac{2\Delta H^{(k)}}{g^2a^3} = \Delta\tau\left(\Upsilon^{(kk)}\Delta\tau + \varsigma^{(k)}\right), \tag{4.11}$$

where $\varsigma^{(k)} = \sum_p\left[\Upsilon^{(kp)} + \left(\Upsilon^{(kp)}\right)^\top\right]\tau^{(p)}$, see Eq. (B.7). It follows from Eq. (4.11) that at every spin update in the MC simulation, the corresponding energy penalty is quadratic depending on the spin increment $\Delta\tau$, which is a direct consequence of the BC choice of the BC. This is a very minor complication, if the spin is updated using the Metropolis algorithm,[106] as compared to, e.g., the Heisenberg model on a periodic lattice, where $\Upsilon^{(kk)} = 0$. However, it is known that the Metropolis algorithm, while effective for studies of systems with discrete spins, is a poor choice for classical spin models: randomly generated orientation of spins often result in a large energy increase and, thus, in a low acceptance ratio. A better choice for the spin update algorithm for classical spin models is the heat bath algorithm,[105] where the updated spin orientation is not

generated randomly but taken from the Boltzmann distribution for the spin. In our case, it has the form:

$$P^{(k)} = \frac{1}{A^{(k)}} e^{-\beta \Delta H_k}, \tag{4.12}$$

where $A^{(k)} = \int \mathrm{d}\Omega_6 \exp[-\beta \Delta H_k]$ and the integration is over all possible directions of $\Delta\tau$. If $\Upsilon^{(kk)} = 0$, this distribution becomes identical (apart from the higher dimensionality of the spin) to the one considered in Ref. [105]. Then, owing to the simple form of $\Delta H^{(k)}$, the normalization factor $A^{(k)}$ can be analytically calculated and the distribution $P^{(k)}$ can be inverted. This allows one to devise a method for generating random numbers with the distribution (4.12) for any value of the local field $\varsigma^{(k)}$.[108, chap. 2] In our case, however, this is not possible, since the normalization factor can be analytically found only for a spin located exactly at the center of a spherical simulation volume $\mathcal{I}$. For all other spins, $P^{(k)}$ is not known analytically and, thus, it is not possible to invert the distribution.

The same problem precludes implementation of the over-relaxation method, which takes advantage of energy conserving local spin motion.[106] In the conventional Heisenberg model, such motion is precession of a spin around the local magnetic field acting. In our system, energy conserving trajectory is more complex owing to the presence of self-interaction. Essentially, it is a six-dimensional rotation that satisfies equation $\Delta H^{(k)} = 0$,

$$\Delta\tau \left(\Upsilon^{(kk)} \Delta\tau + \varsigma^{(k)} \right) = 0. \tag{4.13}$$

for the rotation of spin $\tau^{(k)}$. Solutions of this equation are subject to the obvious constraint,

$$|\tau^{(k)} + \Delta\tau| = 1 \qquad \Leftrightarrow \qquad \Delta\tau \left(\Delta\tau + 2\tau^{(k)} \right) = 0. \tag{4.14}$$

It turns out, however, that in order to find a non-trivial solution for $\Delta\tau$ we need to solve, in general, a cubic equation. In order to show this we diagonalize the interaction matrix $\Upsilon^{(kk)}$ from Eq. (4.8),

$Y^{(kk)} = Q^\top D Q$, where D and Q are diagonal and orthogonal matrices respectively, and introduce three new 6-vectors: $\omega = Q\Delta\tau$, $\psi = Q\varsigma^{(k)}$, and $\beta = 2Q\tau^{(k)}$. Subsequently, we can rewrite the system of equations (4.13) and (4.14) as

$$\begin{cases} \sum_{\alpha=1}^{6} \left(\lambda_\alpha \omega_\alpha^2 + \psi_\alpha \omega_\alpha \right) = 0, \\ \sum_{\alpha=1}^{6} \left(\omega_\alpha^2 + \beta_\alpha \omega_\alpha \right) = 0, \end{cases} \tag{4.15}$$

and look for non-trivial solution. Since the system of equations (4.15) is underdetermined, we can assume that $\omega_3 = \omega_4 = \omega_5 = \omega_6 = 0$, which yields

$$\begin{cases} \omega_1 \left(\lambda_1 \omega_1 + \psi_1 \right) + \omega_2 \left(\lambda_2 \omega_2 + \psi_2 \right) = 0, \\ \omega_1 \left(\omega_1 + \beta_1 \right) + \omega_2 \left(\omega_2 + \beta_2 \right) = 0. \end{cases} \tag{4.16}$$

Finding non-trivial solutions of (4.16) is geometrically equivalent to finding intersection points of an ellipse and a circle, which also cross at the origin of a coordinate plane. It is clear that in general there are up to three solutions and thus system (4.15) can not be reduced to finding roots of a polynomial with degree lower than three. While an analytic solution is still possible using the Cardano formulas, we will not proceed along this route since the resulting procedure is likely to be computationally slow.

To summarize, implementation of MC for systems with self-interaction is a new problem. We are not aware of previous attempts of this sort. At the same time, development and optimization of new algorithms for the type of BC considered here should be done after it is clear that our approach gives insights into the physics of glasses valuable enough to justify the effort. Thus for the simulations reported here we used only already developed methods: the Metropolis algorithm for spin updates combined with the temperature exchange technique.[107] This limits our study to systems with a modest number of spins of about several hundreds. This size should be sufficient to

see the RFOT predicted cooperativity, nevertheless. According to Lubchenko and Wolynes,[16] the cooperative size at the crossover temperature is only about 40 beads.

4.2 TEMPERATURE EXCHANGE MONTE CARLO AND THE ACTIVATED DYNAMICS

Temperature exchange Monte Carlo (MC) is an algorithm intended to improve sampling in MC simulations on complex energy landscapes characteristic of, e.g., spin glasses.[107] For such models, the acceptance ratio of any spin update algorithm becomes very small at low enough temperatures and the system can be effectively trapped in a local metastable minimum of the potential energy surface (PES). Thus, it is difficult to establish thermodynamic averages, which requires fair sampling of the PES.

In the temperature exchange algorithm, several copies (or replicas) of the system with different inverse temperatures θ_i,

$$\theta_i = \beta_i g^2 a^3, \tag{4.17}$$

are simulated *simultaneously* and *independently*. The temperature points must be distributed in such a way that θ_1^{-1}, the highest temperature, is high enough for the system to be equilibrated comparatively easily given specific computational resources. The lowest temperature, however, is often in a region where equilibration is problematic. In the course of the simulation, regular spin updates are performed in individual replicas at their respective temperatures. Occasionally, a temperature exchange trial between copies is performed. The probability of a temperature exchange is determined by the energy difference of the copies so as to preserve the detailed balance.[107] When a copy acquires a higher temperature, it can escape a metastable minimum and reach a new, dissimilar spin configuration. At the same time, when a copy decreases its temperature after the exchange, it becomes localized in an different part of the PES from that of its exchange partner. Thus, after a large number of temperature exchanges, a good sampling of different parts of the PES

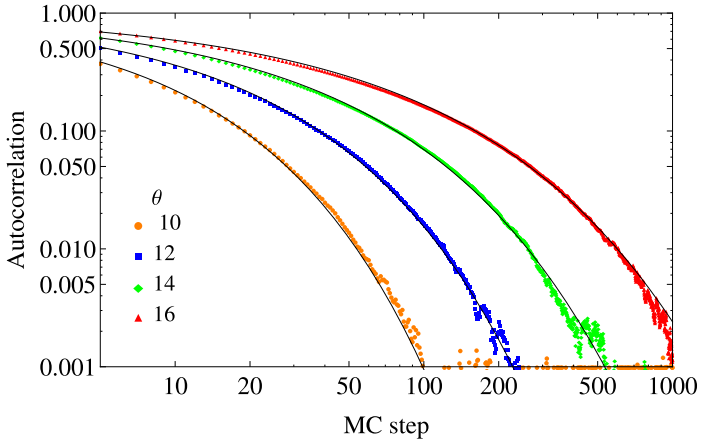

Figure 15.: Auto-correlation function, Eq. (4.18), measured using the simple Metropolis MC without temperature exchange. The solid lines are obtained by a fit with the stretched exponential function, $\exp[-t/t_c]^{\beta_c}$. The simulation is done for $N = 50$, $\chi = 0.6$, $\nu_0 = 0.1$ and $\nu = 0.11$. The MC step is defined as a single full sweep of the sample with the Metropolis algorithm.

can be achieved. The latter is necessary for obtaining an unbiased estimate of any thermodynamic quantity.

4.2.1 *Correlation functions without temperature exchange*

Before beginning the simulation, which will allow us to establish the thermodynamic properties of the model (4.7), we need to accomplish several preparatory steps. First, we determine the highest temperature of the simulation θ_1^{-1}. This temperature is essentially determined by the computational resources : it should be the lowest temperature at which proper equilibration by the Metropolis algorithm is feasible, without temperature exchange. To this end, we have performed the Metropolis MC without temperature exchange to determine the auto-correlation function of the system. The auto-correlation function is defined as

$$c(t) = \frac{1}{N}\sum_i \langle \tau^{(i)}(t_0 + t)\tau^{(i)}(t_0)\rangle, \tag{4.18}$$

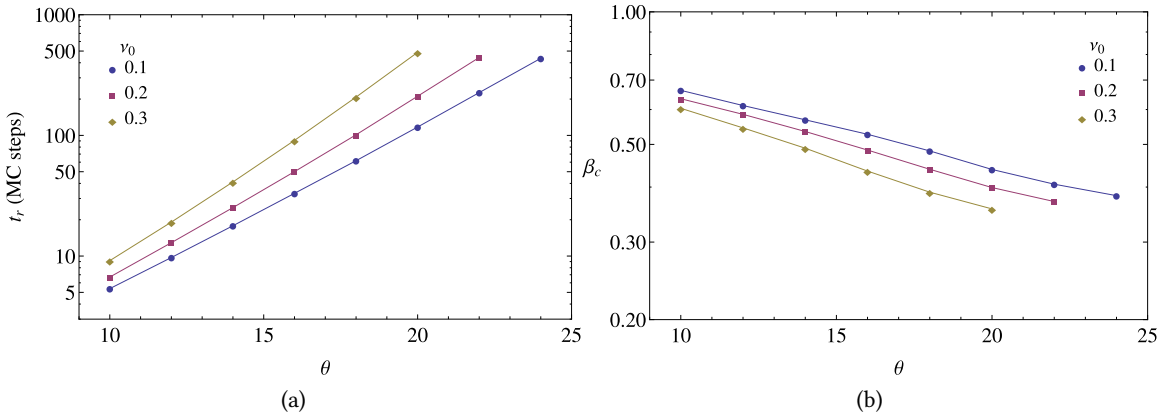

Figure 16.: Temperature dependence of the stretched exponential parameters t_r and β_c, Eq. (4.19), for several values of the Poisson ratio ν_0 inside the simulation volume; $N = 50$, $\chi = 0.6$ and $\nu = 0.11$. The MC step is defined as a single full sweep of the lattice with the Metropolis algorithm.

and is expected to be an exponential function of time for high enough temperatures.[106] Contrary to this expectation we obtain stretched-exponential profiles:

$$c(t) = \exp\left[-\frac{t}{t_r}\right]^{\beta_c}, \tag{4.19}$$

see Fig. 15. Stretched-exponential relaxation is an archetypal feature of glassy dynamics.

The relaxation time t_r and the stretched exponent parameter β_c were obtained for several different combinations of the elastic moduli in the simulation volume and the surrounding matrix. It was found, see Fig. 16, that t_r increases and β_c decreases with the bare value of the Poisson ratio ν_0. The dependence of the ratio on the shear moduli, $\chi = \mu_0/\mu$, is much weaker (not shown on Fig. 16). Importantly, both quantities increase with the inverse temperature θ; the growth law for the relaxation time t_r is super-Arrhenius, a typical feature seen in supercooled liquids. We notice that already at the high temperature from Fig. 16, the relaxation profiles are strongly non-exponential, implying non-trivial dynamics. One may wonder how such small systems could exhibit significant memory effects or a distribution of relaxation times as broad as that transpiring from Fig. 16(b). We remind, however, that an individual point source of stress generically corresponds to several

atoms, and so the physical size in question corresponds to several hundred atoms! On a formal side, the non-exponentiality may stem from the large number, 6, of the spin components, complicated interactions, and the corresponding difficulty in equilibration. It is possible that the frustration present in the spin-spin interaction from Eq. (4.8) sufficiently reproduces the typical frustration in liquids due to mismatch between cohesive forces and steric repulsion.

Last, but not least, Fig. 16(b) indicates that substances with higher values of the Poisson ratio should exhibit relatively more non-exponentiality. This is consistent with results of Chapter 2 and the RFOT theory. Indeed, the parameter $\beta_c \simeq k_B T/\delta F$, where δF is the width of the barrier distribution.[9] On the other hand, $\delta F \propto m$, the fragility index, which is greater for fragile substances. Consistent with these observations, the T-dependence of the relaxation time t_r in Fig. 16(a) becomes more non-Arrhenius with μ_0. Again, this is a signature of the fragile behavior.[8]

4.2.2 *Temperature exchange Monte Carlo simulation*

Having at our disposal the results obtained in the preparatory simulation, we setup the temperature exchange simulation in the following fashion. First, the highest temperature in the simulation is selected as $\theta_1 = 15$. Then, noting that the auto-correlation function drops to about 0.15 after 100 full sweeps of the sample with the simple Metropolis MC, we adopt 100 as the number of full lattice sweeps, N_{fs}, between temperature exchange trials. According to the algorithm,[107] the temperature exchange is done in two steps:

- "Even" exchange: $\theta_1 \rightleftarrows \theta_2$, $\theta_3 \rightleftarrows \theta_4 \ldots \theta_{M-1} \rightleftarrows \theta_M$;
- "Odd" exchange: $\theta_2 \rightleftarrows \theta_3$, $\theta_4 \rightleftarrows \theta_5 \ldots \theta_{M-2} \rightleftarrows \theta_{M-1}$,

where M is the total number of the temperature points.[5]

5 Note that M must be even for the algorithm to work.

The next important quantity we must determine is the *step* of the MC simulation, which provides a measure of a MC simulation length. We define it in the following way: First we perform the "even" temperature exchange trial. Then the simulation is continued for N_{fs} Metropolis updates of the sample for every temperature point. Next, the "odd" temperature exchange trial is performed, followed by another N_{fs} lattice sweeps. This combination constitutes a single step of our temperature exchange simulation.

The next step in the preparation is the optimization of the temperature point. It is done by using 20 iterations of the algorithm introduced by Kerler and Rehberg (for every size of the sample).[109] For a starting distribution of temperature points, we adopt an equidistant one,

$$\theta_m = \theta_1 + (\theta_M - \theta_1)\,\frac{m-1}{M-1}. \tag{4.20}$$

We point out that there is an optimal total number of temperature points M for a specific combination of system size and parameter values. If M is too small, the probability of temperature exchange will be very low because the corresponding energy difference between copies is large. The convergence of the temperature optimization algorithm can be poor under these circumstances. If, on the other hand, the number of temperature points is too large, the transition from the lowest temperature to the highest one will be slow owing to the large number of intermediate steps. The time needed for such a transition is a fundamental characteristic of the temperature exchange algorithm; it is usually called the ergodicity time.

The ergodicity time t_{E} is defined as the average number of the MC steps required for a copy starting at the lowest temperature to reach the highest temperature point of the simulation. Since the highest temperature of the simulation allows for fast equilibration, t_{E} represents the average number of MC steps after which the simulation reaches a statistically independent state. Thus, we have used t_{E} as the time between measurements in the simulation. The results of the simulation

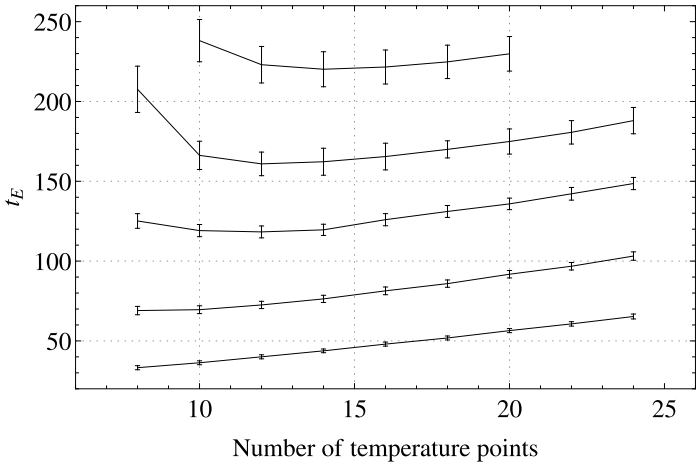

Figure 17.: The ergodicity time as a function of the total number of temperature points for different sample sizes N. The highest and the lowest temperatures of the simulation are $\theta_1 = 15$ and $\theta_M = 50$. The calculation is done after 20 iteration of the temperature optimization algorithm.[109] The data reported for $N = 10$, 20, 30, 40, and 50. Lower lines correspond to lower value of N. Error bars are estimated based on averaging over 20 different samples for each size.

performed to determine t_{E} are reported in Fig. 17. It follows from the graph that there is indeed an optimal number of temperature points for each size of the system.

Based on these results, we have subsequently chosen other parameters for the temperature exchange simulation, as summarized in Table 1. To test the resulting sampling quality, we have estimated the auto-correlation $c(t)$ in the temperature exchange simulation, see Fig. 18(a). The temperature exchange indeed leads to good sampling producing exponentially decreasing auto-correlation function,

$$c(t) \propto \exp\left[-\frac{t}{t_c}\right]. \tag{4.21}$$

The estimated correlation time t_c, Fig. 18(b), is close to half of t_{E} reported in Table 1, which is consistent with the conventional choice of the step between measurements in MC simulations.[6]

6 As the rule of thumb the simulation step between measurements in any MC simulation should be about twice larger the value of the correlation time for corresponding temperature.

N	N_{tp}	t_{E}
10	12	50
20	12	80
30	12	125
50	14	235
90	20	465

Table 1.: Parameters of the temperature exchange MC simulation. N is the number of spins in the sample, N_{tp} is the number of temperature points selected based on the optimal ergodicity time values t_{E} acquired from Fig. 17.

4.2.3 *The thermodynamics of the model*

Using the simulation setup outlined above, we have performed measurements of the potential energy E and heat capacity. Specifically, we have measured the interaction portion

$$E = \frac{H}{g^2 a^3} - \frac{1}{2}\tilde{v} = \frac{1}{2}\sum_{ij} \tau^{(i)} \mathrm{Y}^{(ij)} \tau^{(j)}, \tag{4.22}$$

cf. Eq. (4.7). The heat capacity is estimated in the standard fashion from the fluctuations of the energy, see, e.g., [110, §3.6]:

$$\frac{c}{N} = \frac{\beta^2}{N}\left(\langle E^2\rangle - \langle E\rangle^2\right). \tag{4.23}$$

The results for a broad temperature range are reported in Fig. 19. Each line in the figure consist of high- and low-temperature parts determined in independent simulations. Also we have tested for equilibration by performing a longer simulation with $N_{fs} = 200$. The results are identical to those reported in Fig. 19 and are not shown. Everywhere below error bars are estimated based on simulations for 20 different samples for each system size N.

It is evident from the data presented in Fig. 19 that the system experiences a crossover to a low-temperature regime centered at about $\theta \approx 30$ as evidenced by a mild peak in the T-dependence of the heat capacity. In Fig. 20 we also plot results of simulations for the critical region only, adding

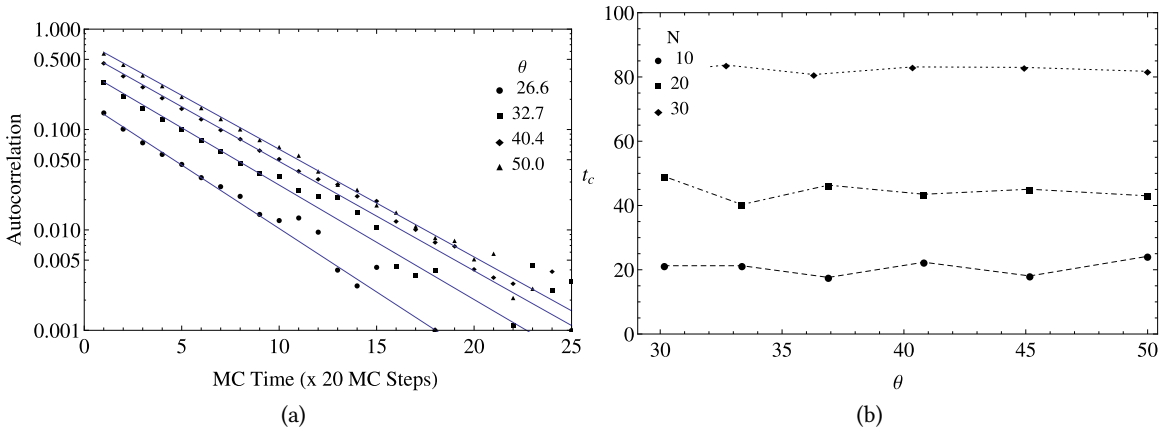

Figure 18.: Auto-correlation function for the temperature exchange MC simulation. (a) Example of the auto-correlation function for $N = 30$. It is evident that $c(t) \propto \exp(t/t_c)$. (b) Correlation time t_c for different samples. Note that t_c does not depend on the temperature and is about $\frac{1}{2}t_{\mathrm{E}}$ consistent with what is expected for the correctly configured temperature exchange simulation. $\chi = 0.71$. $\nu_0 = 0.08$, $\nu = 0.15$.

data for $N = 50$ and $N = 90$. Finite size effects are clearly evident, which is not surprising for such small samples. The latter effects stem mainly from the ruggedness of the boundaries which is expected to become less pronounced for larger samples. It is important to stress, however, that the boundary conditions for this set of simulations were not optimized according to the procedure developed in Section 3.3.

4.2.4 *Dynamics of the model in high- and low-temperature regimes*

We now turn to the next key subject of the present study: the dynamics of the system at low temperatures. In the present MC framework, the dynamics can be recovered from the properties of the PES. We use the following method: After a long equilibration run (in practice using the final spin configuration achieved in the simulation runs discussed in the preceding section) we follow the trajectory of the system in the course of the MC simulation at a constant temperature constant.

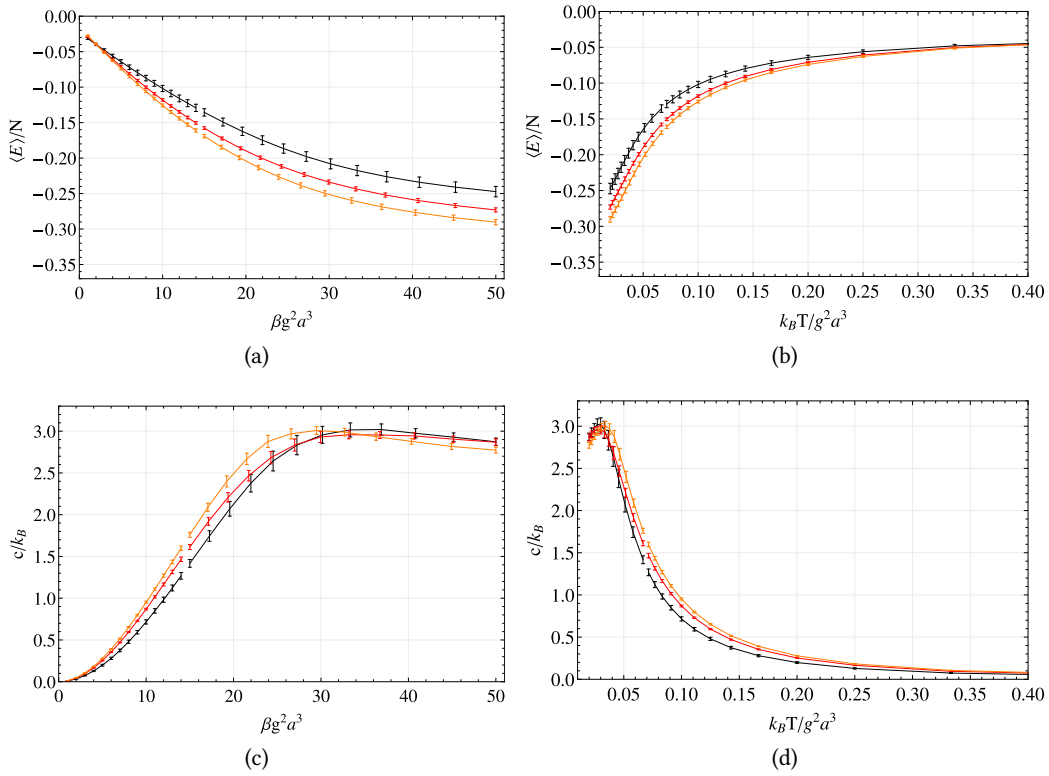

Figure 19.: Potential energy E and heat capacity determined in the temperature exchange MC simulation. Colors label different sample sizes: black for $N = 10$, red for $N = 20$, and orange for $N = 30$. As before $\chi = 0.71$. $\nu_0 = 0.08$, $\nu = 0.15$. Error bars are given base on averaging over 20 different samples for each system size.

The spin state and the energy are written to a file at every lattice sweep which is selected as a unit of time for the simulation reported in this section. We also follow the parameter q,

$$q(\Delta t) = \sum_i \tau^{(i)}(t_0)\tau^{(i)}(t_0 + \Delta t), \tag{4.24}$$

defining the correlation between the spin state at the beginning of the trajectory and after Δt time steps. At the same time, we find energy minima corresponding to the state of the system at each point along the trajectory. This was done by numerically minimizing E, Eq. (4.22), using the Newton algorithm with the initial guess for the search of the energy minimum given by the spin

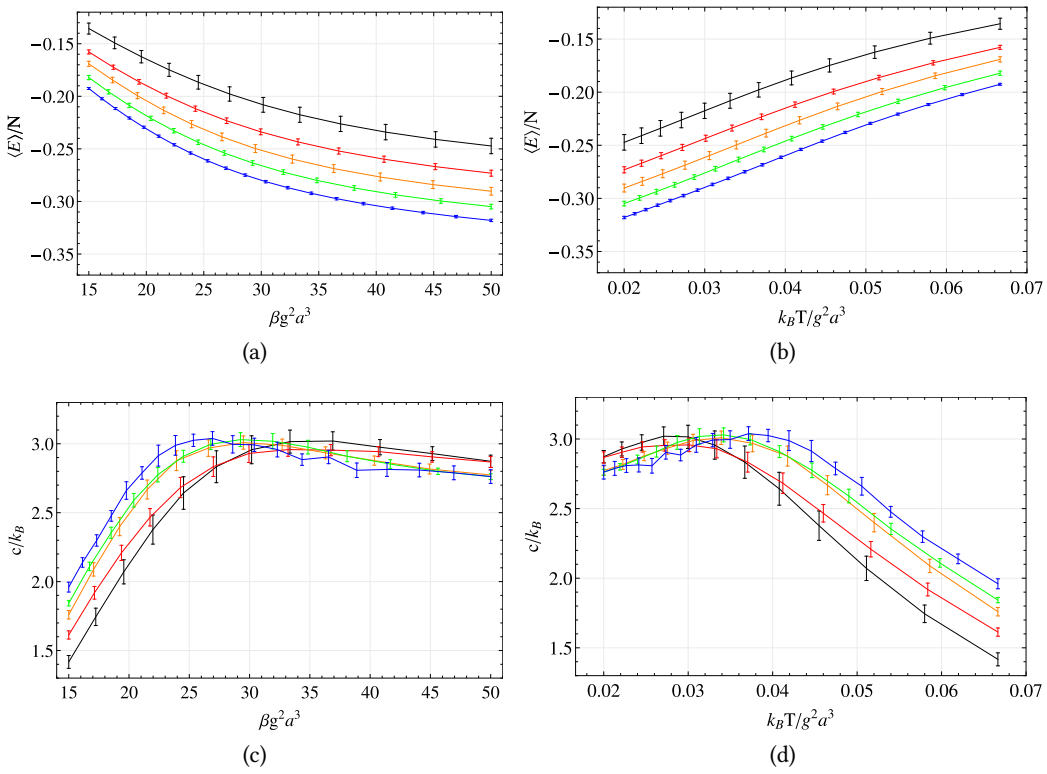

Figure 20.: Potential energy E and heat capacity determined in the temperature exchange MC simulation. Colors label different sample sizes: black for $N = 10$, red for $N = 20$, orange for $N = 30$, green for $N = 50$, and blue for $N = 90$. As before, $\chi = 0.71$. $v_0 = 0.08$, $\nu = 0.15$. Error bars are given based on averaging over 20 different samples for each system size.

configuration at the corresponding step of the simulation. In the present hardware setup,[7] this procedure allowed an accurate descend into a local minima of PES for up to $N = 50$.

Representative results of this procedure for the high-temperature regime $\theta = 20$ and $N = 50$ are shown in Fig. 21. Note that $\theta = 20$ is quite close to the crossover temperature. The results of energy minimization along the trajectory are quite distributed, see Fig. 21(c). The fast drop of the overlap parameter q, Fig. 21(b), shows that the spin configurations in the local minima of the PES corresponding to the nearest points on the simulation trajectory are very different from each

7 The energy minimization was performed using MATHEMATICA on the workstation with two Xeon E5450 CPUs (3.00GHz). For $N = 50$ the procedure requires about 16 Gb of RAM.

other. Note that the beginning of the trajectory was selected at random. Such behavior is expected based on the properties of the Metropolis algorithm for the high-temperature phase. Analysis of the difference between spin configurations shows that after 10 lattice sweeps (the step of the minimization procedure) essentially all the spins in the sample change their orientation. This is consistent with the histogram of q as a function of E shown in Fig. 21(d). It is evident that the simulation samples a wide basin on the PES centered at $q = 0$. On the other hand, two peaks in the histogram reflect a coarse-grained structure of the basin corresponding to two broad local energy minima. Interestingly enough we can distinguish two distinct motifs in the plot of the minimum energy as well, see Fig. 21(c).

A completely different picture is obtained for the low-temperature regime, $\theta = 40$, see Fig. 22. Despite variations of the energy along the trajectory the minimization shows that the system is trapped close to 4 metastable energy minima. This is reflected in Fig. 22(b) displaying slow relaxation of the overlap parameter q. The corresponding histogram of $q(E)$, Fig. 23(a), displays 4 distinct peaks. In Fig. 23(b-d) we visualized[8] the *difference* between the strain corresponding to the spin configurations in the energy minima:

$$\mathrm{C}^{-1/2}\left[\tau^{(i)}(t_0 + \Delta t_i) - \tau^{(i)}(t_0)\right], \qquad i = 1, 2, 3, \tag{4.25}$$

corresponding to energy minima reported in Fig. 22(c).

8 The visualization is performed in MayaVi.

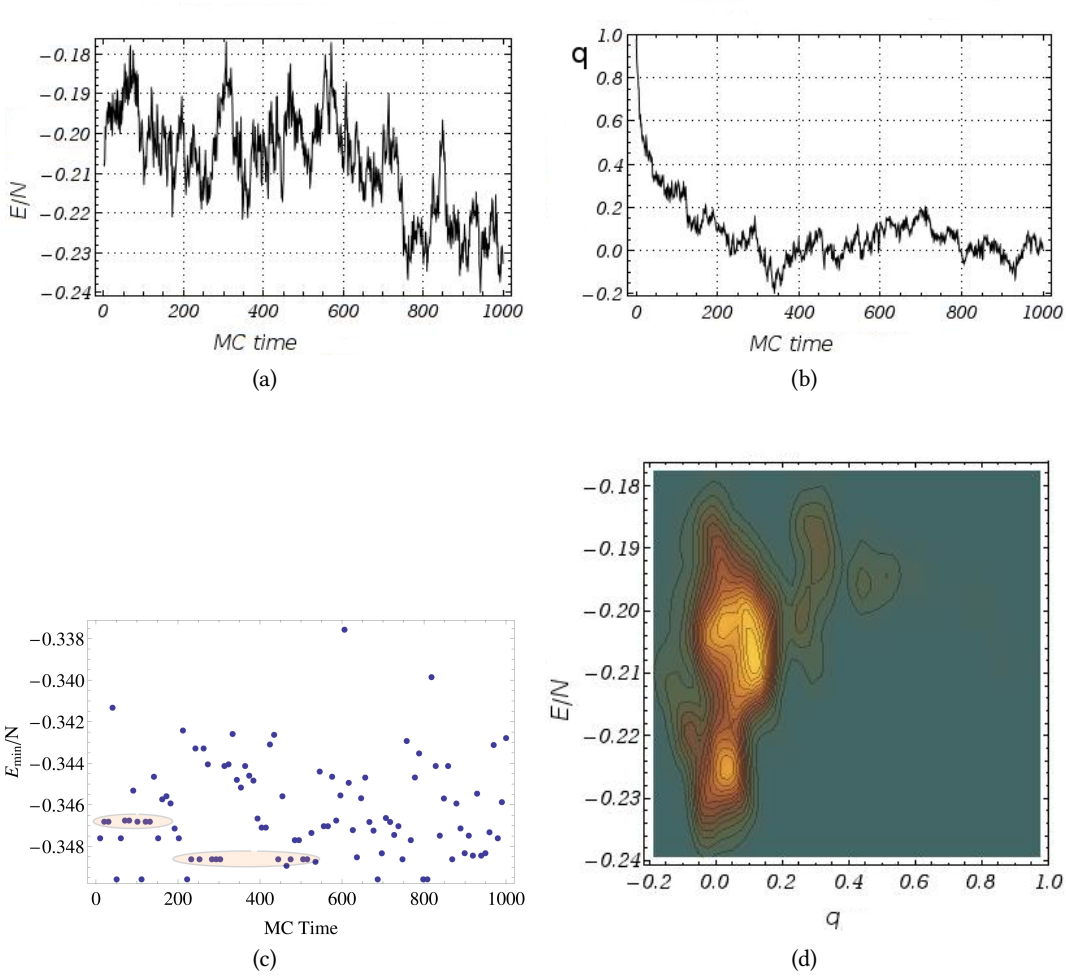

Figure 21.: Analysis of a Monte Carlo (MC) simulation trajectory in the high-temperature regime: $\theta = 20$, $N = 50$, $\chi = 0.71$, $\nu_0 = 0.08$, and $\nu = 0.15$. (a) Energy of the system as a function of time. The unit of time corresponds to a single sweep of the sample by the Metropolis algorithm. (b) Relaxation of the overlap parameter q along the trajectory. (c) Results of minimization of E along the trajectory using the Newton algorithm. The energy of local minima on PES are widely distributed; however, they do exhibit two distinct motifs in the beginning and near the middle of the trajectory. (d) Histogram of the q values a function of E.

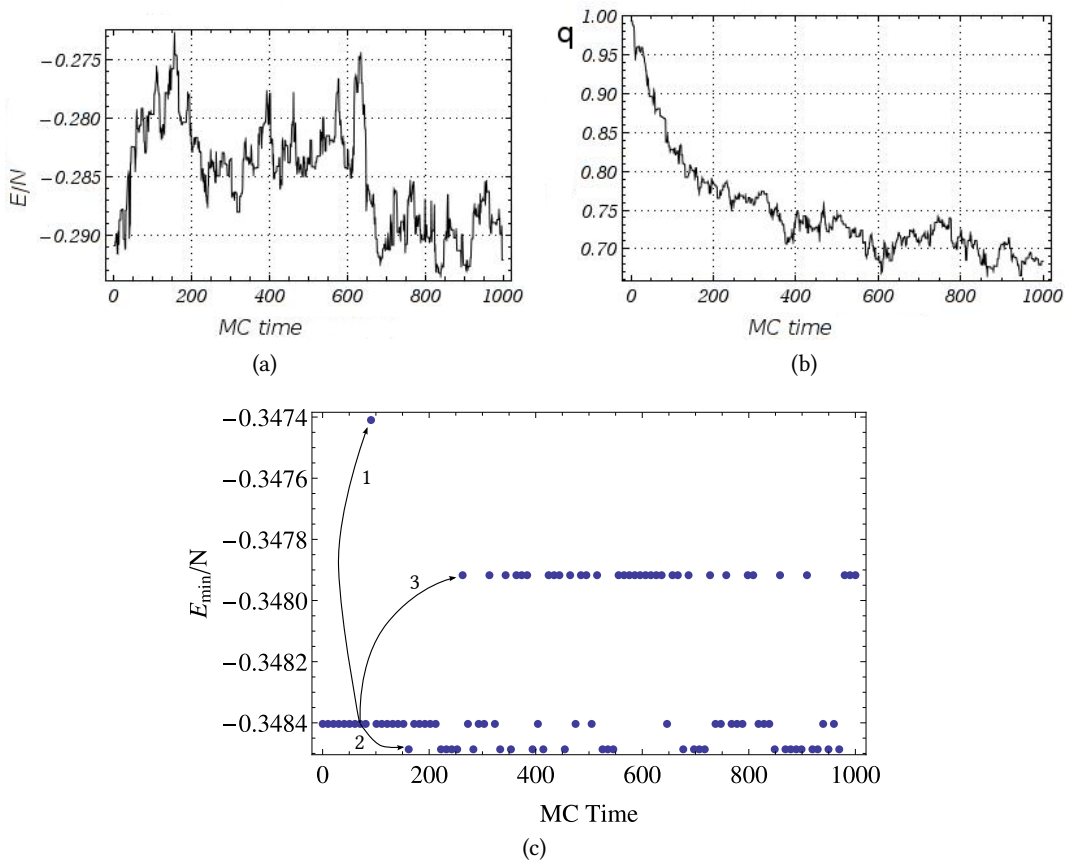

Figure 22.: Analysis of a Monte Carlo (MC) simulation trajectory in the high-temperature regime: $\theta = 40$, $N = 50$, $\chi = 0.71$, $\nu_0 = 0.08$, and $\nu = 0.15$. (a) Energy of the system as a function of time. The unit of time corresponds to a single sweep of the sample by the Metropolis algorithm. (b) Relaxation of the overlap parameter q along the trajectory. (c) Results of minimization of E along the trajectory using the Newton algorithm, showing the system evolves in the vicinity of the 4 metastable energy minima. (d) Histogram of the q values a function of E.

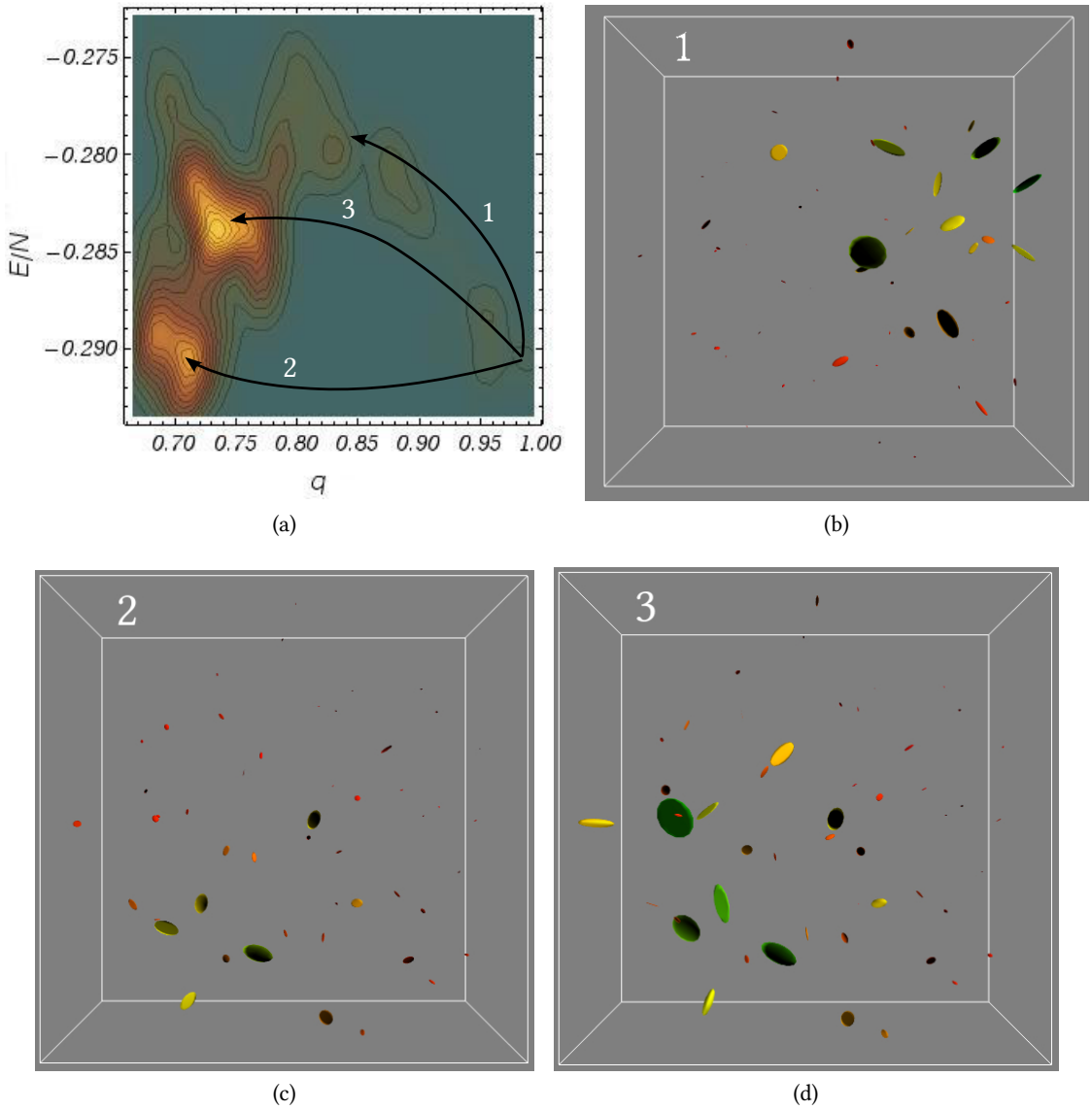

(a) (b)

(c) (d)

Figure 23.: Analysis of the PES for the low-temperature regime: $\theta = 40$, $N = 50$, $\chi = 0.71$, $\nu_0 = 0.08$, and $\nu = 0.15$. (a) Histogram of the q values a function of E. Arrows schematically shows energy basins corresponding to the 4 energy minima in Fig. 22(c). (b-d) Visualization of the difference between spin configurations in the energy minima, Eq. (4.25). The numbers correspond to the arrows in the panel (a). Primary axis of ellipsoids corresponds to eigenvectors of the frozen-in strain differences at lattice sites, cf. Eq. (4.25).

4.2.5 *Discussion*

To summarize, we have set up and performed extensive simulations of the 6-spin model, whose dynamics have been argued earlier to be mutually mappable onto activated transport in liquids; this type of transport precedes the structural glass transition.

The motivations for this part of the project, which proved to be rather laborious, were twofold: For one thing, typical liquid simulations are subject to collisional viscosity, in addition to the long waiting times for the activated transport. As a result, the liquid is probably too slow for the present-day computer to equilibrate in the activated regime. It is hard even to tell for sure how close these simulations are to the activated regime in the first place. There have not been identified, at present, any indicators or order parameters, in a liquid simulation, for the crossover between the high-temperature, collisional transport, and the low-temperature, activated transport, the latter regime being the focus of this work. The difficulty appears to be similar to that faced by field-theoretical techniques, which we have already discussed in Chapter 1: There is no fixed reference frame in the problem. All presently employed parameters, to our knowledge, are not gauge-invariant, i.e., they do not expressly depend exclusively on the mutual distance between the particles. An additional potential problem facing traditional liquid simulations is that the latter must employ mixtures of two differently sized particles, lest the liquid crystallizes before it can achieve any meaningful slowing down. (Simulating actual, anisotropic chemical interactions that could readily provide for such a slowing down is, at present, too computationally costly.) A potential fundamental flaw here is that the resulting dynamics, be they slow or not, are primarily due to the particle exchange, not the multiplicity of packings that drives the activated transport. Such exchange dynamics is clearly irrelevant in actual liquids: For instance, the cost of breaking the Si-O bond in a silicate, an archetypal glass-former, is several eV too high to be relevant to the liquid transport!

In contrast, the spin model is subject neither to the collisional effects nor particle exchange or lack of a convenient reference frame. The multiplicity of the configurations corresponds to the variety of the mutual spin orientations; the order parameters for the reconfigurations are simply the orientations of the individual spins, see Eq. (4.24). The cons of the spin methodology, however, are also many. They include: excessively cumbersome-looking, long-range interactions between the spins, a large number—six—of the spin components, and that the spins can change their orientations continuously, in contrast, for instance, with substitutional impurities or Ising spins, where such changes are discrete and require much less computational power to implement. The long-range interactions can be, at least approximately, dealt with by embedding a finite sample in a medium with distinct, effective elastic constants that are determined self-consistently. There is a price to pay here, as well, since the expression of the elasticity theory become quite cumbersome even for the simplest, spherical cavity; for more complicated cavity shapes, such expressions are not even known yet.

The results of the simulation seem to have justified the effort that went into its implementation. It appears that we have achieved a degree of supercooling far exceeding that achieved in the aforementioned binary mixtures. Judging from the value of the stretching exponent β in Fig. 16(b), we are close to the usual laboratory glass transition, which is about 7-9 orders of magnitude slower than what seems to have been achieved in a liquid simulation. (This difference is hard to pin point more accurately in view of some arbitrariness of the MC time scale.) The following signatures of the glass transition have been seen in our calculation: (1) Non-Arrhenius T-dependence of the relaxation time; (2) Stretched-exponential relaxation profiles, whose temperature dependence conforms with previous results;[9] (3) The degree of deviation from the Arrhenius T-dependence and the exponentiality of relaxations correlates with the Poisson ratio of the substance in an expected fashion.

Furthermore, we have directly observed activated transitions between distinct spin configurations, by monitoring the energy of the system as a function of a similarity gauge between spin

configurations. We have discovered that at sufficiently low temperatures, the system becomes trapped in a small number of well-separated energy minima. This behavior is expected; it corresponds to the so-called Kauzmann entropy crisis [111]: Below a certain, putative temperature often called the Kauzmann temperature, the liquid exhibits only a sub-thermodynamic number of states, in a puzzling contradiction with the Nernst law, which states that above $T = 0$, the log-number of states is always extensive. At a finite system size, such an entropy crisis is expected to take place at a higher temperature than in bulk, because the disallowing dynamics beyond a certain, modest size impose additional constraints on the phase space of the system. Analytical estimates of the size below which the liquid should "run out of states" have been given by Lubchenko and Wolynes.[112] Similar "confinement" effects have been seen in liquid simulations; these, however, are not straightforward to interpret, as we discussed above.

Despite this progress, more work needs to be done to elucidate *spatial* aspects of the slowing down of the spins. The RFOT theory predicts the cooperativity size for the activated reconfigurations should increase with lowering temperature and would, in fact, diverge at the Kauzmann temperature. This divergence is not observable because the barriers, by Eq. (2.1), become infinite when the configurational entropy vanishes. In attempts to infer the cooperativity length from our simulations, we face the difficulty that the spins are oriented randomly, suggesting that the usual, 2-point correlation functions will not be of help, consistent with liquid-based analyses.[113] We hope that recent developments on non-linear, 4-point correlation functions [114] will allow us to make progress on the cooperativity length. This is work in progress.

5

CONCLUSION

We have put forth a radically novel way to think about the structural glass transition. The present methodology exploits the view of supercooled liquids as aperiodic, degenerate crystals. These "crystals" flow on large time and length scales, but are mechanically (meta)stable locally. We have established that the structural degeneracy of these aperiodic crystals can be thought of as a multitude of mutual configurations of frozen-in stress. The latter stress stems from the frustration caused by mismatch between cohesive forces and steric repulsion. The frozen-in stress, as any elastic stress, can be characterized by a stress tensor field, which has six independent entries. The localized sources of stress on different sites interact via usual, nearly harmonic vibrations. The six entries of an individual source of stress can be presented as the components of a six-dimensional spin. We have thus shown that the activated dynamics in supercooled liquids can be mapped onto a Heisenberg model with 6-dimensional spins and complicated, tensorial coupling between the spins. The coupling is very long range, $1/r^3$, similarly to the electric dipole-dipole interaction. The configurational entropy of the liquid, a coveted object in the theory of the glass transition, corresponds to the full entropy of the spin model since the atomic vibrations have been "coarse-grained-out" by mapping of the liquid onto the spins.

The 6-spin Heisenberg model has the advantage of being defined on a fixed lattice and is thus amenable to various field-theoretical approaches and simulations, even though the spin-spin couplings are very complicated and very long-range. As the first step in attacking this complicated problem, we have analyzed the mean-field limit of the model. Already this simple limit turned out to be richer than that for a generic spin model. In addition to the usual Curie point, the model

exhibits a transition between two relative distinct regimes corresponding to frozen-in shear and uniform compression/dilation stress pattern. The transition is controlled by the Poisson ratio and takes place when the ratio is numerically equal to $\frac{1}{5}$. The two regimes themselves have been argued to correspond to strong and fragile liquid behavior.

The next steps in the analysis were motivated by two notions. On the one hand, the spin-spin interaction is very long range, preventing one from use the standard, periodic boundary conditions in a simulation. On the other hand, one must show that the view of a glassy liquid as a collection of local point stresses is internally consistent the same way one must show that the view of a dielectric liquid as a collection of molecular dipoles in internally consistent. We have pursued the latter analogy and have, in fact, established that similarly to how the dielectric susceptibility emerges as a continuum approximation to the response of a collection of disparate molecular dipole, the mechanical metastability of aperiodic, degenerate crystals and corresponding elastic moduli emerge from the present view. We have established that it is internally consistent to treat a compact set of the 6-spins explicitly, while approximating the surrounding material with an elastic continuum with some renormalized elastic constants. This is completely analogous to the cavity construction for dielectric materials by Debye, Onsager, and others. Remarkably, the relation between the bare and renormalized values of the elastic constants has an nontrivial fixed point: The bare and effective values of the Poisson ratio are equal to each other, at any temperature, when the bare Poisson ratio is equal to $\frac{1}{5}$. We have thus established, among other things, an interesting connection between the elasticity theory and the mean-field limit of the 6-spin model.

The elastic cavity construction above has also served as the foundation for our numerical simulation of the 6-spin model. The simulation is remarkably laborious to both implement and execute; the full significance of the results so far and further numerical studies will take some time. Already at present, we believe we have achieved significant progress toward quantitative description of the activated transport. We have established a strongly non-exponential character for the relaxation in the 6-spin model, which matches that of very deeply supercooled liquids,

i.e. on timescales that are possibly 8 to 9 order of magnitude longer than those achieved in direct simulations of glassforming binary mixtures. Another hallmark feature of glassy relaxations, i.e., their being non-Arrhenius is evident from our results. Further systematic studies of the model are needed to see whether the present model yields the experimentally observed fragility range. We have seen a correlation of the aforementioned signatures of glassy physics with the Poisson ratio that is consistent with the conclusions of the first part of the work.

Much work remains to fully establish the consequences of the present microscopic picture. In addition to the aforementioned systematic studies of the fragile vs. strong behavior, we plan to investigate spatial aspects of the activated reconfigurations, including both the cooperativity size and the functional form of the decay of the correlation. Another fundamental question that needs to be clarified is what happens in three dimensions to the Curie point and the strong-to-fragile transition that emerge in the mean field limit. Another obvious direction for further work is including interactions other than purely elastic ones into the formalism. For instance, including the electric dipole-dipole interactions may help us to understand why many ionic liquids behave differently from archetypal glassformers, such as silicates (which, incidentally, also exhibit much ionic bonding!). Likewise, various local anisotropies have been argued [10, 115] to cause deviations of select glass-formers, such as chalcogenides and boron oxide, from predictions of the RFOT theory. The latter takes a very isotropic view of local interactions, similarly to the present formalism. Including such local anisotropies can be done, at least in principle, by a suitable choice of the elastic tensor.

A

THE FOURTH-ORDER GREEN TENSOR FOR A POINT STRESS SOURCE

Consider an infinite medium with a distribution of body force $\mathbf{f}(\mathbf{r})$ different from zero over a finite domain. The distribution produces an elastic response described by the deformation field $\mathbf{u}$ satisfying the following boundary value problem,

$$\begin{cases} \sigma_{ij,j} + f_i = 0, \\ \mathbf{u}(\mathbf{r}) \xrightarrow[r\to\infty]{} 0, \end{cases} \tag{A.1}$$

where the stress σ is related to the deformation $\mathbf{u}$ via the constitutive relation $\sigma = C\varepsilon$, and the elastic strain ε is defined as[41]

$$\varepsilon_{ij} = \frac{1}{2}\left(u_{i,j} + u_{j,i}\right). \tag{A.2}$$

One can solve (A.1) by Fourier transforming $\mathbf{u}$;[43] the result given by

$$u_i(\mathbf{r}) = \int \mathrm{d}V' \gamma^{\mathrm{A}}_{ij}(\mathbf{r} - \mathbf{r}') f_i(\mathbf{r}'), \tag{A.3}$$

where for an isotropic C, the second-order Green tensor γ^{A} is given by

$$\begin{aligned} \gamma^{\mathrm{A}}_{ij}(\mathbf{r} - \mathbf{r}') &= \frac{1}{8\pi^3} \int \mathrm{d}\mathbf{k} \left(\zeta^{-1}\right)_{ij} e^{i\mathbf{k}\mathbf{r}} \\ &= -\frac{1}{16\mu\pi^3} \left(2\delta_{ij}\frac{\partial^2}{\partial x_l x_l} - \frac{1}{1-\nu}\frac{\partial^2}{\partial x_i x_j}\right) \int \mathrm{d}\mathbf{k} \frac{e^{i\mathbf{k}(\mathbf{r}-\mathbf{r}')}}{k^4}, \end{aligned} \tag{A.4}$$

where ζ is from Eq. (2.49). The integral in Eq. (A.4) is over the infinite domain and can be readily found,

$$\int \mathrm{d}\mathbf{k} \frac{e^{i\mathbf{k}\mathbf{r}}}{k^4} = -\pi^2 r. \tag{A.5}$$

Substitution into (A.4) produces the well know Green tensor for a points force inside an infinite, homogeneous, and isotropic medium (Kelvin's solution)[41]

$$\gamma_{ij}^{\mathrm{A}}(\mathbf{r}) = \frac{1}{16\pi\mu\,(1-\nu)} \frac{1}{r} \left[(3-4\nu)\,\delta_{ij} + \frac{x_i x_j}{r^2} \right]. \tag{A.6}$$

A solution for more complex geometries, e.g., a finite, possibly inhomogeneous, body, can be written in the same fashion

$$u_i(\mathbf{r}) = \int \mathrm{dV}' \gamma_{ij}(\mathbf{r}, \mathbf{r}') f_i\,(\mathbf{r}')\,, \tag{A.7}$$

where the tensor γ is not known analytically, in general.

Here we are interested in a situation where, instead of a distributed body force $\mathbf{f}$, the source field is given by the distribution of *stress* ρ. The solution (A.3) and (A.7) are still valid. However, now f_i is replaced by $\rho_{ij,j}$, since the corresponding balance equation is

$$\sigma_{ij,j} + \rho_{ij,j} = 0.$$

Subsequently, applying the Gauss theorem to (A.7) and using $\rho_{ij} = \rho_{ji}$, we get,[116, §3.3]

$$u_i(\mathbf{r}) = -\frac{1}{2} \int \mathrm{dV}' \left[\gamma_{ij,l'} + \gamma_{il,j'} \right] \rho_{jl}\,(\mathbf{r}')\,, \tag{A.8}$$

where the primed indexes label derivatives with respect to components of $\mathbf{r}'$:

$$\frac{\partial\,(\cdot)}{\partial x_i'} = (\cdot)_{,i'}\,.$$

One can define a fourth-order Green tensor G connecting the source stress field ρ with the resulting strain field ε,

$$\varepsilon_{ij} = \int \mathrm{dV}' G_{ijml}(\mathbf{r}, \mathbf{r}') \rho_{ml}(\mathbf{r}') \tag{A.9}$$

Applying the definition of ε, Eq. (A.2), to Eq. (A.8) one obtains the general relation connecting the second-order and the fourth-order Green tensors in a peace-wise homogeneous body of an arbitrary geometry[1]

$$G_{ijml}(\mathbf{r}, \mathbf{r}') = -\frac{1}{4}\left(\delta_{ip}\frac{\partial}{\partial x_j} + \delta_{jp}\frac{\partial}{\partial x_i}\right)\left(\delta_{ql}\frac{\partial}{\partial x'_m} + \delta_{qm}\frac{\partial}{\partial x'_l}\right)\gamma_{pq}(\mathbf{r}, \mathbf{r}'). \tag{A.10}$$

This definition produces for the fourth-order Green tensor corresponding to γ^{A}:

$$\begin{aligned} G^{\mathrm{A}}_{ijml}(\mathbf{r} - \mathbf{r}') &= -\frac{1}{4}\left(\delta_{ip}\frac{\partial}{\partial x_j} + \delta_{jp}\frac{\partial}{\partial x_i}\right)\left(\delta_{ql}\frac{\partial}{\partial x'_m} + \delta_{qm}\frac{\partial}{\partial x'_l}\right)\gamma^{\mathrm{A}}_{pq}(\mathbf{r} - \mathbf{r}') \\ &= -\frac{1}{64\pi^3\mu(1-\nu)}\left(\delta_{ip}\frac{\partial}{\partial x_j} + \delta_{jp}\frac{\partial}{\partial x_i}\right)\left(\delta_{ql}\frac{\partial}{\partial x'_m} + \delta_{qm}\frac{\partial}{\partial x'_l}\right) \\ &\times \left(2(1-\nu)\delta_{pq}\frac{\partial^2}{\partial x_s x_s} - \frac{\partial^2}{\partial x_p x_q}\right)\int \mathrm{d}\mathbf{k}\frac{e^{i\mathbf{k}(\mathbf{r}-\mathbf{r}')}}{k^4}, \end{aligned} \tag{A.11}$$

which has the same form as Eq. (2.58). Noting that

$$\frac{\partial}{\partial x'_i} = -\frac{\partial}{\partial x_i} \tag{A.12}$$

when acting on a function of $\mathbf{r} - \mathbf{r}'$, we also obtain Eq. (3.26).

1 For the validity of Eqs. (A.7) and (A.10) in a peace-wise homogeneous body it is necessary for ρ to vanish at any boundary where elastic moduli changes discontinuously .

B

PHYSICAL MEANING OF THE ESHELBY TENSOR

The Eshelby tensor S is well known in the theory of elasticity. It emerges as a solution to the following problem.[98] Consider an infinite isotropic body $\mathcal{B}$ characterized by an elastic moduli tensor C. The body contains a region, say $\mathcal{I}$, where, e.g., a structural transformation of some sort leads to the appearance of a stress distribution ρ. Such region is usually called a transformed inclusion. Note that elastic moduli are the same both in the material and the inclusion. The stress ρ is usually called "eigenstress". It is incompatible and can model, e.g., a martensitic transformation in the material. It is a source of a body force. Thus an elastic strain ε^{S} appears in the medium to compensate for it. As shown in Appendix A, ε^{S} can be calculated as

$$\varepsilon^{S}_{ij}(\mathbf{r}) = \int_{\mathcal{I}} \mathrm{dV}' G^{A}_{ijml}(\mathbf{r}-\mathbf{r}')\rho_{ml}(\mathbf{r}')\,, \qquad \text{(A.9 revisited)}$$

where the integral is taken over $\mathcal{I}$ since ρ is zero outside. It is often assumed that ρ is uniform.[73, 116]. Under these circumstances, it can be moved outside the integral, while ε is then related to the volume average of G^{A} over $\mathcal{I}$,

$$\varepsilon^{S}_{ij}(\mathbf{r}) = \rho_{ml} \int_{\mathcal{I}} \mathrm{dV}' G^{A}_{ijml}(\mathbf{r}-\mathbf{r}'). \qquad \text{(B.1)}$$

It was shown first by J. D. Eshelby for an elliptical $\mathcal{I}$ that the volume average of G^A in (B.1) does not depend on $\mathbf{r}$ for $\mathbf{r} \in \mathcal{I}$ and, thus, ε^s is homogeneous inside $\mathcal{I}$.[98] The Eshelby solution is usually written in terms of the "eigenstrain" ε^* defined as

$$\varepsilon^* = -C^{-1}\rho, \tag{B.2}$$

and the tensor relating the eigenstrain ε^* with the resulting elastic strain ε^s *inside* $\mathcal{I}$ is called the Eshelby tensor, usually denoted by S,

$$\varepsilon^s = S\,\varepsilon^*. \tag{B.3}$$

From (B.1) and (B.2) we get

$$\varepsilon^s = -\left[\int_{\mathcal{I}} dV' G^A(\mathbf{r}-\mathbf{r}')\right] C\,\varepsilon^*,$$

which provides the definition

$$S = -\int_{\mathcal{I}} dV' G^A(\mathbf{r}-\mathbf{r}')C. \tag{B.4}$$

As shown by Eshelby,[98] S does not depend on $\mathbf{r}$ for $\mathbf{r} \in \mathcal{I}$, if $\mathcal{I}$ is ellipsoidal. This allows one to use Eq. (B.4) to calculate the volume average of ε^s over $\mathcal{I}$,

$$\overline{\varepsilon^s} = \frac{1}{v}\int_{\mathcal{I}} \varepsilon^s\, dV,$$

even for more complicated distributions of ρ. Here, v is the volume of $\mathcal{I}$.

Indeed, using (A.9), changing the order of integration and using $G^A(\mathbf{r}-\mathbf{r}') = G^A(\mathbf{r}'-\mathbf{r})$, which can be checked directly using (3.26), we get for any ellipsoidal inclusion,

$$\overline{\varepsilon^s} = \frac{1}{v}\int_I dV \int_I dV' G^A(\mathbf{r}-\mathbf{r}')\rho(\mathbf{r}') = \frac{1}{v}\int_I dV' \left[\int_I dV G^A(\mathbf{r}'-\mathbf{r})\right]\rho(\mathbf{r}') = -SC^{-1}\overline{\rho}, \tag{B.5}$$

consistent with Eq. (3.67) for $C_0 = C$.

The same idea can be applied for the case of a stressed inhomogeneity, i.e. when the elastic moduli inside $\mathcal{I}$ are different from those of in the rest of body $\mathcal{B}$. For example, for a *spherical* $\mathcal{I}$ characterized by an isotropic elastic moduli tensor C_0 and an isotropic body $\mathcal{B}$ with elastic moduli tensor C, the strain *inside* $\mathcal{I}$ created by a uniform ρ, non-zero inside $\mathcal{I}$ only, is given by Eq. (3.67),

$$\varepsilon^S = -QS\,\rho, \tag{3.67 revisited}$$

where Q is given by Eq. (3.53). At the same time, ε^S can be calculated using Eq. (A.9) which gives,

$$SQ = -\int_{\mathcal{I}} dV' G(\mathbf{r},\mathbf{r}'), \tag{B.6}$$

where the Green tensor $G(\mathbf{r},\mathbf{r}')$ is now a sum of G^A and the image field Green tensor G^I. The latter is known analytically for the case of an isotropic spherical inhomogeneity inside an isotropic matrix considered here,[100] see Section 3.3 for discussion. Still, calculating, the volume average over $\mathcal{I}$, $\overline{G^I}$, is a formidable task owing to a very complex nature of the tensor. However, we note, in the 6-vector representation, discussed in Section 2.3, there is an important reciprocity relation,

$$G(\mathbf{r},\mathbf{r}') = [G(\mathbf{r}',\mathbf{r})]^\top \tag{B.7}$$

which allows one to write, similarly to Eq. (B.5),

$$\overline{\varepsilon^S} = \frac{1}{v}\int_I dV \int_I dV' G(\mathbf{r},\mathbf{r}')\rho(\mathbf{r}') = \frac{1}{v}\int_I dV' \left[\int_I dV G(\mathbf{r}',\mathbf{r})\right]^\top \rho(\mathbf{r}') = -[QS]^\top \overline{\rho}. \tag{B.8}$$

Since S and Q are isotropic tensors, they are symmetric, and so we get finally for *any* distribution of ρ inside spherical $\mathcal{I}$,

$$\overline{\varepsilon^S} = -QS\,\overline{\rho}. \tag{3.106 revisited}$$

C

THE FOURTH-ORDER IMAGE FIELD GREEN TENSOR FOR A SPHERE

In this appendix we provide the expression for the image field part of the fourth-order Green tensor for an isotropic spherical inhomogeneity embedded in an isotropic matrix. As shown in Section 2.5, a fourth-order Green tensor can be calculated using Eq. (A.10), if the corresponding second-order Green tensor is known. The second-order Green tensor for an isotropic spherical inhomogeneity embedded in an isotropic matrix with distinct elastic moduli was analytically found by L. J. Walpole in [100]. Despite the very simple form of Eq. (A.10) the actual calculation is tedious owing to the complex form of Walpole's solution. The result of the calculation is rather lengthy. We present it here in the system of notation used by Walpole. Note that this forces us to redefine some symbols which have already been used in this manuscript. However, it is important to simplify reference to Walpole's paper as much as possible.

We denote the shear modulus and Poisson ratio inside the inhomogeneity by μ and ν respectively. The corresponding parameters for the matrix are $\tilde{\mu}$ and $\tilde{\nu}$. The position of a concentrated source of stress is labeled by $\bar{\mathbf{r}} = \bar{x}_i$ while the position of an observation point is labeled by $\mathbf{r} = x_i$. In the following we will label equations from Ref. [100] referenced here using the corresponding equation numbers from [100] and adding the prefix "W".

In his paper, Walpole builds the solution for an elastic singularity in the spherical inclusion using expansions in terms of harmonic functions such as, e.g.,

$$|\mathbf{r} - \bar{\mathbf{r}}|^{-1} = \left[r\sqrt{1 - 2\left(\frac{\upsilon\bar{r}}{r}\right) + \left(\frac{\bar{r}}{r}\right)^2} \right]^{-1} = \sum_{n=0}^{\infty} \frac{H^n}{r^{2n+1}}, \tag{W.2.15}$$

where

$$v = \frac{x_i \bar{x}_i}{r\bar{r}}, \qquad H^n = (r\bar{r})^n P_n(v). \tag{W.2.16}$$

Here P_n refers to the Legendre polynomial of degree n; see [100] for full description. Walpole uses different Latin capital letters to denote harmonic functions relative to derivatives of H^n. In our case the number of the derivatives is large and it is reasonable to introduce the following definition:

$$H_M^n = \begin{cases} (r\bar{r})^n \, P_{n+M}^{(M)}(v), & n \geq 0,\, M \geq 0; \\ 0, & n < 0,\, M < 0 \end{cases} \tag{C.1}$$

where the superscript in the parentheses indicates the order of the derivative. Using well known relations between the Legendre polynomials,[117, §10.10]

$$P'_{n+1} = (2n+1)P_n + P'_{n-1}, \qquad P'_{n+1} - xP'_n = (n+1)P_n,$$

which can be generalized to

$$\begin{aligned} P_{m+n+1}^{(m+1)} &= [2(m+n)+1]\, P_{n+m}^{(m)} + P_{m+n-1}^{(m+1)}, \\ P_{m+n+1}^{(m+1)} - xP_{m+n}^{(m+1)} &= (m+n+1)P_{n+m}^{(m)}, \end{aligned}$$

we get the following relations for the derivatives of H_M^n with respect to coordinates of the source $\bar{x}_i$ or the observation point,

$$\begin{aligned} \frac{\partial H_M^n}{\partial x_i} &= \bar{x}_i H_{M+1}^{n-1} - x_i \bar{r}^2 H_{M+1}^{n-2}, \\ \frac{\partial H_M^n}{\partial \bar{x}_i} &= x_i H_{M+1}^{n-1} - \bar{x}_i r^2 H_{M+1}^{n-2}. \end{aligned} \tag{C.2}$$

We also can obtain the recurrence relation

$$H_M^n = [2\,(m+n)-1]\,H_{M-1}^n + (r\bar{r})^2 H_M^{n-2}. \tag{C.3}$$

Also needed will be the following coefficients defined by Walpole in [100]

$$\begin{aligned}
\tilde{q}_n &= [n^2 + (1-2\tilde{\nu})n + 1 - \tilde{\nu}]\tilde{\mu} + (n-1)[(3-4\tilde{\nu})n + 2(1-\tilde{\nu})]\mu,\\
q_n &= (n+2)[(3-4\nu)n + (1-2\nu)]\tilde{\mu} + [(n-1)^2 + (3+2\nu)(n-1) + 3(1+\nu)]\mu,\\
a_n &= (n+2)\Big/[(n-1)\mu + (n+2)\tilde{\mu}],\\
\tilde{q}_{n+1}b_n &= 2\mu[3(1-\nu) + (1-2\nu)n][n(3-4\tilde{\nu}) + 5 - 6\tilde{\nu}]\Big/[(n-1)\mu + (n+2)\tilde{\mu}],\\
\tilde{q}_{n+1}c_n &= 2n(2n+1)\Big/[(n-1)\mu + (n+2)\tilde{\mu}],\\
q_{n-1}d_n &= \mu\epsilon_n[(1-2\nu)n - 2 + \nu]\Big/[(n-1)\mu + (n+2)\tilde{\mu}],\\
2q_{n+1}g_n &= (n+3)(n+2)(2n+5)\Big/(2n+3),\\
p_n &= (3-4\nu)a_n - (2n+1)[n + 4(1-\nu)]d_n,\\
s_n &= a_n + (2n+1)[n + 8(1-\nu)]d_n,\\
t_n &= a_n + n(2n+1)d_n,\\
v_n &= [(a_n - b_n - t_{n+2})\Big/(2n+3)] + [n + 4(1-\nu)]d_n,\\
w_n &= g_{n-2} + t_n\Big/(2n-1),
\end{aligned}$$

where

$$\epsilon_n = \begin{cases} 1, & n > 0;\\ 0, & n \le 0. \end{cases}$$

Now we can define the following functions, which are generalization of U_N^n, V_N^n, and W_N^n used by Walpole

$$
\begin{aligned}
U_{1,M}^{n,i} &= v_n H_{M+1}^{n-i} + p_n H_M^{n-i}, \\
U_{2,M}^{n,i} &= -v_{n+2} H_{M+2}^{n-i}, \\
U_{3,M}^{n,i} &= 2v_{n+1} H_{M+2}^{n-i} - (t_{n+1} + s_{n+1}) H_{M+1}^{n-i}, \\
U_{4,M}^{n,i} &= \left[s_{n+1} + t_{n+1} - 2(2n+5)v_{n+1}\right] H_{M+1}^{n-i} + 2v_{n+1} H_{M+2}^{n-i} - 2(2n+1)t_{n+1} H_M^{n-i}, \\
V_{1,M}^{n,i} &= c_n H_{M+1}^{n-i}, \\
V_{2,M}^{n,i} &= -c_{n+2} H_{M+2}^{n-i}, \\
V_{3,M}^{n,i} &= 2c_{n+1} H_{M+2}^{n-i}, \\
V_{4,M}^{n,i} &= 2c_{n+1} \left[H_{M+2}^{n-i} - (2n+5) H_{M+1}^{n-i}\right], \\
W_{1,M}^{n,i} &= w_{n+2} H_{M+1}^{n-i}, \\
W_{2,M}^{n,i} &= -w_{n+4} H_{M+2}^{n-i}, \\
W_{3,M}^{n,i} &= 2w_{n+3} H_{M+2}^{n-i}, \\
W_{4,M}^{n,i} &= 2w_{n+3} \left[H_{M+2}^{n-i} - (2n+5) H_{M+1}^{n-i}\right), \\
W_{5,M}^{n,i} &= t_{n+2} H_{M+1}^{n-i}, \\
W_{6,M}^{n,i} &= t_{n+3} H_{M+1}^{n-i}.
\end{aligned}
$$

For $M = i = 0$, we return to the corresponding definitions of Walpole, e.g., $U_{N,0}^{n,0} = U_N^n$. Next we define the following series,

$$
\begin{aligned}
G_{N,M}^i &= \sum_{n=0}^{\infty} \frac{(\mu - \tilde{\mu}) U_{N,M}^{n,i} + (\nu - \tilde{\nu}) \tilde{\mu} V_{N,M}^{n,i}}{a^{2n+5}}, \\
\hat{G}_{N,M}^i &= (\mu - \tilde{\mu}) \sum_{n=0}^{\infty} \frac{W_{N,M}^{n,i}}{a^{2n+5}},
\end{aligned}
\tag{C.4}
$$

where a is the radius of the homogeneity. We also use the following notations:

$$\gamma = \frac{r^2}{a^2} - 1, \qquad \varepsilon = \frac{\bar{r}^2}{a^2} - 1.$$

We are now ready to write the image field part of the fourth-order Green tensor. The equation below was obtained applying Eq. (A.10) to the image field part of the second-order Green tensor derived by Walpole in [100]. It is a complex combination of series defined by Eq. (C.4). Note that the source must be inside the inhomogeneity, $\bar{r} < a$, or the series (C.4) diverges. We have

$$\begin{aligned}
&64\pi\mu(1-\nu)G^{\mathrm{I}}_{ijkl}(\mathbf{r},\bar{\mathbf{r}}) = 4C_1\delta_{ij}\delta_{kl} + 2C_2(\delta_{il}\delta_{jk} + \delta_{ik}\delta_{jl}) + \\
&+ C_3\left[x_l(\delta_{ik}x_j + x_i\delta_{jk}) + x_k(\delta_{il}x_j + x_i\delta_{jl})\right] + C_4\left[x_l(\delta_{ik}\bar{x}_j + \bar{x}_i\delta_{jk}) + x_k(\delta_{il}\bar{x}_j + \bar{x}_i\delta_{jl})\right] + \\
&+ C_5\left[\bar{x}_j(\delta_{ik}\bar{x}_l + \delta_{il}\bar{x}_k) + \bar{x}_i(\delta_{jk}\bar{x}_l + \delta_{jl}\bar{x}_k)\right] + C_6\left[x_j(\delta_{ik}\bar{x}_l + \delta_{il}\bar{x}_k) + x_i(\delta_{jk}\bar{x}_l + \delta_{jl}\bar{x}_k)\right] + \\
&+ 2\delta_{ij}\left[C_7(\bar{x}_k x_l + x_k\bar{x}_l) + 2C_8 x_k x_l + 2C_9\bar{x}_k\bar{x}_l\right] + 2\delta_{kl}\left[C_{10}(\bar{x}_i x_j + x_i\bar{x}_j) + 2C_{11}x_i x_j + 2C_{12}\bar{x}_i\bar{x}_j\right] + \\
&+ C_{13}(\bar{x}_i x_j + x_i\bar{x}_j)(\bar{x}_k x_l + x_k\bar{x}_l) + 2(\bar{x}_k x_l + x_k\bar{x}_l)(C_{14}x_i x_j + C_{15}\bar{x}_i\bar{x}_j) + \\
&+ 2(\bar{x}_i x_j + x_i\bar{x}_j)(C_{16}x_k x_l + C_{17}\bar{x}_k\bar{x}_l) + 4\bar{x}_i\bar{x}_j(C_{18}x_k x_l + C_{19}\bar{x}_k\bar{x}_l) + \\
&+ 4x_i x_j(C_{20}x_k x_l + C_{21}\bar{x}_k\bar{x}_l),
\end{aligned} \tag{C.5}$$

where

$$\begin{aligned}
C_1 &= \frac{1}{2}a^2 G^0_{4,0} + \frac{1}{2}a^2\gamma\varepsilon\hat{G}^0_{4,0} - (r^2 + \bar{r}^2)\hat{G}^0_{6,0}, \\
C_2 &= a^4 G^1_{1,1} + \frac{1}{2}a^2 G^0_{3,0} + (a^2 - r^2)(a^2 - \bar{r}^2)\hat{G}^1_{1,1} + \frac{1}{2}a^2\gamma\varepsilon\hat{G}^0_{3,0}, \\
C_3 &= -a^4\bar{r}^2 G^3_{1,2} + 2\bar{r}^2 G^1_{2,1} - \frac{1}{2}a^2\bar{r}^2 G^2_{3,1} + (-2a^2 + 2\bar{r}^2)\hat{G}^1_{1,1} - (a^2 - r^2)\bar{r}^2(a^2 - \bar{r}^2)\hat{G}^3_{1,2} + \\
&\quad + 2\gamma\varepsilon\bar{r}^2\hat{G}^1_{2,1} + \varepsilon\hat{G}^0_{3,0} - \frac{1}{2}a^2\gamma\varepsilon\bar{r}^2\hat{G}^2_{3,1} + 2a^2\hat{G}^1_{5,1}, \\
C_4 &= a^4 G^2_{1,2} + \frac{3}{2}a^2 G^1_{3,1} + (a^2 - r^2)(a^2 - \bar{r}^2)\hat{G}^2_{1,2} + \frac{3}{2}a^2\gamma\varepsilon\hat{G}^1_{3,1},
\end{aligned}$$

$$C_5 = -a^4r^2G^3_{1,2} + 2r^2G^1_{2,1} - \frac{1}{2}a^2r^2G^2_{3,1} + 2(-a^2+r^2)\hat{G}^1_{1,1} - a^4\gamma\varepsilon r^2\hat{G}^3_{1,2} +$$
$$+ 2\gamma\varepsilon r^2\hat{G}^1_{2,1} + \gamma\hat{G}^0_{3,0} - \frac{1}{2}a^2\gamma\varepsilon r^2\hat{G}^2_{3,1} + 2a^2\hat{G}^1_{5,1},$$
$$C_6 = -2a^4G^2_{1,1} + a^4r^2\bar{r}^2G^4_{1,2} + 4G^0_{2,0} - 2r^2\bar{r}^2G^2_{2,1} + \frac{1}{2}a^2G^1_{4,1} + 4\hat{G}^0_{1,0} -$$
$$- 2(a^4\gamma\varepsilon - a^2\bar{r}^2 + r^2(a^2\varepsilon + \bar{r}^2))\hat{G}^2_{1,1} + a^4\gamma\varepsilon r^2\bar{r}^2\hat{G}^4_{1,2} +$$
$$+ \frac{2}{a^4}\hat{G}^0_{2,0}\left[a^4(1+\gamma\varepsilon) + a^2(-1+\varepsilon)r^2 + 2(-a^2+r^2)\bar{r}^2\right] - 2\gamma\varepsilon r^2\bar{r}^2\hat{G}^2_{2,1} + \frac{1}{2}a^2\gamma\varepsilon\hat{G}^1_{4,1} -$$
$$- a^2(r^2+\bar{r}^2)\hat{G}^2_{5,1} + (-r^2-\bar{r}^2)\hat{G}^1_{6,1},$$
$$C_7 = 2G^0_{2,0} - r^2\bar{r}^2G^2_{2,1} + \frac{1}{2}a^2G^1_{4,1} + \frac{2}{a^4}\hat{G}^0_{2,0}(a^2-r^2)(a^2-2\bar{r}^2) - \gamma\varepsilon r^2\bar{r}^2\hat{G}^2_{2,1} +$$
$$+ \frac{1}{2}a^2\gamma\varepsilon\hat{G}^1_{4,1} - a^2r^2\hat{G}^2_{5,1} + (-r^2-\bar{r}^2)\hat{G}^1_{6,1},$$
$$C_8 = \bar{r}^2G^1_{2,1} + \gamma\varepsilon\bar{r}^2\hat{G}^1_{2,1} + a^2\hat{G}^1_{5,1},$$
$$C_9 = -\frac{1}{2}a^2r^2G^2_{4,1} + \gamma\hat{G}^0_{4,0} - \frac{1}{2}a^2\gamma\varepsilon r^2\hat{G}^2_{4,1} - 2\hat{G}^0_{6,0} + r^2(r^2+\bar{r}^2)\hat{G}^2_{6,1},$$
$$C_{10} = 2G^0_{2,0} - r^2\bar{r}^2G^2_{2,1} + \frac{1}{2}a^2G^1_{4,1} + 2\varepsilon(\gamma + \frac{r^2}{a^2})\hat{G}^0_{2,0} - \gamma\varepsilon r^2\bar{r}^2\hat{G}^2_{2,1} +$$
$$+ \frac{1}{2}a^2\gamma\varepsilon\hat{G}^1_{4,1} - a^2\bar{r}^2\hat{G}^2_{5,1} + (-r^2-\bar{r}^2)\hat{G}^1_{6,1},$$
$$C_{11} = -\frac{1}{2}a^2\bar{r}^2G^2_{4,1} + \varepsilon\hat{G}^0_{4,0} - \frac{1}{2}a^2\gamma\varepsilon\bar{r}^2\hat{G}^2_{4,1} - 2\hat{G}^0_{6,0} + \bar{r}^2(r^2+\bar{r}^2)\hat{G}^2_{6,1},$$
$$C_{12} = r^2G^1_{2,1} + \gamma\varepsilon r^2\hat{G}^1_{2,1} + a^2\hat{G}^1_{5,1},$$
$$C_{13} = 4G^1_{2,1} - 2r^2\bar{r}^2G^3_{2,2} - a^2G^2_{3,1} + \frac{1}{2}a^2r^2\bar{r}^2G^4_{3,2} +$$
$$+ \frac{1}{2}a^2G^2_{4,2} + \frac{2}{a^4}\hat{G}^1_{2,1}\left[a^4(1+\gamma\varepsilon) + a^2(-1+\varepsilon)r^2 + 2(-a^2+r^2)\bar{r}^2\right] -$$
$$- 2\gamma\varepsilon r^2\bar{r}^2\hat{G}^3_{2,2} + \frac{2}{a^2}\hat{G}^0_{3,0} + (-\varepsilon r^2 - \gamma(a^2\varepsilon + \bar{r}^2))\hat{G}^2_{3,1} +$$
$$+ \frac{1}{2}a^2\gamma\varepsilon r^2\bar{r}^2\hat{G}^4_{3,2} + \frac{1}{2}a^2\gamma\varepsilon\hat{G}^2_{4,2} - a^2(r^2+\bar{r}^2)\hat{G}^3_{5,2} + (-r^2-\bar{r}^2)\hat{G}^2_{6,2},$$
$$C_{14} = -4\bar{r}^2G^2_{2,1} + r^2\bar{r}^4G^4_{2,2} - \frac{1}{2}a^2\bar{r}^2G^3_{4,2} - \frac{4}{a^4}\hat{G}^0_{2,0}(a^2-2\bar{r}^2) -$$
$$- \frac{2\bar{r}^2}{a^4}\hat{G}^2_{2,1}\left[a^4(1+\gamma\varepsilon) + a^2(-1+\varepsilon)r^2 + 2(-a^2+r^2)\bar{r}^2\right] + \gamma\varepsilon r^2\bar{r}^4\hat{G}^4_{2,2} +$$
$$+ \varepsilon\hat{G}^1_{4,1} - \frac{1}{2}a^2\gamma\varepsilon\bar{r}^2\hat{G}^3_{4,2} - 2a^2\hat{G}^2_{5,1} + a^2r^2\bar{r}^2\hat{G}^4_{5,2} - 2\hat{G}^1_{6,1} + \bar{r}^2(r^2+\bar{r}^2)\hat{G}^3_{6,2},$$

$$
\begin{aligned}
C_{15} &= r^2 G^2_{2,2} - \frac{1}{2}a^2 r^2 G^3_{3,2} + \gamma\varepsilon r^2 \hat{G}^2_{2,2} + \gamma \hat{G}^1_{3,1} - \frac{1}{2}a^2\gamma\varepsilon r^2 \hat{G}^3_{3,2} + a^2 \hat{G}^2_{5,2},\\
C_{16} &= \bar{r}^2 G^2_{2,2} - \frac{1}{2}a^2 \bar{r}^2 G^3_{3,2} + \gamma\varepsilon \bar{r}^2 \hat{G}^2_{2,2} + \varepsilon \hat{G}^1_{3,1} - \frac{1}{2}a^2\gamma\varepsilon \bar{r}^2 \hat{G}^3_{3,2} + a^2 \hat{G}^2_{5,2},\\
C_{17} &= -4r^2 G^2_{2,1} + r^4 \bar{r}^2 G^4_{2,2} - \frac{1}{2}a^2 r^2 G^3_{4,2} -\\
&\quad - \frac{4}{a^4}\hat{G}^0_{2,0}(a^2 - 2r^2) - \frac{2r^2}{a^4}\hat{G}^2_{2,1}\left[2a^4\gamma\varepsilon - a^2\bar{r}^2 + r^2(a^2\varepsilon + \bar{r}^2)\right] +\\
&\quad + \gamma\varepsilon r^4 \bar{r}^2 \hat{G}^4_{2,2} + \gamma \hat{G}^1_{4,1} - \frac{1}{2}a^2\gamma\varepsilon r^2 \hat{G}^3_{4,2} -\\
&\quad - 2a^2 \hat{G}^2_{5,1} + a^2 r^2 \bar{r}^2 \hat{G}^4_{5,2} - 2\hat{G}^1_{6,1} + r^2(r^2 + \bar{r}^2)\hat{G}^3_{6,2},\\
C_{18} &= \frac{1}{2}a^2 G^2_{3,2} + \frac{1}{2}a^2\gamma\varepsilon \hat{G}^2_{3,2},\\
C_{19} &= -r^4 G^3_{2,2} + \frac{2r^2}{a^4}\hat{G}^1_{2,1}(r^2 - a^2) - \gamma\varepsilon r^4 \hat{G}^3_{2,2} - a^2 r^2 \hat{G}^3_{5,2},\\
C_{20} &= -\bar{r}^4 G^3_{2,2} + \frac{2\varepsilon\bar{r}^2}{a^2}\hat{G}^1_{2,1} - \gamma\varepsilon \bar{r}^4 \hat{G}^3_{2,2} - a^2 \bar{r}^2 \hat{G}^3_{5,2},\\
C_{21} &= -a^2 G^2_{4,1} + \frac{1}{2}a^2 r^2 \bar{r}^2 G^4_{4,2} + \frac{2\hat{G}^0_{4,0}}{a^2} + (-\varepsilon r^2 - \gamma(a^2\varepsilon + \bar{r}^2))\hat{G}^2_{4,1} +\\
&\quad + \frac{1}{2}a^2\gamma\varepsilon r^2 \bar{r}^2 \hat{G}^4_{4,2} + 4(r^2 + \bar{r}^2)\hat{G}^2_{6,1} - r^2\bar{r}^2(r^2 + \bar{r}^2)\hat{G}^4_{6,2}.
\end{aligned}
$$

No further simplification of the result was attempted since it is clear that the expressions given above can be realistically used only with the aid of a computer. Furthermore, for fast calculation of the Green tensor it is *necessary* to use the Clenshaw algorithm for series summation,[118, §5.4.2] which is possible since H^n_M obeys the three-term recurrence relation

$$
H^{n+1}_M(v) = \alpha_n H^n_M + \beta_n H^{n-1}_M, \tag{C.6}
$$

where

$$
\alpha_n = \frac{2(n+M)+1}{n+1} r\bar{r}, \qquad \beta_n = -\frac{n+2M}{n+1}(r\bar{r})^2. \tag{C.7}
$$

Then, any sum of the type

$$\sum_{n=0}^{N} \varsigma_n H_M^n = (\beta_1 y_2 + \varsigma_0) H_M^0 + y_1 H_M^1, \tag{C.8}$$

where coefficients y_i are calculated from the recurrence relation:

$$\begin{aligned} &y_{N+1} = y_{N+2} = 0, \\ &y_n = \alpha_n y_{n+1} + \beta_{n+1} y_{n+2} + \varsigma_n, \qquad\qquad n = N, N-1, \cdots, 1. \end{aligned} \tag{C.9}$$

Thus, the most convenient, from the practical standpoint, form of G^{I}, is a sum of the series of the type given by Eq. (C.8). Such simplification as well as the implementation of numerical computation of G^{I} was done using MATHEMATICA.

Even with the aid of the Clenshaw algorithm, numerical computation of G^{I} for large (several hundred particles) lattices is prohibitively long. To further shorten the computation time, Eq. (C.5) was optimized for the computation of the Green tensor for $a = 1$ and a single configuration of the source and the observation points: the source is located at the Ox axis, $\bar{\mathbf{r}} = (\bar{x}_1, 0, 0)$, and the observation point is on the xOy plane, $\mathbf{r} = (x_1, x_2, 0)$. To compute G^{I} for arbitrary $\mathbf{r}$ and $\bar{\mathbf{r}}$, the corresponding coordinate system K is first transformed (rotated) into the coordinate system K' where positions of the source and the observation points are as described above. Then the Green tensor is computed using the highly optimized version of Eq. (C.5) with the aid of the Clenshaw algorithm for $a = 1$ for scaled positions of the source and the observer in K', $(\bar{x}_1'/a, 0, 0)$ and $(x_1'/a, x_2'/a, 0)$ respectively (prime labels vector components in K' coordinate system). After that the result is transformed back into K and scaled using the obvious property,

$$\mathrm{G}^{\mathrm{I}}(\mathbf{r}, \bar{\mathbf{r}}) = \frac{1}{a^3} \mathrm{G}^{\mathrm{I}}\left(\frac{\mathbf{r}}{a}, \frac{\bar{\mathbf{r}}}{a}\right). \tag{C.10}$$

Thus optimization allows one to reduce the computation time in MATHEMATICA by orders of magnitude. For all the calculations reported in this manuscript number of terms is the series (C.4) was set to 300.

D

NOTES ON PREPARATION OF THE SAMPLES

We take a large (10^5 lattice points) spherical RCP lattice generated according to the Bennett algorithm[101] and generate our (much smaller) sample by cutting out spherical chunks of a given radius according to the following algorithm:

1: Read radius of the sample from input: $Input \rightarrow R$

2: Increment R by some number of nearest neighbor distances a: $R + m \times a \rightarrow R_a$. By default, $m = 1$ and $a = 1$.

3: Read large RCP lattice from the input: $Input \rightarrow \mathbf{r}_i$, $i = 0, 1, \ldots, N-1$. N is the number of lines in the corresponding file.

4: Calculate the radius R_b of the RCP lattice:[1] $|\mathbf{r}_0 - \mathbf{r}_N| \rightarrow R_b$

5: The provided RCP lattice must be big enough: $R_b > R_a + M$. Abort program otherwise. By default, $M = 5.0$.

6: Find a center of the chunk: $\mathbf{r}_N - \frac{R_a}{R_b} \times (\mathbf{r}_0 - \mathbf{r}_N) \rightarrow \mathbf{r}_c$

7: **for** $i = 0$ to $N - 1$ **do**

8: Find the distance from i-th lattice point to the center of the chunk: $|\mathbf{r}_i - \mathbf{r}_c| \rightarrow d$

9: **if** $d < R$ **then**

10: **return** $\mathbf{r}_i - \mathbf{r}_c$ {Return coordinates of the point to the output using $\mathbf{r}_c$ as the origin of a coordinate system}

11: **end if**

1 This algorithm uses the property of the Bennett procedure to build a random lattice around a cluster of three particles. Thus first three lines of the input give the "center" of the lattice while the last line gives coordinates of a particle located at the outermost shell of the lattice.

12: **end for**

The procedure was applied many times to generate many different sample lattices. For the simulation we used sets of samples containing equal number of lattice points, e.g., $N = 50$. For such samples the interaction matrix $\mathrm{Y}^{(ij)}$ was computed using the following procedure:

1: Load lattice coordinates of a sample: $Input \rightarrow \mathbf{r}_i \in \mathbb{L}$.

2: Find the center of the sample $\mathbf{r}_c$: $f(\mathbf{r}_c) = \min_{\mathbf{x}\in\mathbb{L}} f(\mathbf{x})$, where $f(\mathbf{x}) = \frac{1}{|\mathbb{L}|}\sum_{\mathbf{y}\in\mathbb{L}}|\mathbf{x}-\mathbf{y}|$, where $|\mathbb{L}|$ denotes number of elements in $\mathbb{L}$.

3: Shift the lattice to the new coordinate system with the origin in $\mathbf{r}_c$: $\mathbb{L} \rightarrow \mathbb{M} = \{\mathbf{y} : \mathbf{y} = \mathbf{x} - \mathbf{r}_c, x \in \mathbb{L}\}$.

4: Find $r_{max} = \max \mathbb{M}$.

5: Find lattice points which form the surface of the sample: $\mathbb{S} = \{\mathbf{y} \in \mathbb{M} : r_{max} - a/2 > |\mathbf{y}| \leq r_{max}\}$.

6: Find $r_{mean} = a/2 + \frac{1}{|\mathbb{S}|}\sum_{y\in\mathbb{S}}|y|$.

7: Calculate self-interaction $\mathrm{G}^{\mathrm{I}}(\mathbf{y},\mathbf{y})$ for every spin, using R as the radius of the inclusion $\mathcal{I}$

$$R = \begin{cases} r_{mean}, & \mathbf{y} \notin \mathbb{S}; \\ |\mathbf{y}| + a/2, & \mathbf{y} \in \mathbb{S}. \end{cases}$$

8: Using $R = r_{mean}$ find the image part of the interaction, $\mathrm{G}^{\mathrm{I}}(g(\mathbf{x}), g(\mathbf{y}))$, where

$$g(\mathbf{x}) = \begin{cases} \left(r_{mean} - \frac{a}{2}\right)\frac{\mathbf{x}}{|\mathbf{x}|}, & \mathbf{x} \in \mathbb{S}; \\ g(\mathbf{x}) = \mathbf{x}, & x \in \mathbb{M} \setminus \mathbb{S}. \end{cases}$$

9: Find direct interaction $G^{\mathrm{A}}(\mathbf{x},\mathbf{y})$ for every $\mathbf{x},\mathbf{y} \in \mathbb{M}$.

10: Apply eq. (4.8) to compute $\mathrm{Y}^{(ij)}$ and return the results.

Here R denotes the radius of the inclusion $\mathcal{I}$ used to calculate the image part of $\mathrm{Y}^{(ij)}$. The procedure for calculating G^{I} was outlined in app. C.

BIBLIOGRAPHY

[1] M. Piperno, C. Collina, R. Gallotti, J.-P. Raynal, G. Kieffer, F.-X. le Bourdonnec, G. Poupeau, and D. Geraads, "Obsidian exploitation and utilization during the Oldowan at Melka Kunture (Ethiopia)," in *Interdisciplinary approaches to the Oldowan*, edited by E. Hovers and D. R. Braun (Springer, 2009), pp. 111–128.

[2] E. Trinkaus, "Early modern humans," Annu. Rev. Anthropol. **34**, 207 (2005).

[3] B. Wood and J. Baker, "Evolution in the genus *Homo*," Annu. Rev. Ecol. Evol. Syst. **42**, 47 (2011).

[4] V. Lubchenko and P. G. Wolynes, "Theory of structural glasses and supercooled liquids," Annu. Rev. Phys. Chem. **58**, 235 (2007).

[5] M. D. Ediger, C. A. Angell, and S. R. Nagel, "Supercooled liquids and glasses," J. Phys. Chem. **100**, 13200 (1996).

[6] V. Lubchenko and P. G. Wolynes, "Theories of structural glass dynamics: mosaics, jamming, and all that," in *Structural glasses and supercooled liquids: theory, experiment, and applications*, edited by P. G. Wolynes and V. Lubchenko (John Wiley & Sons, Inc., 2012) Chap. 10, pp. 341–379.

[7] T. R. Kirkpatrick, D. Thirumalai, and P. G. Wolynes, "Scaling concepts for the dynamics of viscous liquids near an ideal glassy state," Phys. Rev. A **40**, 1045 (1989).

[8] C. A. Angell, "Formation of glasses from liquids and biopolymers," Science **267**, 1924 (1995).

[9] X. Xia and P. G. Wolynes, "Fragilities of liquids predicted from the random first order transition theory of glasses," PNAS **97**, 2990 (2000).

[10] P. Rabochiy and V. Lubchenko, "Microscopic calculation of the free energy cost for activated transport in glass-forming liquids," J. Chem. Phys. **138**, 12A534, 12A534 (2013).

[11] G. N. Greaves, "Poisson's ratio over two centuries: challenging hypotheses," Notes Rec. R. Soc. **67**, 37 (2013).

[12] A. L. Greaves, G. N. Greer, R. S. Lakes, and T. Rouxel, "Poisson's ratio and modern materials," Nature Mater. **10**, 823 (2011).

[13] R. H. Cole, "Dielectrics in physical chemistry," Annu. Rev. Phys. Chem. **40**, PMID: 18338977, 1 (1989).

[14] D. Bevzenko and V. Lubchenko, "Stress distribution and the fragility of supercooled melts," J. Phys. Chem. B **113**, 16337 (2009).

[15] Y. Singh, J. P. Stoessel, and P. G. Wolynes, "The hard sphere glass and the density functional theory of aperiodic crystals," Phys. Rev. Lett. **54**, 1059 (1985).

[16] V. Lubchenko and P. G. Wolynes, "Barrier softening near the onset of nonactivated transport in supercooled liquids: implications for establishing detailed connection between thermodynamic and kinetic anomalies in supercooled liquids," J. Chem. Phys. **119**, 9088 (2003).

[17] R. Casalini, M. Paluch, and C. M. Roland, "Dynamic crossover in supercooled liquids induced by high pressure," J. Chem. Phys. **118**, 5701 (2003).

[18] T. R. Kirkpatrick and P. G. Wolynes, "Connections between some kinetic and equilibrium theories of the glass transition," Phys. Rev. A **35**, 3072 (1987).

[19] T. R. Kirkpatrick and P. G. Wolynes, "Stable and metastable states in mean-field potts and structural glasses," Phys. Rev. B **36**, 8552 (1987).

[20] W. Götze, *Complex dynamics of glass-forming liquids: a mode-coupling theory* (Oxford University Press, 2009).

[21] F. A. Lindemann, Physik. Z. **11**, 609 (1910).

[22] V. Lubchenko, "A universal criterion of melting," J. Phys. Chem. B **110**, 18779 (2006).

[23] V. Lubchenko and P. G. Wolynes, "Theory of aging in structural glasses," J. Chem. Phys. **121**, 2852 (2004).

[24] C. Angell, "Spectroscopy simulation and scattering, and the medium range order problem in glass," J. Non-Cryst. Solids **73**, 1 (1985).

[25] L. Martinez and C. A. Angell, "A thermodynamic connection to the fragility of glass-forming liquids," Nature **410**, 663 (2001).

[26] J. D. Stevenson and P. G. Wolynes, "Thermodynamic-kinetic correlations in supercooled liquids: a critical survey of experimental data and predictions of the random first-order transition theory of glasses," J. Phys. Chem. B **109**, 15093 (2005).

[27] R. W. Hall and P. G. Wolynes, "Microscopic theory of network glasses," Phys. Rev. Lett. **90**, 085505 (2003).

[28] V. Lubchenko, "Charge and momentum transfer in supercooled melts: why should their relaxation times differ?" J. Chem. Phys. **126**, 174503, 174503 (2007).

[29] D. Turnbull, "Formation of crystal nuclei in liquid metals," J. Appl. Phys. **21**, 1022 (1950).

[30] A. Zhugayevych and V. Lubchenko, "An intrinsic formation mechanism for midgap electronic states in semiconductor glasses," J. Chem. Phys. **132**, 044508, 044508 (2010).

[31] R. W. Hall and P. G. Wolynes, "The aperiodic crystal picture and free energy barriers in glasses," J. Chem. Phys. **86**, 2943 (1987).

[32] S. M. Sharma and S. Sikka, "Pressure induced amorphization of materials," Prog. Mater. Sci. **40**, 1 (1996).

[33] G. C. Serghiou, R. R. Winters, and W. S. Hammack, "Pressure-induced amorphization and reduction of t-nb_2o_5," Phys. Rev. Lett. **68**, 3311 (1992).

[34] R. J. Hemley, A. P. Jephcoat, H. K. Mao, L. C. Ming, and M. H. Manghnani, "Pressure-induced amorphization of crystalline silica," Nature **334**, 52 (1988).

[35] G. Baldi, M. Zanatta, E. Gilioli, V. Milman, K. Refson, B. Wehinger, B. Winkler, A. Fontana, and G. Monaco, "Emergence of crystal-like atomic dynamics in glasses at the nanometer scale," Phys. Rev. Lett. **110**, 185503 (2013).

[36] S. Sarkar, X. Ren, and K. Otsuka, "Evidence for strain glass in the ferroelastic-martensitic system $Ti_{50-x}Ni_{50+x}$," Phys. Rev. Lett. **95**, 205702 (2005).

[37] J. S. Rowlinson and B. Widom, *Molecular theory of capillarity* (Clarendon Press, Oxford, 1982).

[38] N. Ashcroft and N. Mermin, *Solid state physics* (Saunders College, 1976).

[39] A. Loidl, "Orientational glasses," Annu. Rev. Phys. Chem. **40**, 29 (1989).

[40] W. Cochran, "Crystal stability and the theory of ferroelectricity," Phys. Rev. Lett. **3**, 412 (1959).

[41] L. D. Landau and E. M. Lifshitz, *Theory of elasticity* (Pergamon Press, 1986).

[42] S. R. Shenoy, T. Lookman, and A. Saxena, "Spin, charge, and lattice coupling in multiferroic materials," in *Magnetism and structure in functional materials*, edited by A. Planes, L. Mañosa, and A. Saxena (Springer, 2005) Chap. 2, pp. 3–25.

[43] C. Teodosiu, *Elastic models of crystal defects* (Springer, 1982).

[44] L. J. Walpole, "Elastic behavior of composite materials: theoretical foundations," Adv. App. Mech. **21**, 169 (1981).

[45] M. M. Mehrabadi and S. C. Cowin, "Eigentensors of linear anisotropic elastic materials," Q. J. Mech. Appl. Math. **43**, 15 (1990).

[46] D. I. Uzunov, *Iintroduction to the theory of critical phenomena: mean field, fluctuations and renormalization* (World Scientific, 1993).

[47] C. J. Thompson, *Classical equilibrium statistical mechanics* (Clarendon Press, 1988).

[48] F. D. Nobre and C. Tsallis, "Classical infinite-range-interaction Heisenberg ferromagnetic model: metastability and sensitivity to initial conditions," Phys. Rev. E **68**, 036115 (2003).

[49] A. Abramowitz and I. Stegun, eds., *Handbook of mathematical functions* (Dover, 1964).

[50] R. Monasson, "Structural glass transition and the entropy of the metastable states," Phys. Rev. Lett. **75**, 2847 (1995).

[51] J. Schmalian and P. G. Wolynes, "Stripe glasses: self-generated randomness in a uniformly frustrated system," Phys. Rev. Lett. **85**, 836 (2000).

[52] N. Goldenfeld, *Lectures on phase transitions and the renormalization group* (Addison-Wesley, 1992).

[53] E. Zeidler, *Quantum field theory I: basics in mathematics and physics* (Springer, 2006).

[54] J. L. Black and B. I. Halperin, "Spectral diffusion, phonon echoes, and saturation recovery in glasses at low temperatures," Phys. Rev. B **16**, 2879 (1977).

[55] A. L. Burin, D. Natelson, D. D. Osheroff, and Y. Kagan, "Interactions between tunneling defects in amorphous solids," in *Tunneling systems in amorphous and crystalline solids*, edited by P. Esquinazi (Springer, 1998) Chap. 5, pp. 223–315.

[56] D. C. Vural and A. J. Leggett, "Universal sound absorption in amorphous solids: a theory of elastically coupled generic blocks," J. Non-Cryst. Solids **357**, 3528 (2011).

[57] E. R. Grannan, M. Randeria, and J. P. Sethna, "Low-temperature properties of a model glass. i. elastic dipole model," Phys. Rev. B **41**, 7784 (1990).

[58] E. R. Grannan, M. Randeria, and J. P. Sethna, "Low-temperature properties of a model glass. ii. specific heat and thermal transport," Phys. Rev. B **41**, 7799 (1990).

[59] C. C. Yu, "Phase transitions of interacting elastic defects," Phys. Rev. Lett. **69**, 2787 (1992).

[60] J. Felsteiner, "Structure of the ordered state of ortho-hydrogen at absolute zero," Phys. Rev. Lett. **15**, 1025 (1965).

[61] V. N. Novikov and A. P. Sokolov, "Poisson's ratio and the fragility of glass-forming liquids," Nature **431**, 961 (2004).

[62] A. P. Sokolov, V. N. Novikov, and A. Kisliuk, "Fragility and mechanical moduli: do they really correlate?" Philos. Mag. **87**, 613 (2007).

[63] Y. Singh, J. P. Stoessel, and P. G. Wolynes, "Hard-sphere glass and the density-functional theory of aperiodic crystals," Phys. Rev. Lett. **54**, 1059 (1985).

[64] Z. E. Usatenko and M. P. Kozlovskii, "Thermodynamic characteristics of the classical *n*-vector magnetic model in three dimensions," Phys. Rev. B **62**, 9599 (2000).

[65] V. Lubchenko, R. J. Silbey, and P. G. Wolynes, "Electrodynamics of amorphous media at low temperatures," Mol. Phys. **104**, 1325 (2006).

[66] V. N. Novikov and A. P. Sokolov, "Correlation of fragility and poisson's ratio: difference between metallic and nonmetallic glass formers," Phys. Rev. B **74**, 064203 (2006).

[67] G. P. Johari, "On poisson's ratio of glass and liquid vitrification characteristics," Philos. Mag. **86**, 1567 (2006).

[68] D. H. Torchinsky, J. A. Johnson, and K. A. Nelson, "A direct test of the correlation between elastic parameters and fragility of ten glass formers and their relationship to elastic models of the glass transition," J. Chem. Phys. **130**, 064502, 064502 (2009).

[69] S. N. Yannopoulos and G. P. Johari, "Glass behaviour: poisson's ratio and liquid's fragility," Nature **442**, E7 (2006).

[70] J. D. Stevenson, A. M. Walczak, R. W. Hall, and P. G. Wolynes, "Constructing explicit magnetic analogies for the dynamics of glass forming liquids," J. Chem. Phys. **129**, 194505, 194505 (2008).

[71] B. A. DiDonna and T. C. Lubensky, "Nonaffine correlations in random elastic media," Phys. Rev. E **72**, 066619 (2005).

[72] D. J. Bacon, D. M. Barnett, and R. O. Scattergood, "Anisotropic continuum theory of lattice defects," Prog. Mater Sci. **23**, 51 (1979).

[73] T. Mura, *Micromechanics of defects in solids* (Martinus Nijhoff, 1987).

[74] E. Kröner, "Dia- and para-elasticity," in *Theory of crystal defects. Proc. of the summer school held in Hrazany in September 1964* (Academic Press, 1966).

[75] W. Känzig, "Paraelasticity, a mechanical analog of paramagnetism," J. Phys. Chem. Solids **23**, 479 (1962).

[76] A. Nowick and W. Heller, "Anelasticity and stress-induced ordering of point defects in crystals," Adv. Phys. **12**, 251 (1963).

[77] R. M. Lynden-Bell and K. H. Michel, "Translation-rotation coupling, phase transitions, and elastic phenomena in orientationally disordered crystals," Rev. Mod. Phys. **66**, 721 (1994).

[78] P. Curie, Ann. de Chim. et de Phys. (VII) **5**, 289 (1895).

[79] P. Langevin, Ann. de Chim. et de Phys. (VI) **5**, 70 (1905).

[80] P. Debye, "Einige Resultate einer kinetischen Theorie der Isolatoren," Physik. Z. **13**, 97 (1912).

[81] P. Debye, *Polar molecules* (Dover, 1945).

[82] H. A. Lorentz, *The theory of electron*, 2nd edition, Leipzig (B. G. Teubner, 1916).

[83] J. D. Jackson, *Classical electrodynamics* (Wiley, 1975).

[84] J. Wyman, "Polarization and dielectric constant of liquids," J. Am. Chem. Soc. **58**, 1482 (1936).

[85] H. Müller, Physik. Z. **34**, 689 (1932).

[86] L. Onsager, "Electric moments of molecules in liquids," J. Am. Chem. Soc. **58**, 1486 (1936).

[87] F. N. H. Robinson, *Macroscopic electromagnetism* (Oxford: Pergamon, 1973).

[88] J. H. Hannay, "The Clausius-Mossotti equation: an alternative derivation," Eur. J. Phys. **4**, 141 (1983).

[89] J. G. Kirkwood, "The dielectric polarization of polar liquids," J. Chem. Phys. **7**, 911 (1939).

[90] E. Kröner, "Allgemeine Kontinuumstheorie der Versetzungen und Eigenspannungen," Arch. Ration. Mech. Anal. **4**, 18 (1960).

[91] V. Namias, "Application of the Dirac delta fuction to electric charge and multipole distributions," Am. J. Phys. **45**, 624 (1977).

[92] J. Van Bladel, *Singular electromagnetic fields and sources* (IEEE Press, 1991).

[93] L. D. Landau and E. M. Lifshitz, *Electrodynamics of continuous media*, 2nd edition (Pergamon Press, 1984).

[94] G. Stell, "The dielectric constant and mean electostatic energy of molecular fluids," in *The collected works of Lans Onsager*, edited by P. C. Hemmer, H. Holden, and S. Kjelstrup Ratkje (World Scientific, 1996), pp. 673–675.

[95] J.-P. Hansen and I. R. McDonald, *Theory of simple liquids* (Academic Press, 2006).

[96] G. Stell, G. N. Patey, and J. S. Høye, "Dielectric constant of fluid models: statistical mechanical theory and its quantitative implementation," Adv. Chem. Phys. **48**, 183 (1981).

[97] J. D. Eshelby, "The force on an elastic singularity," Phil. Trans. Roy. Soc. A **244**, 87 (1951).

[98] J. D. Eshelby, "The determination of the elastic field of an ellipsoidal inclusion, and related problems," Proc. Roy. Soc. A **241**, 376 (1957).

[99] K. Robinson, "Elastic energy of an ellipsoidal inclusion in an infinite solid," J. Appl. Phys. **22**, 1045 (1951).

[100] L. J. Walpole, "An elastic singularity in a spherical inclusion: the green tensor," Proc. Roy. Soc. A **458**, 705 (2002).

[101] C. H. Bennett, "Serially deposited amorphous aggregates of hard spheres," J. Appl. Phys. **43**, 2727 (1972).

[102] K. Hukushima and H. Kawamura, "Monte Carlo simulations of the phase transition of the three-dimensional isotropic heisenberg spin glass," Phys. Rev. B **72**, 144416 (2005).

[103] L. A. Fernandez, V. Martin-Mayor, S. Perez-Gaviro, A. Tarancon, and A. P. Young, "Phase transition in the three dimensional heisenberg spin glass: finite-size scaling analysis," Phys. Rev. B **80**, 024422 (2009).

[104] H. Kawamura, "Two models of spin glasses - Ising versus Heisenberg," J. Phys. Conf. Ser. **233**, 012012 (2010).

[105] J. A. Olive, A. P. Young, and D. Sherrington, "Computer simulation of the three-dimensional short-range Heisenberg spin glass," Phys. Rev. B **34**, 6341 (1986).

[106] D. P. Landau and K. Binder, *A guide to Monte Carlo simulation in statistical physiscs*, 2nd ed. (Cambridge University Press, 2005).

[107] K. Hurushima and K. Nemoto, J. Phys. Soc. Jpn. **65**, 1604 (1996).

[108] N. Madras, *Lectures on Monte Carlo methods* (AMS, 2002).

[109] W. Kerler and P. Rehberg, "Simulated-tempering procedure for spin-glass simulations," Phys. Rev. E **50**, 4220 (1994).

[110] R. K. Pathria, *Statistical mechanics* (Pergamon Press, 1972).

[111] W. Kauzmann, "The nature of the glass state and the behavior of liquids at low temperatures," Chem. Rev. **43**, 219 (1948).

[112] V. Lubchenko and P. G. Wolynes, "Intrinsic quantum excitations of low temperature glasses," Phys. Rev. Lett. **87**, 195901 (2001).

[113] C. Cammarota and G. Biroli, "Patch-repetition correlation length in glassy systems," EPL (Europhysics Letters) **98**, 36005 (2012).

[114] L. Berthier and G. Biroli, "Theoretical perspective on the glass transition and amorphous materials," Rev. Mod. Phys. **83**, 587 (2011).

[115] P. Rabochiy and V. Lubchenko, "Liquid state elasticity and the onset of activated transport in glass formers," J. Phys. Chem. B **116**, 5729 (2012).

[116] J. Qu and M. Cherkaoui, *Fundamentals of micromechanics of solids* (John Wiley & Sons, Inc., 2006).

[117] H. Bateman, *Higher transcendental functions*, edited by A. Erdélyi, Vol. 2 (McGraw-Hill, 1953).

[118] W. H. Press, S. A. Teukolsky, W. T. Vetterling, and B. P. Flannery, *Numerical recipes: the art of scientific computing* (Cambridge University Press, 2007).